MINISTÈRE DE L'ENSEIGNEMENT SUPÉRIEUR ET DE LA RECHERCHE SCIENTIFIQUE

----------o----------

UNIVERSITÉ FERHAT ABBAS

SÉTIF

THÈSE

présentée par

LOUAHDI Rachid

Pour obtenir le titre de **Docteur d'état**

de l'Institut d'Optique et de Mécanique de Précision

OPTION

Technologie

THE EFFECT OF DEFECT ANNIHILATION ON THE SEGREGATION KINETICS OF SULPHUR IN BOTH QUENCHED AND COLD WORKED NICKED

Date de soutenance : 14 novembre 1999

Devant le jury composé de :

Président :	Mr. D. BENACHOUR	Prof. Université de Sétif
Rapporteur :	Mr. A. BOUCENNA	Prof. Université de Sétif
Examinateurs :	Mr. D. HAMANA	Prof. Université de Constantine
	Mr. R. HALIMI	Prof. Université de Constantine
	Mr. E.H. OUAKDI	M.C. Université de Sétif

Année 1998/99

ACKNOWLEDGEMENTS

Most of this work was done in the laboratory of materials engineering of ISITEM (Institut des Sciences de l'Ingénieur en Thermique, Energétique et Matériaux), the university of Nantes, France. Part of it was carried out in the institute of mechanical engineering of the university of Sétif, Algeria.

I would like to express my special thanks to Professor Guy Saindrenan, Dr. René Le Gall, Dr. Pascal Paillard and all the other members of staff and technicians for the friendly welcome and for all the co-operation I was granted during all my short stays in the materials engineering laboratory of ISITEM (Nantes).

A series of the corrosion tests was carried out in the institute of industrial chemistry at Sétif university, Algeria. The help of Dr. A. Kahoul in carrying out these tests is gratefully acknowledged.

My thanks go to Professor Ahmed Boucenna for having kindly accepted to supervise this work.

My respectful thanks go to Professor D. Benachour, Rector of Sétif university, for having granted me the honnour of being the president of my submission jury.

My gratitude is hereby expressed to Professors D. Hamana and R. Halimi, from the physics institute of Constantine university, for having kindly accepted to be members of this jury.

I would also like to thank my friend and colleague, Dr. E.H. Ouakdi for his everlasting encouragement and for accepting to be a member of my submission jury.

The Auger analyses were carried out by Mr. J.P. Roche of the Ecole Centrale de Nantes. His co-operation is gratefully acknowledged.

The DSC and resistivity measurements would not have been possible without the help of Mr. B. Bauché and Mr. P. Molinié of the Institute of Materials of Nantes (IMN), I am indebted to them for their kindness.

REMERCIEMENTS

La plus grande partie de ce travail a été réalisée au laboratoire de génie des matériaux de l'ISITEM, université de Nantes, France. Une partie a été réalisée à l'institut d'optique et de mécanique de précision de l'université de Sétif, Algérie.

Je tiens à remercier tout particulièrement MM. Guy Saindrenan, professeur, P. Paillard et R. Le Gall, maîtres de conférence, tous à l'ISITEM de l'accueil amical qu'ils m'ont toujours réservé et de l'aide sans limites qu'ils m'ont accordé. Une série des essais de corrosion a été effectuée à l'institut de chimie industrielle de l'université de Sétif. Que le Dr. A. Kahoul qui m'a aidé à exécuter ces essais trouve ici l'expression de ma gratitude la plus sincère.

Mes remerciements vont aussi au professeur Ahmed Boucenna de L'institut de physique de l'université de Sétif pour avoir accepté la tâche de promoteur de ma thèse.

Le Professeur D. Benachour, Recteur de l'université de Sétif, m'a fait l'honneur de présider mon jury de thèse, qu'il trouve ici l'expression de mes respectueux remerciements.

Que le Professeur D. Hamana, directeur de l'unité de recherche Physique des matériaux et applications (université de Constantine) et le Professeur R. Halimi, directeur de recherche à la même unité, soient tout particulièrement remerciés d'avoir accepté de participer à ce jury.

Je voudrais aussi remercier mon ami et collègue, Dr. E.H. Ouakdi, pour ses encouragements inlassables et pour avoir accepté de participer au jury de Thèse.

Je remercie Monsieur J.P. Roche de l'école centrale de Nantes d'avoir effectué les analyses Auger avec beaucoup de soins. Les mesures de calorimétrie différentielle et de résistivité n'auraient pas été possibles sans l'aide de MM B. Bauché et P. Molinié de l'institut de matériaux de Nantes, Je tiens à leur exprimer ma gratitude la plus sincère.

REMERCIEMENTS

La plus grande partie de ce travail a été réalisée au laboratoire de génie des matériaux de l'ISITEM, université de Nantes, France. Une partie a été réalisée à l'institut d'optique et de mécanique de précision de l'université de Sétif, Algérie.

Je tiens à remercier tout particulièrement MM. Guy Saindrenan, professeur, P. Paillard et R. Le Gall, maîtres de conférence, tous à l'ISITEM de l'accueil amical qu'ils m'ont toujours réservé et de l'aide sans limites qu'ils m'ont accordé. Une série des essais de corrosion a été effectuée à l'institut de chimie industrielle de l'université de Sétif. Que le Dr. A. Kahoul qui m'a aidé à exécuter ces essais trouve ici l'expression de ma gratitude la plus sincère.

Mes remerciements vont aussi au professeur Ahmed Boucenna de L'institut de physique de l'université de Sétif pour avoir accepté la tâche de promoteur de ma thèse.

Le Professeur D. Benachour, Recteur de l'université de Sétif, m'a fait l'honneur de présider mon jury de thèse, qu'il trouve ici l'expression de mes respectueux remerciements.

Que le Professeur D. Hamana, directeur de l'unité de recherche Physique des matériaux et applications (université de Constantine) et le Professeur R. Halimi, directeur de recherche à la même unité, soient tout particulièrement remerciés d'avoir accepté de participer à ce jury.

Je voudrais aussi remercier mon ami et collègue, Dr. E.H. Ouakdi, pour ses encouragements inlassables et pour avoir accepté de participer au jury de Thèse.

Je remercie Monsieur J.P. Roche de l'école centrale de Nantes d'avoir effectué les analyses Auger avec beaucoup de soins. Les mesures de calorimétrie différentielle et de résistivité n'auraient pas été possibles sans l'aide de MM B. Bauché et P. Molinié de l'institut de matériaux de Nantes, Je tiens à leur exprimer ma gratitude la plus sincère.

CONTENTS

GENERAL INTRODUCTION

Metals are often subjected to operations which introduce in them quantities of crystalline imperfections well above the saturation levels. The metals in these conditions are said to be supersaturated in defects and are therefore in a non equilibrium state. Amongst these operations, rapid cooling from a high temperature (quenching), irradiation and plastic deformation during various shaping processes are the most frequently encountered in practice. Metals undergo subsequent heat treatments destined to bring the material back to its equilibrium state. An acceleration of the migration of defects, impurities and even alloying elements is found to occur during these heat treatments leading, contrary to the objectives initially sought, to a deterioration of the mechanical and the electrochemical properties of the material.

Early observations of interfacial segregation accompanying the return to equilibrium of a metal supersaturated in vacancies go back to nearly thirty years ago. The work of Aust *et al* [1] established that, during the cooling of a metal, the regions in the vicinity of grain boundaries harden as a result of their enrichment in solute atoms. The development of the nuclear industry has also motivated a considerable amount of research on similar phenomena occurring in irradiated material.

The recovery of a cold worked metal takes place through a recrystallisation of the deformed grains preceded by a vacancy elimination stage, and it is established that each of these stages generates an acceleration of interfacial segregation.

The object of this work is to treat the particular case of the effect on the properties of sulphur segregation occurring during the heat treatment of quenched and cold worked nickel, and to determine the role of each of the point defect elimination and the recrystallisation processes on the segregation kinetics. The main reason behind this choice is the existence in the literature of substantial amount of data concerning the segregation of sulphur in nickel, in equilibrium conditions (i.e. during the heat treatment of a fully annealed

material) readily available as a basis for comparison . Other equally important reasons are given in chapter III where more details on the Ni-S system are also provided.

A brief review of some of the work reported in the literature concerning general aspects such as the main two types of segregation (surface and grain boundary), its origins and its effects on the properties is presented in chapter I.

Chapter II introduces the concepts of equilibrium and non equilibrium segregation. The thermodynamic and kinetic aspects of the former, which has been extensively studied, are briefly outlined with particular reference to the Ni-S system . Non equilibrium (**dynamic**) segregation is the object of our work and is dealt with in the subsequent chapters.

In chapter IV, and after a brief introduction summarising the main aspects of recovery and recrystallisation, the experimental techniques used to study the recovery and recrystallisation of cold rolled nickel together with those used to study the segregation accompanying it are elaborated. The segregation results are interpreted in terms of the results obtained from the work on recrystallisation, highlighting the influence of each of the recrystallisation stages on the segregation kinetics. Indirect indication of grain boundary segregation is given by the results obtained from tensile and electrochemical tests carried out on the cold rolled and then heat treated material.

In order to clearly emphasise the effect of vacancies, work on quenched and then annealed nickel is undertaken. After a concise introduction on vacancies, details on the experimental work carried out on their creation and elimination , the resulting segregation and the consequences on the intergranular properties of nickel are given in chapter V.

Chapter VI Summarises the mechanisms operating during dynamic (non-equilibrium) segregation of sulphur in cold worked and in quenched nickel.

A summary of the main points stemming from our contribution to the subject is finally presented in the form of a conclusion.

CHAPTER I

A LITERATURE SURVEY ON SEGREGATION TO THE SURFACE AND TO THE GRAIN BOUNDARIES OF METALS AND ITS EFFECTS ON THEIR PROPERTIES

In this chapter an attempt is made to review some of the work done on segregation in some commercial metals, and its effects on the mechanical and the electrochemical properties. The relationship between surface and intergranular segregation is emphasised.

1. Metallurgical aspects of segregation

At temperatures sufficiently high to promote diffusion, elements in solid solution accumulate at defect sites such as grain boundaries and free surfaces [2,3]. At equilibrium, these elements which may be present as residual impurities at concentrations of a few parts per million, can concentrate by factors of many thousands at these sites [4-7]. In engineering materials, enrichment of natural impurities at defect sites is responsible for many forms of intergranular mechanical failure such as low temperature brittleness and creep embrittlement [8-11]. Since it is usually impracticable to reduce the bulk level or to reduce the diffusion activity of all possible residual impurities, it is important to identify the nature and enrichment of the most harmful segregants associated with a given material and a particular heat treatment or, say, welding procedure. This may be done by Auger electron fractography in which the intergranular service failure is simulated by tensile or impact failure of a small sample of the material at low temperature in ultra-high vacuum [8,12,13]. The composition of the interfacial atomic layer is then directly identified by examining the exposed grain boundary by Auger electron spectroscopy.

In commercial materials, however, the impurities segregated to grain boundaries, while impairing certain mechanical properties during service life [14], are often insufficient to promote the low temperature intergranular brittleness necessary to expose the grain boundaries for Auger electron examination.

In order to overcome this experimental limitation, procedures have been set up for the quantitative determination of grain boundary segregation by recourse to the more accessible measurements of segregation at the free surface [15-17]. For this purpose equilibrium surface segregation levels have been measured in the Fe-Sn system [5] in order to relate surface enrichment parameters with those already available for grain boundaries in that system [4].

Besides this application of surface segregation to indicate grain boundary segregation levels, the phenomenon is worthy of study and understanding in its own right[18,19]. Phosphorus in steels destined to receive galvanneal coatings is found to influence the evolution of the coating structure as well as the final properties of the coating . It is postulated that phosphorous which segregates to the sheet steel surface during recrystallization annealing affects the kinetics of the Fe-Zn reaction as the sheet steel is subsequently dipped in a molten zinc bath of a continuous galvanising line [20-22]. The surface segregation of magnesium from aluminium alloys causes difficulties in adherence of coatings such as porcelain enamel to the metal [23] or results in a considerably enhanced propensity of aluminium alloys to stress corrosion in humid environments . Also, trace levels of sulphur in nickel, diffusing rapidly to the surface, have been shown to have many important effects on the reaction of nickel with oxygen, increasing the kinetics of oxidation in the early stages and also reducing the stability of the oxide scale formed [24].

More details on the effects of interfacial impurity and alloying element segregation in some widely used systems are presented in the following sections.

2. Segregation in some common systems

2.1 Aluminium alloys

Considerable work is reported in the literature about the segregation behaviour of magnesium in Al-Mg alloys, both in the as quenched and in the quenched and aged conditions. Indirect evidence of grain boundary segregation in Al-Mg alloys is based mainly on their grain boundary corrosion behaviour [25] and sometimes on their mechanical properties [26-28]. Both EDX (energy dispersive X-ray analysis) and EELS (electron energy loss spectroscopy) have been used to attempt to observe directly the segregation of magnesium to grain boundaries in Al-Mg systems. Enrichment was seen both by EELS [29] and by EDX [30].

TEM/STEM-EDX analysis showed magnesium enrichment at many of the as quenched boundaries observed [31].

Other aluminium alloys have been studied from the view point of the relationship microstructure-intergranular corrosion-stress corrosion cracking behaviour. Calvele and De Micheli [32], Maitra and English [33] and Byrne [34] have shown the importance of electrochemical methods in the study of the susceptibility of Al-6%Zn-2.5%Mg-1.7%Cu-.02%Cr to intergranular corrosion due to intergranular segregation. Two breakdown potentials were identified in the potentiodynamic anodic polarisation curves. The first was attributed to the Mg and Zn enriched phase in the vicinity of the grain boundaries, indicating segregation of these elements to these regions, and the second was attributed to the matrix.

2.2. Stainless steels

Intergranular corrosion and stress corrosion cracking of austenitic stainless steels have occurred in a number of industrial applications. Many of these failures have been correctly attributed to sensitisation of the steel. Sensitisation is a term used to describe the depletion of chromium along grain boundaries that occurs as the result of the growth of chromium rich carbides [35,36]. Research has now shown that although sensitisation greatly accelerates corrosion and stress corrosion cracking, its occurrence is not a necessary condition for intergranular attack of stainless steels in all environments. Intergranular failures occurred in non-sensitised materials [37-40]. It has been assumed, and demonstrated to some extent, that in the absence of chromium depletion impurity segregation to grain boundaries causes this intergranular damage [41-43].

In low alloy ferritic steels, grain boundary segregation has been examined by Auger electron spectroscopy after fracturing the samples intergranularly in the high vacuum environment required for this technique [44]. In austenitic alloys,

grain boundary segregation has been harder to study because of the difficulty associated with making these alloys fracture intergranularly in a high vacuum. In austenitic steels that are heavily doped with impurity elements, intergranular fracture has been obtained when the samples have been charged with hydrogen [45-49]. But in austenitic steels that are not heavily doped, it has been difficult to investigate this segregation. Consequently, segregation to the free surface is frequently used to obtain qualitative information about what elements are segregating to an interface at a particular temperature and how this segregation may change with alloy composition and may affect the intergranular properties of the material. In a comprehensive study conducted by Briant [50], in which Auger electron spectroscopy was used to measure surface segregation in austenitic stainless steels having compositions similar to types 304L, 316L, 304 or 347 , it was found that segregation of impurity elements could occur at temperatures between 300 and 500°C. Although nitrogen was found to segregate most rapidly, phosphorus, sulphur and silicon were also observed on the surfaces. Cold work or the presence of martensite accelerated segregation. Sulphur segregation was found to occur in both Mn containing and Mn free stainless steels, although the presence of manganese greatly retarded segregation. The retardation was attributed to the role of manganese in lowering the activity of sulphur in the alloy. Both silicon and nickel were found to segregate to the surfaces, with the segregation of the latter being affected by that of the former. Additions of up to 0.8% niobium were found to increase phosphorus segregation. This increase was attributed to the role of niobium in lowering the carbon activity in the steel, and reducing phosphorus-carbon competition. Table I-1 summarises results of various works carried out on austenitic stainless steels [45,49,51], clearly showing that both surface and grain boundary segregations are qualitatively similar. The same elements segregate to both interfaces. The kinetics of segregation are reasonably similar in both situations, and evidence of the site competition between sulphur, phosphorus

and nitrogen that is detected on surfaces has also been found on grain boundaries [45]. In contrast, equilibrium concentrations of the segregant on the surface are usually higher than on the grain boundaries, the decrease in free energy accompanying surface segregation being greater than that accompanying grain boundary segregation. These findings are similar to those in other studies that have compared surface segregation with grain boundary segregation [52,53].

Element	Surface segregation			Grain boundary segregation		
	Time (h) To reach equilibrium	Auger peak height ratio	Competitive Interactions observed	Time (h) to reach equilibrium	Auger peak height ratio	Competitive Interactions observed
N	0.7	0.14	C,P,S	<5	0.09	
P	20	0.8	N,S	5-24	0.2-0.4	N,S
S	70	1	N,P	-	~ 0.1	

Table I-1. A comparison of grain boundary and surface segregation at 650°C in austenitic stainless steels [45,49,51].

The influence of intergranular segregation on corrosion and stress corrosion cracking of stainless steels is shown in Table I-2 [45]. Briant and Anderson [45] have shown that sulphur segregation increases intergranular stress corrosion cracking in austenitic stainless steels tested in 288°C water with a pH of 2.5. They found that in Mn containing alloys aged for 100h at 500, 550, 600, 650 and 700°C, little intergranular stress corrosion cracking was observed below 600°C. In alloys that did not contain manganese, intergranular stress corrosion was observed even at 500 and 550°C. This is consistent with the segregation behaviour observed by Briant [50]. Silicon has also been reported to increase intergranular corrosion of stainless steels, particularly at high electrochemical

is in agreement with the results found by Briant [50] which would suggest that silicon should segregate to grain boundaries and therefore be available to affect intergranular corrosion. They would also suggest that niobium additions should not decrease phosphorous segregation to grain boundaries and hence its effect on intergranular corrosion. Also it would appear, from a comparison with AES studies carried out on cold worked material [50], that low temperature heat treatment of cold worked material lead to segregation induced corrosion . This low temperature segregation could explain why commercial purity steels subjected to long time irradiation at approximately 300°C become very susceptible to intergranular stress corrosion cracking whereas high purity materials, at least in some cases, do not [54].

Element	Laboratory tests	Industrial applications
P	Huey test (65%HNO_3), HNO_3/Cr^{+6}	Nitric acid plants, dye plants, heat exchangers, Boiling water reactors
Si	HNO_3/Cr^{+6}	Nitric acid plants, heat exchangers, boiling water reactors
S	Stress corrosion test in pH 2.5 water	Oil refinery, waste water treatment plants, heat exchangers, boiling water reactors

Table I-2. A summary of laboratory experiments which have demonstrated the importance of impurity elements in causing intergranular corrosion and industrial applications where similar conditions might exist [45].

2.3 Segregation of sulphur in nickel

Not as much work on segregation in pure metals, as in alloys, is reported in the literature. This is presumably because of the long held idea that impurities exist in pure metals in concentrations too small to engender any segregation related problems. The present work sets out to bring evidence that it is far from being the case.

One of the few investigations on the thermodynamics and the kinetics of sulphur segregation taking place during the heating of fully annealed different grades of nickel carried out by Larère [55] provided the following results:

- the kinetics of surface and grain boundary segregation of sulphur are proportional to the square root of heating time. This is in agreement with the McLean model [56];
- values of the free enthalpies of sulphur segregation at both interfaces are in good agreement with Fowler's formalism [57].
- the maximum sulphur concentration at the grain boundary (45 at.%) is equivalent to that at the free surface. This is possibly due to the fact that the interface concentration is controlled by the number of available sites.

The influence of sulphur segregation on the corrosion behaviour of nickel, in both an alkaline (K2SO4 + LIOH at a pH of 9.5) and an acidic (1 M H2SO4) medium is reported by Rabu *et al* [58]. Sulphur segregation was shown to increase the dissolution rate. The increase was less significant in the alkaline medium, and intergranular corrosion was more evident in the acidic medium.

3. Electrochemical aspects of segregation induced intergranular corrosion

Preferential attack due to grain boundary segregation is found to take place at high energy grain boundaries, the regions of the surface where these boundaries emerge being mainly constituted of loosely linked atoms in comparison with the rest of the metal as a consequence of the disorder existing in these regions [59].

This type of corrosion, although very localised, was found to reach considerable depths.

The understanding of the role of microstructural features requires the characterisation of the metallurgical heterogeneities responsible for the localised cell action. The electrochemical theory of corrosion emphasises the importance of electrode potentials and polarisation phenomena for an accurate interpretation of intergranular reactions. Various electrochemical techniques (potentiostatic, potentiodynamic,....etc.) in which the potential, the current and the quantity of electricity are rigorously controlled have been developed [60]. The tests carried out dealt mainly with the detection of precipitation and chromium depleted areas in light elements and nickel-chromium steels [61]. The results obtained are, however, only macroscopic and yield no information on the intrinsic and local properties of grain boundaries. These tests also proved to be inadequate for intergranular corrosion in water quenched, precipitate- free, materials despite the fact that grooves were otherwise seen to form at the emergence of grain boundaries on the surfaces of precipitate-free stainless steels [62]. A variety of other alloys were observed to undergo preferential intergranular corrosion, displayed in the form of emerging grooves, when the potential was chosen in the initial rise of the transpassive peak [63], and an evaluation of the attack is obtained from a measure of the groove parameters (angle, depth and width). To explain the appearance of these grooves, it was suggested that a grain boundary dissolution current, $\mathbf{I}_{g.b.}$, existed as well as the surface dissolution current , $\mathbf{I}_s$. A relationship between $\mathbf{I}_{g.b}$, $\mathbf{I}_s$ and the intergranular groove angle α is given by :

$$I_{g.b.} = I_s(\sin\frac{\alpha}{2})^{-1}.$$

Figure I-1 is a schematic representation of a model describing the preferential attack taking place at the grain boundaries [64]. In general, $\mathbf{I}_{g.b}$>**Is** and therefore, an intergranular groove is obtained. It is shown that the value, α, at which the

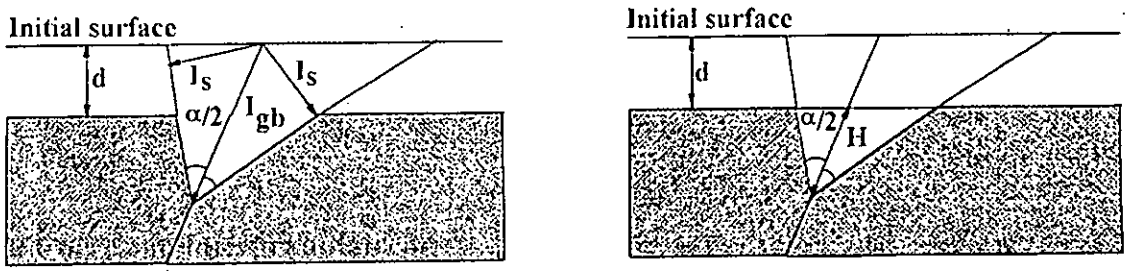

(a) (b)

Figure I-1. A schematic representation of the preferential attack taking place at the grain boundaries [91].
(a) a representation of the dissolution currents existing at the grain boundaries
(b) a representation of the parameters (H, α) of the resulting intergranular groove

groove angle stabilises is independent of the quantity of electricity crossing the metal [64] but is considerably affected by the chemical composition of the GB. The groove characteristics (angle α, height **H**) can therefore be taken as indications of the progress of intergranular attack. This is exploited in the present work to investigate intergranular corrosion due sulphur segregation to the grain boundaries of nickel.

4. Physical origins of segregation and segregation induced intergranular de-cohesion

Several explanations are reported in the literature concerning the driving force for segregation. The decrease in free energy accompanying the passage of a solute atom from the bulk to the interface results from one of the following phenomena :

- Relaxation of the elastic energy resulting from the solute atom finding a better accommodation site in the interface [65].
- The formation of more geometrically favourable chemical bonds at the grain boundary [66]. The grain boundary consists, according to this model, of structural units linked together to form a chain. This partly explains the stability of segregation, since the chemical bonds made by the impurity are stronger in the GB than in the matrix.
- An overall decrease in the grain boundary interfacial energy [67].

It is well known that the lower the solubility in a matrix, the easier its segregation to interfaces will be [67], thus leading to an increase in segregation with decreasing temperature. It should however be borne in mind that unlike precipitation where saturation is the driving force, segregation appears even in a non-saturated solution, and nothing prevents it from taking place at the same time as precipitation.

It is reported in some literature that intergranular cohesion greatly depends on the elctronic properties of metals [68,69]. The embrittling impurities are

electronegative with respect to the matrix, and therefore attract towards them the electronic charges of the matrix atoms, thus leading to a weakening of the metal-metal bonds near the boundary .

The role of sulphur in bringing about a spectacular decrease in ductility of several ferrous and nickel base alloys during hot working in certain temperature ranges is summarised according to some research workers in the following steps [69]:

- Microcracks are initiated, under the effect of stress, at the triple points where flow cannot take place.
- The impurity atoms segregate to the microcracks, and then accumulate, through superficial diffusion and for surface tension considerations, at the tips of these cracks.
- The decrease in surface tension thus obtained leads to a decrease in the work necessary for crack opening. This in turn facilitates crack propagation until failure occurs.

The results obtained in the present work on the Ni-Si system enabled us to put forward a mechanism based on the so called "impurity drag theory" which will be exposed and detailed further in the text.

P.S. It is admitted that the part on stainless steels is rather too long. This is so because the original idea consisted of investigating nickel and then extending the findings to stainless steels as widely used nickel containing alloys. Although the considerable amount of work limited the investigation to pure nickel, it was decided not to shorten the part on stainless steels because of the valuable information it contains, and the qualitative agreement that was found between our results and those surveyed on stainless steels.

CHAPTER II

THERMODYNAMIC AND KINETIC ASPECTS OF SEGREGATION

In this chapter the most widely known thermodynamic and kinetic models describing equilibrium segregation are briefly outlined, insisting more particularly on the results relevant to our work (i.e., the expressions that enabled us to calculate "apparent diffusion coefficients").

1. Introduction

Two segregation modes have been reported in the literature; equilibrium and non-equilibrium segregation. Equilibrium segregation deals with interface enrichments resulting from normal diffusion processes under the sole control of the diffusion coefficient of the segregating specie in the metal [70]. Non-equilibrium segregation corresponds to cases where the diffusion of the segregating element is accelerated by the presence of unstable or metastable defects. The driving force in these cases is linked to the return of the metal to its equilibrium condition.

2. Thermodynamic aspects of equilibrium segregation

From the thermodynamic point of view, segregation is regarded as a special case of adsorption, where the diffusing specie comes from the metal instead of coming from the surrounding gaseous phase.

Considering the interface Φ to be a phase in its own right, Gibbs [71] established the following relationship linking the enrichment of the interface Φ with impurity I, $\Gamma^{\phi}_{(I,M)}$, to the surface tension of the interface, γ^{Φ}, and to the chemical potential of I in the phase Φ, μ^{ϕ}_{I} :

$$\Gamma^{\Phi}_{I,M} = \frac{\partial \gamma^{\phi}}{\partial \mu^{\phi}_{I}}$$

The application of this model to segregation is, however, not very convenient since it requires the knowledge of the surface tension which cannot be measured at the temperatures at which segregation takes place.

Other models involving parameters more readily disposed to experimental acquisition are developed. Most of these models are based on either statistical or chemical thermodynamics considerations. Although they contain numerous

simplifying hypothesise, they nevertheless satisfactorily account for the reality. While one type of these models ignores possible interactions between atoms in the segregated layer (ideal solution), the other introduces a term taking into account this interaction (regular solution).

2.1 Segregation models assuming no atomic interactions

One of the first adsorption models to be known is that of Langmuir [72], and is derived from the kinetic theory of gases. The rate of surface coverage θ_I (ratio of sites occupied by adsorbed atoms to the available sites) is given by:

$$\frac{\theta_I}{1-\theta_I} = P_I.K(T).e^{\frac{-\Delta G_I^{ads}}{RT}}$$

where ΔG_I^{ads} is the free enthalpy of adsorption, and P_I is the bulk concentration of the impurity.

Mc Lean [56] puts forward a similar expression describing grain boundary segregation:

$$\frac{Y_I^{\phi}}{1-Y_I^{\phi}} = C_I^B.e^{\frac{-\Delta G_I^{gbs}}{RT}}$$

Where Y_I^{ϕ} represents the ratio of the grain boundary concentration to the maximum grain boundary concentration ($Y_I^{\phi} = C_I^{\phi}/C_{I(\max)}^{\phi}$), C_I^B is the bulk concentration of the impurity and ΔG_I^{gbs} represents the free enthalpy of grain boundary segregation of the impurity *I*.

This model is equally well applicable to surface segregation provided ΔG_I^{gbs} is replaced with ΔG_I^{ss}, the free enthalpy of surface segregation.

2.2 Segregation models taking into account atomic interactions

The introduction of the term W, representing the energy of interaction between first nearest neighbour atoms in the segregated layer, in the adsorption model of Fowler and Guggenheim [73] takes into account the interaction aspect. The isotherm thus becomes:

$$\frac{\theta_I}{1-\theta_I} = K(T).P_I.e^{\frac{-(\Delta G_I^{ads} - 2N \cdot W \cdot \theta_I)}{R \cdot T}}$$

$2N$ is the number of atoms in the segregated layer.

Lagües [74] who studied segregation to free surfaces, found a similar expression:

$$\frac{Y_I}{1-Y_I} = C_I^B.e^{\frac{-(\Delta G_I^{seg} - 2N \cdot W \cdot Y_I)}{R \cdot T}}$$

Larere [55] who applied to binary alloys, a model put forward by Guttmann [75,76] for grain boundary segregation in ternary alloys, found a similar expression as that of Lagües.

Table II-1 gives values of free enthalpies of segregation and interaction energies for sulphur segregation in nickel, calculated by various authors.

Figure II-1 represents the evolution of the surface coverage rate with temperature for high purity nickel (< 1ppm sulphur) . It clearly appears that the curves of Langmuir-McLean and of Fowler-Lagües representing surface segregation are nearly identical. This is due to the weak interaction energy of sulphur on the surface of nickel. It also appears that for temperatures less than 800°C, the surface coverage rate at equilibrium remains very near to saturation, and that the McLean approximation for segregation to grain boundaries can only

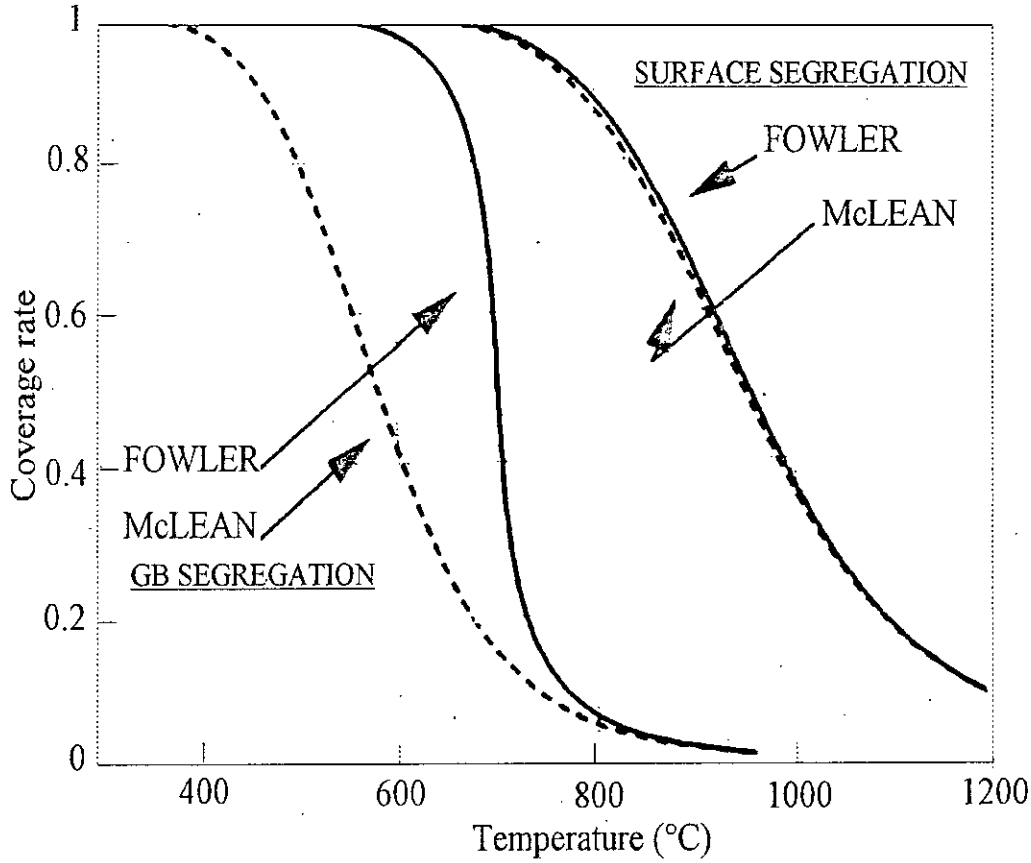

Figure II-1. Curves representing the evolution of the interface coverage rate with temperature during the equilibrium segregation of sulphur in high purity nickel (<1ppm S).

be used at high temperatures corresponding to small values of the coverage rate. The temperature of 700°C can therefore be considered to be a critical one, below which the grain boundary is saturated with sulphur and above which the coverage rate decreases rapidly to become negligible for temperatures greater than 800°C.

Ref	$\Delta G_S^{\circ surf}$ (kJ.mol^{-1})	W_S^{surf} (kJ.mol^{-1})	$\Delta G_S^{\circ joint}$ (kJ.mol^{-1})	W_S^{joint} (kJ.mol^{-1})	Observation
[55]	-140±7	-1.5	-	-	Ni270 (800<T<950°C)
[55]	-	-	-98	-32	T = 1200°C
[77]	-175	-	-	-	adsorption
[78]	-123	-	-	-	

Table II-1. Thermodynamic data for sulphur segregation to nickel interfaces.

3. Kinetic aspects of equilibrium segregation

Lagües [74] puts forward the following two step mechanism for segregation:

1) The segregating atoms diffuse thermally to the "skin". The skin is the region just underneath the surface (x=0) and where diffusion is normal to the surface. The "skin" can be made of more than one atom plane.

2) The atoms then pass from a state of dissolution in the "skin" to a state of segregation.

On the basis of this mechanism, and using Fick's laws of diffusion, the physical model describing the formation of the segregation layer can be obtained through the solution of the following system:

- Initial conditions:

$$C_1^B(x, t = 0) = C_B(x)$$

$$C_I^{\phi}(t=0) = C_0$$

C_I^B and C_I^{ϕ} are the bulk and the interface concentrations of the impurity respectively.

- Boundary conditions:

1- $$C_I^B(x=0,t) = f(C_I^{\phi})$$

2- $$d.\left(\frac{dC_I^{\phi}}{dt}\right) = D.\left(\frac{\partial C_I^B}{\partial x}\right)_{x=0}$$

where d is the thickness of the interface. This parameter disappears if the concentration is given per unit area.

This condition stems from the conservation of mass principle. The flux of matter leaving the volume is distributed in the interface (in the case of a grain boundary, the multiplication factor ½ appears in the relationship accounting for the fact that this kind of interface is fed from two sides).

3- $$\left(\frac{\partial C_I^B}{\partial x}\right)_{x\to\infty} = 0$$

This condition considers the diffusion medium to be semi-infinite, i.e. it implies that at a remote distance, the flux is nil and therefore the concentration is constant.

-Fick's second law:

$$D_I^B.\frac{\partial^2 C_I^B}{\partial x^2} = \frac{\partial C_I^B}{\partial t}$$

McLean [56] put forward the following analytical solution :

$$\frac{C_I^{\phi}(t)}{C_I^B(x=0,t)} = \beta = \text{ constant,}$$

which is a simplification of the relationship:

$$C_I^B(x=0,t) = f(C_I^{\phi}(t))$$

McLean's relationship is only valid at the very first instances of diffusion, during which the concentration of the interface remains low.

Assuming that neither the enthalpy of segregation nor the temperature change, C_i^ϕ has to remain very much less than unity for β to remain constant. This condition being satisfied, McLean obtains the following expression:

$$\frac{C^\phi(t) - C^\phi(t=0)}{C^\phi(t\to\infty) - C^\phi(t=0)} = 1 - e^{s^2}.erf(s)$$

where $S = \frac{2\sqrt{D.t}}{\beta.d}$ in the case of a grain boundary

$S = \frac{\sqrt{D.t}}{\beta.d}$ in the case of a surface.

This expression can further be simplified through a limited development near the origin:

$$\frac{C^\phi(t) - C^\phi(t=0)}{C^\phi(t\to\infty) - C^\phi(t=0)} \approx \frac{2.s}{\sqrt{\pi}}$$

If the concentration at the interface at t=0 is also assumed to be negligible (which is strictly not the case in the first instances) and β to remain constant and equal to the equilibrium value $\beta = \frac{C^\phi(t\to\infty)}{C_B}$, the following approximate solution is obtained:

$C^{gb}(t) = \frac{4.C_B}{d}.\sqrt{\frac{D.t}{\pi}}$ in the case of grain boundary segregation,

$C^s(t) = \frac{2.C_B}{d}.\sqrt{\frac{D.t}{\pi}}$ in the case of free surface segregation.

4. Non-equilibrium (dynamic) segregation

Non-equilibrium segregation may take place during the return of a metal to its equilibrium state, i.e. during the recovery and recrystallisation of a cold worked metal (containing an excess of dislocations and point defects), or during the annealing of a metal supersaturated in point defects resulting from processes such as quenching [79-81] or irradiation [82-84].

Although, this type of segregation has been previously reported and considerable efforts of theoretical studies have been undertaken [85-87], no satisfactory thermodynamic or kinetic model based on experimental evidence has been proposed to describe the phenomenon.

The main object of our work is to investigate non-equilibrium segregation of sulphur taking place during the heat treatment of quenched and cold worked pure nickel and its consequences on the intergranular properties of the material.

CHAPTER III

MATERIAL STUDIED

Nickel is considered to be a strategic material. It is widely used as an alloying element in stainless alloys, super-alloys, ferro-nickels, inconels, ...etc.. It is also used as a coating material for copper and ferrous alloys, since it has good mechanical properties (hardness of annealed pure nickel = 85HB)[88] and its hardness can be improved by adding small quantities of phosphorous and boron [89]. The major limitations lie in its intergranular brittleness and poor corrosion resistance in acid solutions.

The most important reasons that lead to the choice of the Ni-S system as a subject for our study are as follows :

- The great majority of experimental results presented in the literature show unambiguously the role of sulphur in impairing the intergranular properties of nickel.
- The availability of thermodynamic and kinetic data concerning equilibrium segregation of sulphur in nickel [55].
- The separation, for nickel, between the recrystallisation stage and the vacancy elimination stage on the temperature scale, which is not the case for all f.c.c. metals (copper, for example, does not have two distinct stages). This enables the determination of the effect of each stage separately on the segregation phenomenon.
- To confirm whether very low impurity contents would have any effects on high purity materials . Various results presented in the literature tend to suggest that a minimum sulphur content is necessary to lead to intergranular brittleness. Merica and Waltenberg [90] showed, as early as 1925, that at least 5ppm of sulphur were necessary to cause the embrittlement of nickel during forging. Nearly fourty years later , Olsen *et al* [91] and Oliver [92] put forward the values of 5 and 7ppm respectively as minimum sulphur contents for any embrittlement to occur. However, none of these workers gave any explanation as to the existence of such minimum levels.

The material studied in this work is high purity nickel 270 of Wiggins Alloys (UK), containing only 0.5ppm sulphur. The chemical analysis is given in table III-1. The relatively high content of carbon results from the fact that the metal is obtained from metal-carbonyl compounds by powder metallurgy techniques.

Element	Fe	Mn	C	O	S	Σ others
Weight (ppm)	30	20	70	21	0.5	50

Table III-1: Chemical composition of Ni 270 (determined by spark emission spectrometry).

The previous studies conducted on the equilibrium segregation of sulphur in nickel [55] pointed to the fact that only sulphur segregates in measurable quantities despite the considerable quantity of the other elements compared to that of sulphur.

The atomic radii of sulphur and nickel are equal to 1.84 A° and 0.78 A° respectively, giving a ratio greater than 2.3. Sulphur tends, therefore, to be preferentially located in expanded sites in contrast to the normal sites of nickel, in order to minimise the elastic energy of the crystal. These expanded sites are more readily available on the free surface and grain boundaries, and also near vacancies and dislocations. This is furthermore emphasised by the values of the free energies of equilibrium segregation to these interfaces: -140 kJ. mol^{-1} to the free surface and -98kJ.mol^{-1} to grain boundaries (the activation energy for heterodiffusion is found to be 192 kJ.mol^{-1}) [93]. Studies were carried out on the solubility of sulphur in nickel monocrystals [94] and polycrystals [95], and the maximum solubility was found to be 450 ppm in monocrystalline nickel and 510 ppm in the polycrystalline material, at a temperature of 1200°C. The Ni-S

equilibrium diagram (figure III-1) [96] shows that the solubility of sulphur in nickel varies considerably with temperature, and that although the solubility limit at temperatures below 700°C is not accurately determined it is reasonable to admit that at these temperatures (the importance of which in relation to this work will become more evident in the part on the experimental procedure) the small amount of sulphur existing in Ni 270 should, in equilibrium conditions, remain in solution (i.e., precipitation is excluded).

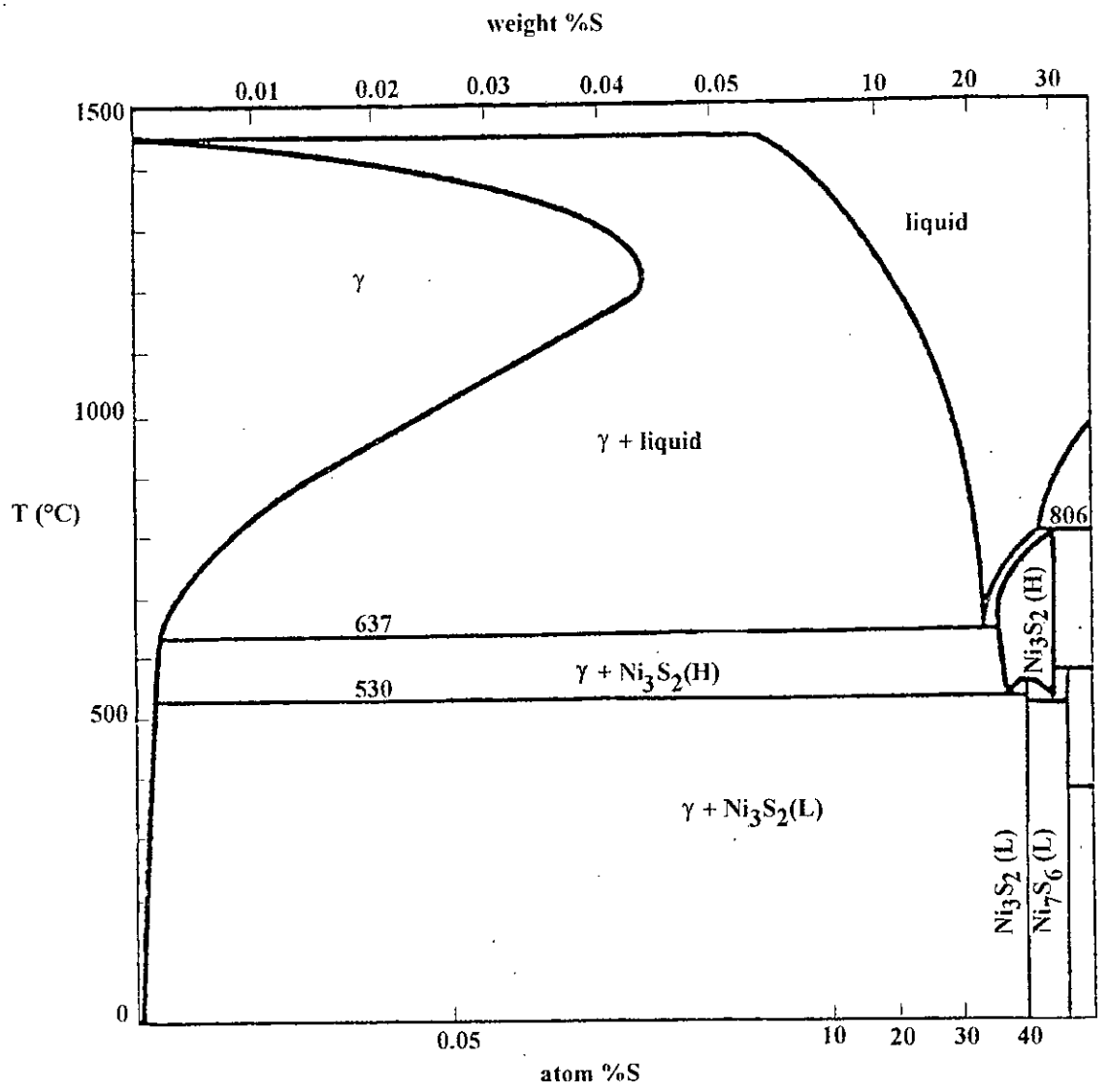

Figure III-1. Phase diagram of the Ni-S system [3]

CHAPTER IV

SEGREGATION TAKING PLACE DURING THE RECOVERY AND RECRYSTALLISATION OF COLD WORKED NICKEL

This chapter is divided into four parts. Part one, besides including an introduction on plastic deformation and on recrystallisation, contains the details on the experimental procedure carried out to study the recovery and recrystallisation of cold worked nickel, as well as the results obtained.

The Auger electron spectrometry, AES, undertaken to study surface segregation accompanying the recovery and recrystallisation is presented in part two. Part three deals with the effect of this segregation on brittleness and intergranular corrosion of the material. A comparison between surface and grain boundary segregation makes the fourth and last part of this chapter.

1. Recovery and recrystallisation of cold worked nickel

1.1 Introduction

1.1.1 Plastic deformation

A pure metal deformed to small plastic strains (usually less than 10%) exhibits a dislocation substructure where individual dislocations are easily identified in transmission electron microscopy. As the strain increases the dislocations rearrange themselves into a more well defined cell structure and at high strains the microstructure is most appropriately characterised as a subgrain structure where the average sub-boundary misorientation is typically 3° or more [97]. This picture applies to métals which deform by slip. Large variations, however, are found between different metals, the important parameter in this context being the stacking fault energy. In high stacking fault f.c.c. metals like aluminium and nickel, cell formation starts at strains less than 10% and at stains larger than 50%, well developed sub boundaries becomes a characteristic structural element [98]. By alloying this picture may of course become drastically distorted. A considerable amount of vacancies is also created during plastic deformation.

A number of mathematical expressions linking the applied stress to the quantity of defects generated by plastic deformation is reported in the literature [99,100]. Bailey [99] puts forward the following relationship which enables the calculation of the dislocation density in a metal under a given stress :

$$\rho = \left(\frac{\sigma}{\alpha . m . b . \mu} \right)^2 ,$$

where μ is Coulomb's modulus (MPa), b is the Burgers vector, m is the Taylor factor (= 3.06 for f.c.c. metals) and α is a constant of the order of **0.5**.

Another relationship put forward by Saada [100] links the number of point defects generated during plastic deformation to the amount of the work done $\sigma d\varepsilon$.

$$dn = \frac{A}{\mu . b^3} . \sigma d\varepsilon \quad ,$$

where n is the number of point defects per unit volume, ε is the true deformation and A is a constant equal to **1/3**.

This expression is, however, not applicable to the entire deformation range, simply because the physical phenomena leading to the creation of point defects are not the same at all stages of the plastic deformation. Merklin [101], for instance, found a saturation in defects corresponding to 80% deformation, whereas Saada's relationship predicts an increase in the density of defects over the entire deformation range.

The defects (vacancies, dislocations) induced in a metal by plastic deformation can have a considerable effect on the diffusion process and hence on the segregation kinetics. It clearly appears , therefore, that the study of the recovery and recrystallisation processes in nickel is more than justified.

1.1.2 Recrystallisation

A material with a microstructure of dislocations, subgrains or grains may lower its energy by the processes of recovery, recrystallisation or grain growth. Until comparatively recently, the distinctions between these processes appeared to be reasonably clear, but the increasing sophistication of the tools for microstructural characterisation now shows that the borderlines between these phenomena are often blurred and newly discovered microstructural changes may not easily fit into well defined categories [102]. It is now known that all three of the above phenomena may occur in the following ways. They may occur heterogeneously throughout the material, such that they may be formally described in terms of nucleation and growth stages. In this case they are described as *discontinuous* processes. Alternatively, recovery, recrystallisation or grain growth may occur uniformly, such that the microstructures evolve

gradually with no identifiable nucleation and growth stages. In this case, the prefix *continuous* is used to describe the phenomena [103].

The micromechanisms operating during the changes occurring in a deformed metal when heated to a temperature below its melting point can be summarised in the following points :

- Defect clustering and annihilation.

-The annihilation of dislocations of opposite signs and the formation of dislocation loops.

-The rearrangement of dislocations to form more stable configurations.

-The absorption of point defects and dislocation loops by moving grain boundaries.

-The reduction in the total grain boundary area.

Once a nucleus is formed, the driving force for the growth of this nucleus is the difference in dislocation density between the nucleus and the surrounding deformed matrix. The grain boundaries of the nuclei which reach a critical size would then advance in the matrix until the driving force for grain boundary (GB) migration becomes too weak to counteract the force opposing this migration. GB migration is a complex phenomenon due to the effect of point defects, impurity atoms and precipitates. The following relationship gives the speed of a moving GB [104] :

$$V = m.F^n ,$$

where m is a term known as the mobility of the boundary, F is the resultant of all the forces acting on the boundary and n is a coefficient which is usually different from 1 (in the case of course where the relationship between V and F is not linear).

The mobility is made up of two terms in the following manner :

$$\frac{1}{m} = \frac{1}{m_I} + \frac{1}{m_{II}} ,$$

where m_I is an intrinsic mobility factor and m_{II} is an impurity concentration dependant factor.

The force F is the resultant of two most important forces :

- The force due to the difference between the dislocation densities on both sides of the boundary which is given by :

$$F_d = \Delta\rho.\mu.b^2 ,$$

where $\mu.b^2$ is the energy of a unit length of dislocation and $\Delta\rho$ is the difference in dislocation density.

- The surface force which is given by :

$$F_s = 2.\frac{\gamma}{r} ,$$

where γ is the interfacial energy and r the mean radius of the grain.

Even though these two forces act simultaneously, F_d is the dominating force as long as the matrix has not recrystallised entirely, i.e. during primary recrystallisation, whereas F_s dominates during grain growth.

The recovery and recrystallisation of a cold worked structure is experimentally investigated using either heavy techniques which are not always easy to carry out such as transmission electron microscopy, or more accessible techniques involving a study of the relationship between the structural defects and a macroscopic quantity such as electrical resistivity or the energy dissipated during the annealing of the cold worked metal. Knowing that the recovery and recrystallisation processes take place through a dissipation in the form of heat of the mechanical energy stored as defects introduced during plastic deformation of the metal, the recording of the heat given off during the annealing of the cold worked metal enables the determination of not only the temperature but also the energy involved at each rcrystallisation stage. This widely used technique is known as differential scanning calorimetry (DSC). Two major drawbacks must, however, be taken into account when using this method :

- the energies involved are so small (~150 $\mu W.g^{-1}$) that a considerable amount (mass) of material is necessary regardless of the precision of the detectors used.
- the recovery and recrystallisation stages may overlap on the temperature scale which sometimes makes the distinction between them impossible. This is not found to happen for nickel for which the vacancy elimination and the recrystallisation stages are clearly separated for true deformations $\varepsilon < 1$.

Clarebrough et al [105] who measured the energy released during recovery of a cold worked nickel of a similar composition as the one studied in this work, using differential scanning calorimetry , found two peaks centred at 120 and 270°C respectively, and a third one centred at a deformation dependant temperature. The first two peaks were attributed to the annihilation of the point defects, whereas the third was attributed to the recrystallisation stage. The electrical resistivity measurements carried out by Sosin et al [106] on the same material lead to similar conclusions.

1.1.2.1 Recrystallisation kinetics

Recrystallisation kinetics are a function of the nucleation rate $\dot{N}$ and the growth rate $\dot{G}$ which often vary from one point to another in the material (spatial variation) and with the transformation time (time variation). Several theories have been proposed to describe recrystallisation kinetics. The most widely used one is the classical theory of Johnson and Mehl [107], Avrami [108] and Kolmogorov [109], commonly referred to as the JMAK theory.

Assuming that the nucleation sites are randomly distributed and that grain growth occurs isotropically at a constant rate, the **JMAK** theory yields the following relationship between the recrystallised fraction, X (the recrystallised area in a given region over the total area of that region), and the annealing time, t :

$$X = 1 - \exp(-kt^n) .$$

Rewriting this equation in a double log form yields the following expression:

$$\ln[-\ln(1-X)] = \ln k + n \ln t$$

This relationship is known as the JMAK equation, where k and n (the JMAK exponent) are constants. In the case of three dimensional nucleation, n is equal to **3** when all the nuclei are formed at zero time (i.e. site saturation nucleation) and equal to **4** when nuclei appear at a constant rate in a non recrystallised material (continuous nucleation). Lower values of n are found in such conditions as growth in less than three dimensions or heterogeneous nucleation on planar or linear defects [110].

Several early experimental investigations on recrystallisation kinetics are reported in the literature [110,111]. Humphreys et al [110] and Rollett et al [111] provide extensive literature surveys on the recrystallisation of a wide variety of materials. The exponent is generally found to be much smaller , typically around 2 and sometimes even less than 1. Humphreys et al [110] conclude that the deviation of recrystallisation kinetics from the ideal linear JMAK plots and the low values of the exponent n found in many experimental investigations are in most cases directly attributable to the inhomogeneity of the microstructure. This leads to a non-random distribution of nucleation sites and stored energy , and to a growth rate which decreases with time. Hutchinson et al [112] found inhomogeneous recrystallisation in cold rolled copper. They showed that the decrease with time of the measured growth rate of the recrystallising grains was entirely due to inhomogeneous distribution of the stored energy. Vandermeer et al [113] also showed that the amount of heat evolved per unit recrystallised volume decreased as recrystallisation proceeded. Although this was interpreted as being due to recovery, inhomogeneous distribution of stored energy may, partially at least, explain these results.

Many investigations on recrystallisation kinetics using computer simulation techniques are reported in the literature [114-116]. Very little detailed experimental work has, however, been recently carried out.

1.1.2.2 The influence of impurity concentration and temperature

The role played by impurity atoms during recrystallisation is translated by their influence on either the mobility or the driving force. The impurity drag theory of Lücke and Detert [117] suggests that the impurity atoms play a retarding role. This theory can be summarised as follows :

- Impurity atoms segregate to the grain boundary which is considered as a low potential energy region ;
- They then form a cloud acting as an obstacle to GB movement, leading to a decrease in the displacement speed.
- At sufficiently high speeds, the boundary can break away from the impurity cloud ,thus regaining a speed comparable to the case of a pure metal.

Figure IV-1 represents the evolution of the GB migration speed with increasing driving force for different impurity concentrations, as given by Cahn [118]. For small concentrations, the V versus F curve approximates the straight line ($V=M.F$) corresponding to a pure metal. As the concentration increases, the curve takes up an S shape with an unstable part in which the speed can switch, in a discontinuous fashion, from one branch of the curve to another. The author did not give any explanation for this behaviour.

The change in temperature leads to a change in the diffusion coefficient as well as in the potential energy. Figures IV-2 represents the evolution of the GB migration speed with temperature for different impurity concentrations, as given by Lücke and Stüve [119]. It can easily be seen that the greater the impurity concentration, the higher the temperature at which the transition from an impurity free GB to a GB loaded with impurities takes place. This is experimentally translated by a decrease in recrystallisation temperature when the purity of the metal is improved.

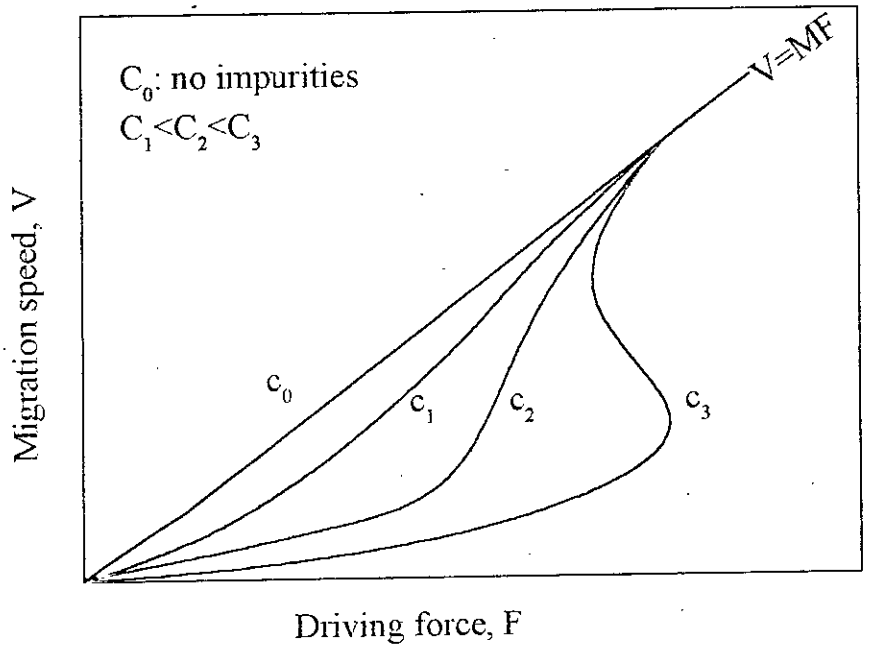

Figure IV-1. Variation of the GB migration speed with driving force for different impurity concentrations [118].

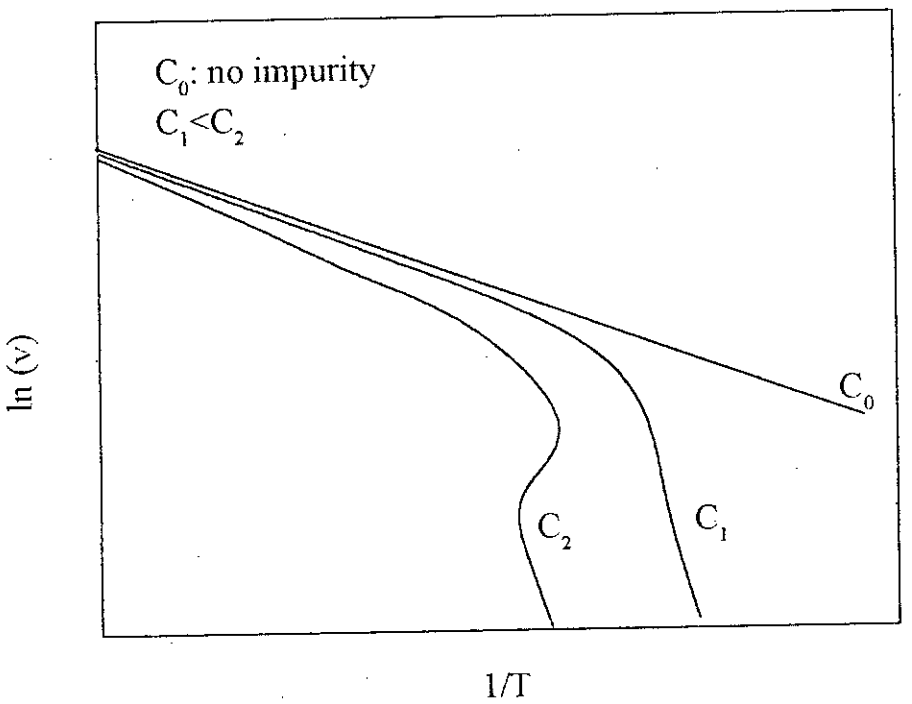

Figure IV-2. Variation of the GB migration speed with temperature for different impurity concentrations [119].

1.2 Experimental work carried out to study the recovery and recrystallisation of nickel

The object of this part of the investigation is to determine the temperatures as well as the kinetics of the different recrystallisation stages.

1.2.1 Differential scanning calorimetry (DSC)

Recovery and recrystallisation of a metal are accompanied by the dissipation, in the form of heat, of the energy stored during cold work in the form of defects. It is therefore possible to follow the different recovery stages of a cold worked metal by measuring the heat given off during an annealing treatment. This is frequently done by differential scanning calorimetry.

1.2.1.1 Specimen preparation

The material is delivered in the form of sheets which are first of all homogenised for 5 hours at 850°C inside evacuated silica capsules. They are then rolled at room temperature, using a conventional laboratory rolling mill. The desired true reductions in thickness are obtained after several passes of less than 0.05 mm each, in order to avoid excessive heating of the material. The true reduction in thickness is defined as:

$$\varepsilon = \ln\left(\frac{e_i}{e_f}\right),$$

where e_i and e_f are the initial and final thicknesses, respectively.

Specimens in the form of rods of prallelipepedic cross sections , are cut from the laminated sheets using a conventional laboratory cutting machine equipped with a low speed diamond wheel. They are lightly polished mechanically down to a reasonable surface finish using 4000 grade polishing paper and then electropolished in a solution of 70% (volume) ethanol, 12% water, 10% 2-butoxyethanol and 8% perchloric acid, in order to remove the layer affected by

mechanical polishing (~5μm) and finally thoroughly cleaned in acetone. A number of these rods making up a mass of $27g \pm 10^{-3}g$ are finally stacked inside the calorimetric cell.

1.2.1.2. Testing equipment and procedure

The equipment used in this work is a SETARAM differential scanning calorimeter , type Calvet HT 1000, schematically represented in figure IV-3. It contains two cells placed in the same calorimetric bloc and mounted in opposition so that the collected potential is proportional to the difference in heat flow between the two cells. The signal originating from the flux meters is amplified using a low voltage amplifier and then collected on a digital recorder together with the temperature of the calorimetric bloc, measured by an S type thermocouple. The numerated signals are subsequently transmitted to a personal computer which also drives a digital regulator controlling the temperature of the calorimetric bloc.

The cold worked specimens go into the working cell and the fully annealed (5 hours at 850°C) specimens, prepared in the same manner as the cold rolled specimens, go into the reference cell.

The first step in the experiment consists of stabilising the thermal flux at the starting temperature. After that, an ascent at a rate of 10°C/h is carried out until the final temperature (650°C) is reached. After a period of stabilisation of about 5 min at this temperature, a free descent is undertaken. A complete new cycle is repeated once the starting temperature is reached in order to determine the base line.

1.2.2 Electrical resistivity measurements

The introduction of vacancies into a metal by any of the known methods such as quenching, irradiation or cold work produces changes in both its physical and mechanical properties. The electrical resistivity is one of the simplest properties

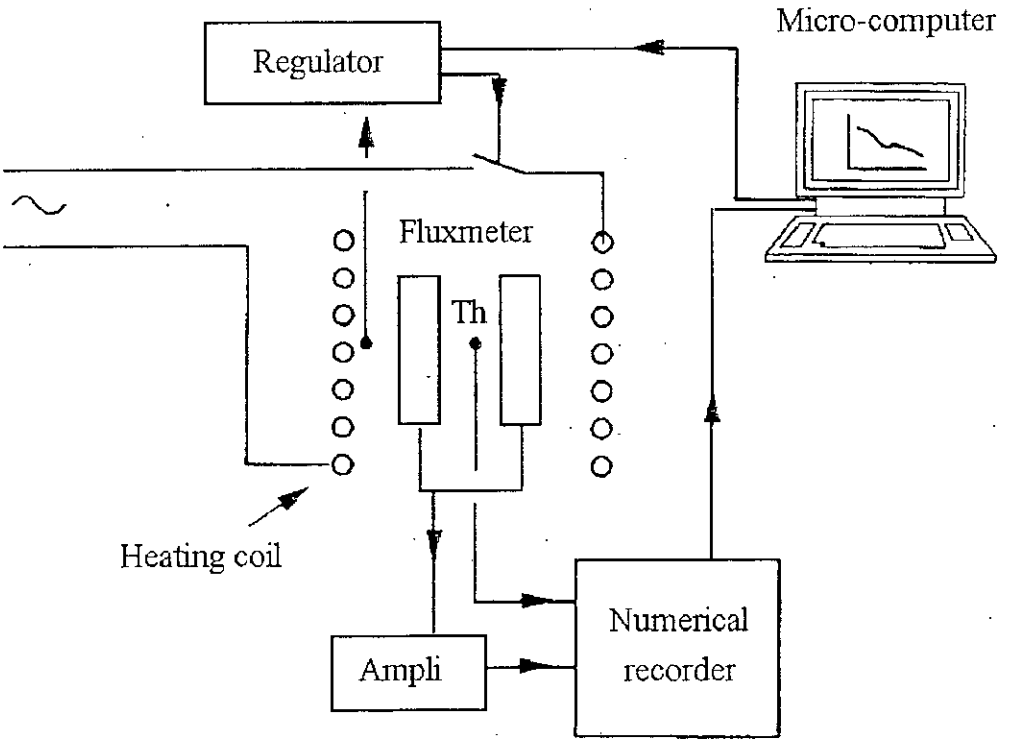

Figure IV-3. Schematic representation of the DSC set-up .

which can be employed to investigate changes in vacancy concentration, and consequently is widely used.

The resistivity of a metal can be separated into a temperature independent portion due to imperfections in the metal, ρ_i, and a temperature dependent portion due to thermal vibrations, ρ_T,:

$$\rho = \rho_i + \rho_T.$$

At low temperatures, thermal vibrations are very low and the resistivity consists almost entirely of ρ_i. This is why measurements are made, whenever possible, at the temperature of liquid helium (4.2 K).

The equipment used is a laboratory made apparatus. A current of 1 mA is sent across a 23 mm x 2 mm x 1.5 mm specimen, cut from sheets homogenised and then cold rolled to various true reductions in thickness as described before . Measurements of the resulting voltage are taken at the temperature of liquid helium (4.2 K), in order to minimise the resistivity due to thermal vibration. In order to avoid the cumbersome task of having to determine accurately the specimen dimensions, the resistivity is also measured at room temperature and the resistivity ratio $\rho_{4.2} / \rho_{293}$ is taken as a significant quantity of the test.

1.2.3 Microhardness testing

The hardness of a material represents a good indication of its microstructural state, and therefore provides a viable means to study recrystallisation.

The equipment used is a microhardness tester mounted on a Neophot 21 optical microscope. In order to obtain a mean representative value, a minimum of 10 measurements spread over different grains were taken on specimens, cut from sheets cold rolled and then heat treated in evacuated silica capsules as described before.

1.2.4 In-situ scanning electron microscopy investigation of recrystallisation

Specimens of 5x1.2x0.5mm^3 were cut from sheets, cold rolled to desired true reductions in thickness ranging from 0.25 to 1.12. They were subsequently mechanically polished down to a 1μm diamond surface finish, and then electropolished as described before.

In-situ isothermal heating was carried out inside a Leica Stereoscan 440 scanning electron microscope. The specimen was spot welded to a thin foil (12mm x 2mm x 16μm) of tantalum which was resistance heated inside the SEM vacuum system. The temperature was measured with a thin (50μm), k type, thermocouple spot welded to the specimen. The temperature of the specimen attained 455°C in less than 2 seconds. The residual pressure inside the SEM vacuum chamber was maintained below 5.10^{-5} Pa The images were obtained using secondary electrons generated at 10 kV EHT, 2.3 nA primary beam current and -100V bias voltage. The specimen was tilted to 20°. Photographs were taken after every 5 minutes or even less when necessary (as is the case for heavy deformations), until the recrystallisation was seen to be complete. The area of recrystallised grains was measured, using an image analysis software named Global Lab Image from Data Translation Incorporation (USA), in order to determine the recrystallised fraction **X** which was equal to the recrystallised area in a chosen region divided by the total area of that region (0.24 mm^2).

The results were presented in the form of curves representing the recrystallised fraction **X** against annealing time for different deformations, and recrystallisation starting and finishing times against true strain. Double log graphs were also plotted and JMAK exponents calculated in the range $0.003<X<0.995$.

1.3 Experimental results and discussions

1.3.1 Recovery and recrystallisation of cold worked nickel

Figure IV-4(a) represents a typical DSC curve. The curves of the first ascent (recrystallisation) and second ascent (base line) are separated. This is due to the change in the specific heat of the material during recrystallisation. The difficulty in determining with accuracy the temperatures of both the beginning and the end of recrystallisation, as well as the area under the peak representing the recovered energy, is clearly evident. The temperature corresponding to the maximum of the peak is therefore taken to be the recrystallisation temperature and the values of the recovered energies are given with an unknown error.

Figure IV-4(b) represents the variation of the recovered energy (mW/g) with annealing temperature for deformations ranging from 0.2 to 0.8, after subtraction of the base line from the curve of figure V-4(a).

Two clearly distinct peaks appear :

- The first one is centred at about 250°C, a temperature which seams to be independent of deformation. This peak is absent for deformations less than 0.3.
- The second peak occurs at a temperature which decreases with increasing deformation.

There is a reasonable qualitative and quantitative agreement between the results obtained in this study and others obtained by Clarebrough et al [105] on a similar grade nickel , as shown by table IV-1. The first peak is attributed by these authors to vacancy annihilation and the second to recrystallisation.

	Heat flux ($mJ.g^{-1}$)	
	Clarebrough [105] (ε=0.53)	This study (ε=0.6)
Recovery (200-350°C)	234	186
Recrystallisation	840	772

Table IV-1. DSC results obtained in comparable conditions.

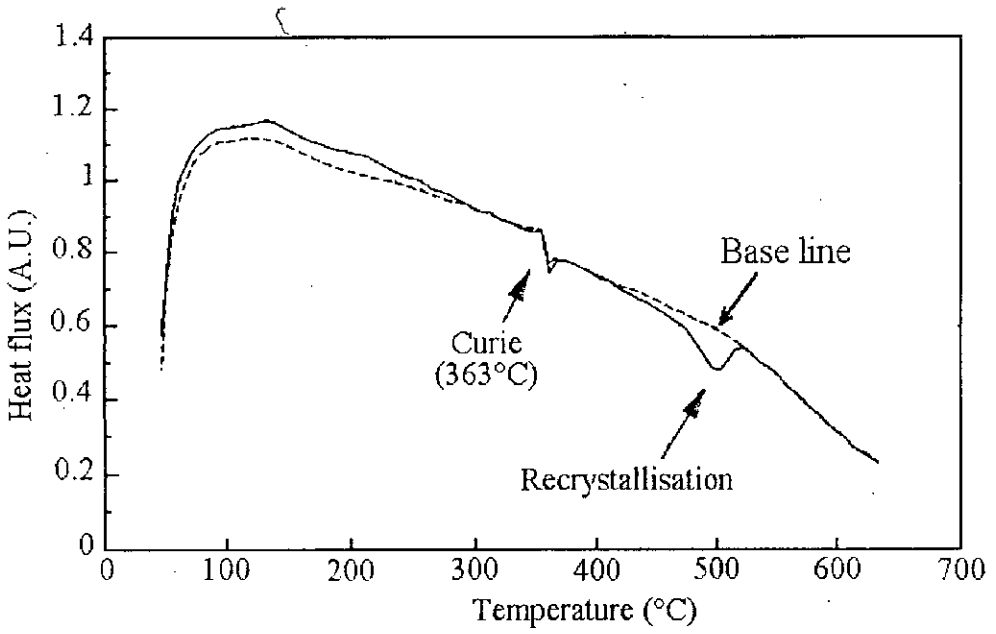

Figure IV-4(a) DSC curve for nickel cold rolled to 0.2 true strain.

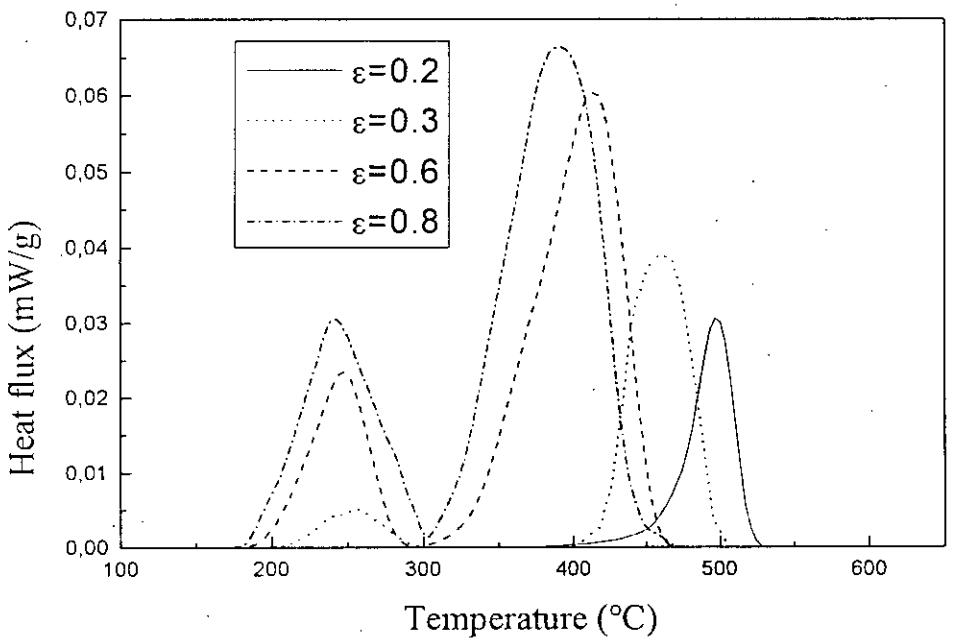

Figure IV-4(b). Variation of heat flow with temperature for nickel, cold rolled to true strains of 0.2,0.3, 0.6 and 0.8.

In order to confirm the role of vacancies in the first peak, DSC runs were carried out on specimens that were annealed for 1 hour at 1200°C and then quenched in cold water. A comparison between the energy recovery curve of the quenched material which shows only one peak centred at around 250°C and that of the cold worked material , represented together in figure IV-5, yields further evidence of the role of vacancies in the first peak since they are the only defects existing in supersaturation in the quenched material. The vacancy concentration is calculated by dividing the recovered energy corresponding to the first peak by the energy of formation of a vacancy (1.58 eV [136]). The values obtained are given in table IV-2, together with concentrations calculated from Saada's relationship [100](see section 1.1.1).

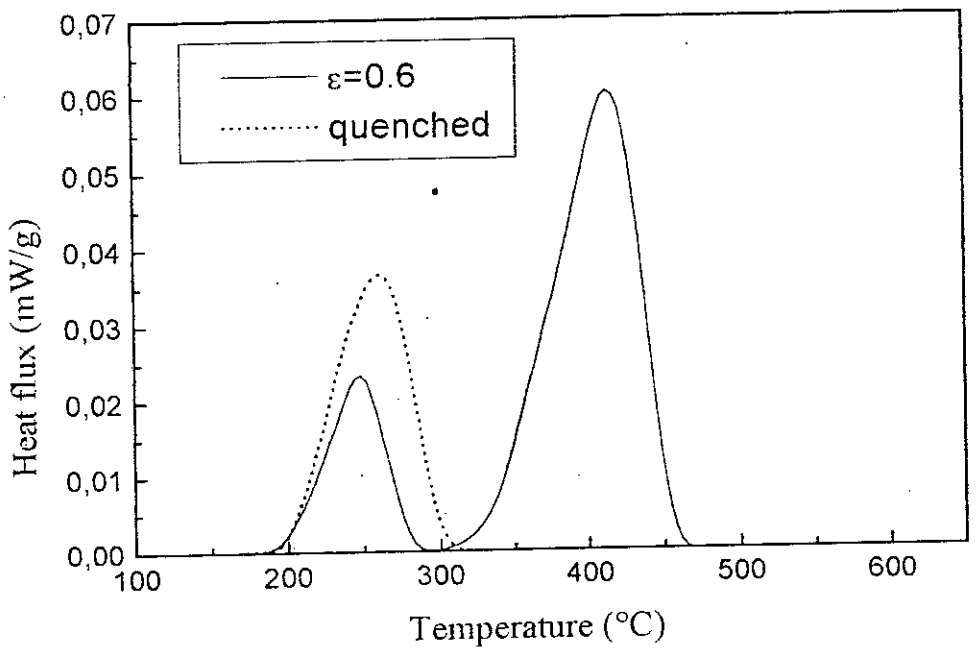

Figure IV-5. Heat flow against temperature for a nickel specimen quenched from 1200°C, and another specimen cold rolled to 0.6 true strain.

Deformation	0.2	0.3	0.4	0.6	0.8
Recovered energy ($mJ.g^{-1}$)	-	44	124	186	310
Vacancy concentration (ppm)	-	17	48	72	119
Calculated concentration (ppm) [100]	100	200	400	700	1100

Table IV-2. Vacancy concentrations calculated for different true strains.

Although in both cases the vacancy concentration increases linearly with deformation, as shown on figure IV-6, the values determined from Saada's relationship are nearly 10 times those determined from DSC measurements. This indicates that nearly 90% of the vacancies are annihilated during cold work.

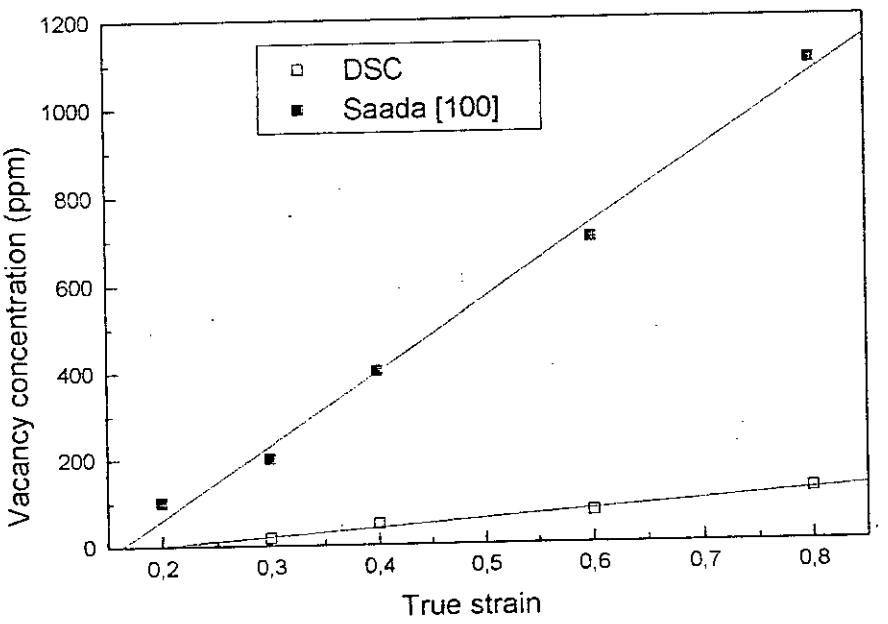

Figure IV-6. Variation of vacancy concentration with true strain, calculated from the first peak of the DSC curves of figure V-4(b) and from Saada's expression.

The micrographs of figure IV-7 yield further evidence of the role of vacancies in the first peak. Figure IV-7(a) does not show any new grains for the material deformed to 0.2 true strain and then heat treated for 3 hours at 315°C, whereas recrystallization is unambiguously apparent for the same material heat treated for the same period at 455°C, figure IV-7(b). The in-situ investigation carried out inside the SEM confirmed that no recrystallisation occurs at 315°C (figure IV-7(c)) in contrast to 455°C where the formation of new, strain free, grains is clearly evident , figure IV-7(d).

The data related to the recrystallisation stage, corresponding to the second peak on the DSC plot, is summarised in table IV-3.

True strain	0.2	0.3	0.4	0.6	0.8
Stress as obtained from the plasticity function (Mpa)	370	430	500	590	650
Recovered energy (area under the peak), $mJ.g^{-1}$	210	300	390	772	903
Temperature at the maximum of the peak (°C)	500	460	445	415	395
Dislocation density calculated from DSC (10^{10} cm^{-2})	2.6	3.8	4.9	9.7	11
Theoretical dislocation density [99]($10^{10}cm^{-2}$)	1.6	2.2	2.8	3.8	4.8

Table IV-3. Data obtained from the second DSC peak.

The excess in electrical resistivity due to cold work, which is also an indication of the quantity of defects introduced into the material, is depicted in figure IV-8 where the resistivity ratio , $R = \rho_{4.2} / \rho_{293}$, is plotted against deformation. ρ_{293} and $\rho_{4.2}$ represent the electrical resistivities of the deformed material measured at 293K and 4.2 K (liquid helium) respectively. The curve exhibits a tendency towards stabilisation at high deformation ratios. This tendency is equally exhibited by the curve of figure IV-9 representing the dislocation density as calculated from the second peak of the DSC curves (table IV-3), assuming that

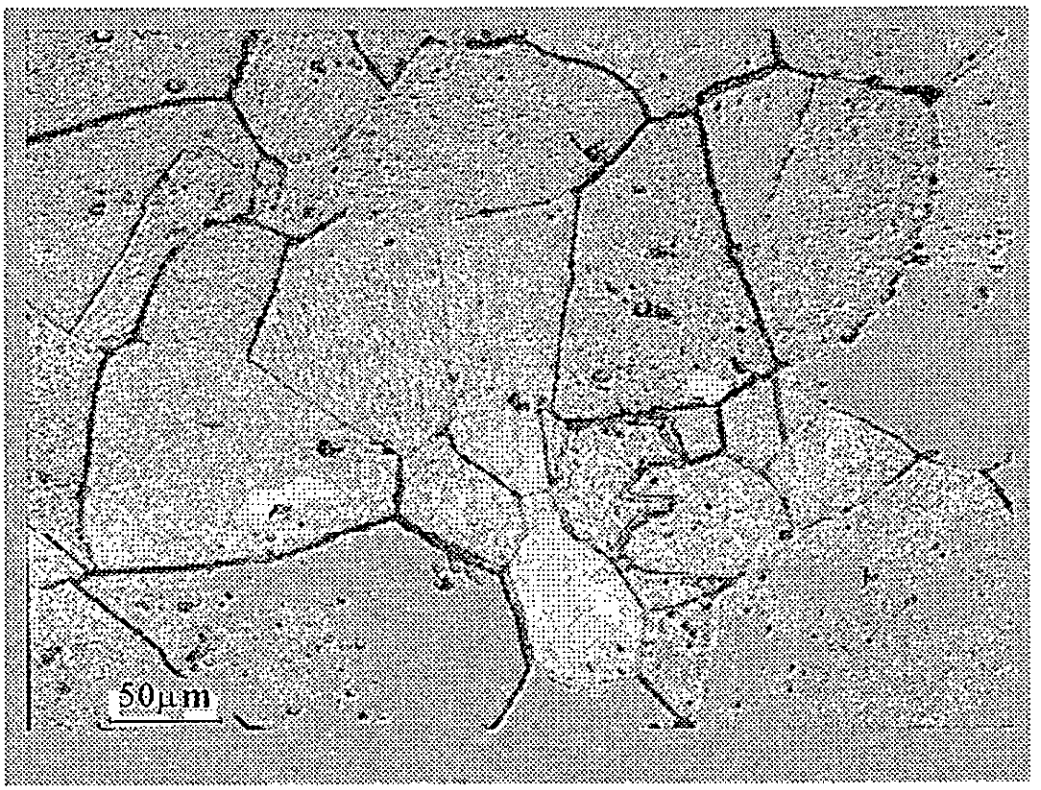

(a)

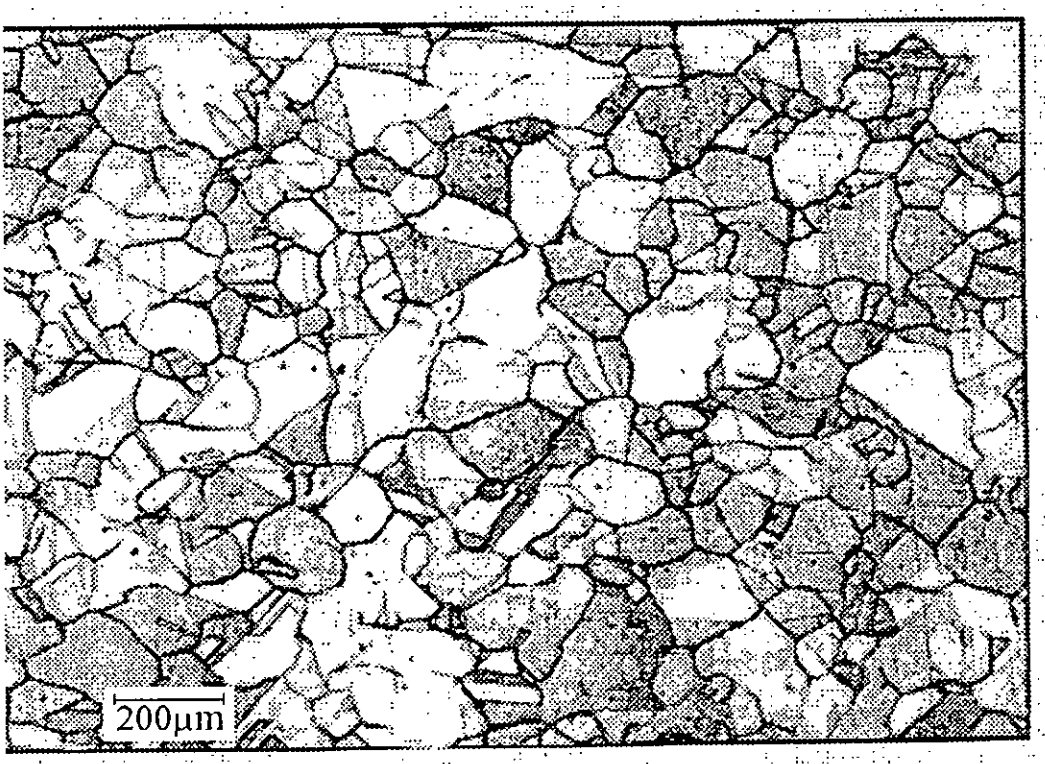

(b)

Figure IV-7. Optical micrographs showing the evolution of the microstructure in the course of heat treatment of the material deformed to 0.2 true strain . (a) 3 hours at 315°C, the microstructure remains unchanged, (b) 3 hours at 455°C, the microstructure is nearly entirely recrystallised.

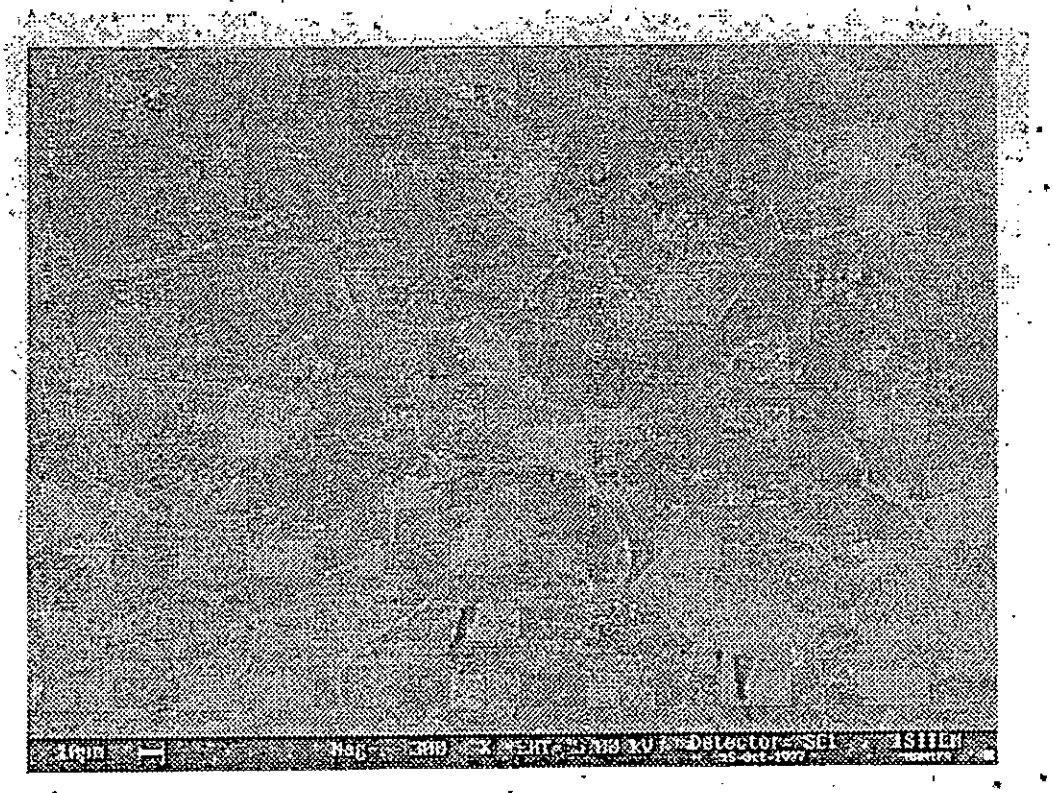

(c)

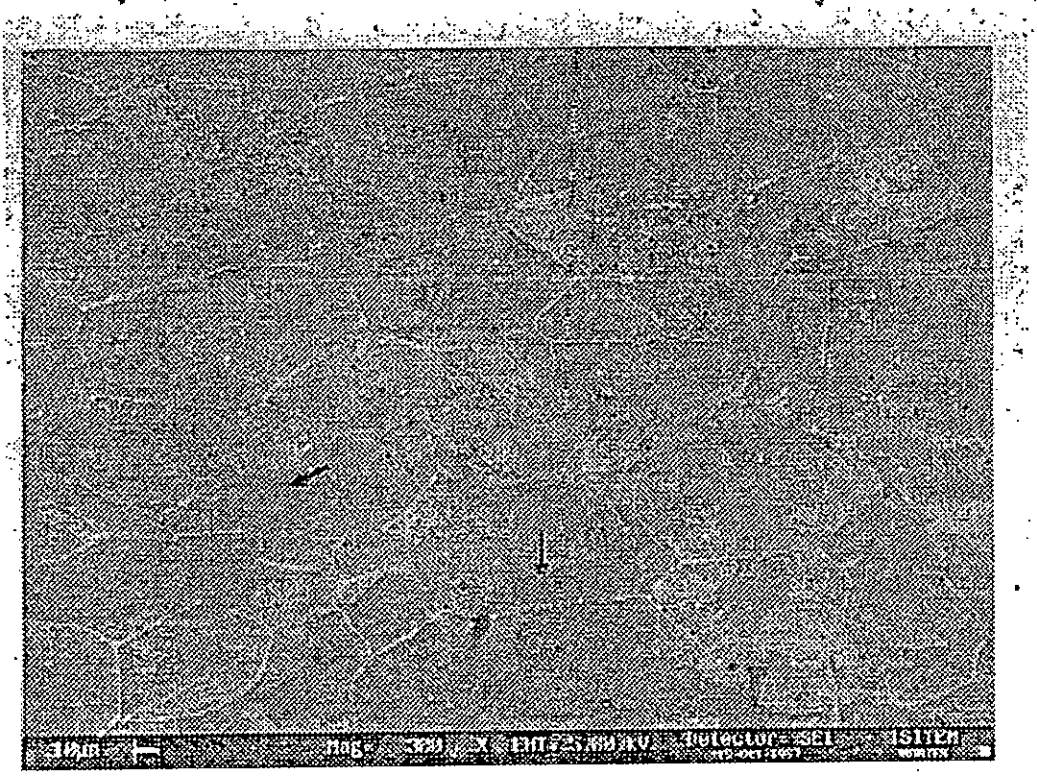

(d)

Fig IV-7. (followed). SEM micrograph showing: (c) the absence of new grains after 3 hours at 315°C. (d) Developing new grains (arrows) just over 1 hour at 455°C.

all the energy recovered during recrystallization is due to dislocation annihilation and taking the energy of a dislocation line to be equal to $7x10^{-11}$ $J.cm^{-1}$ [105]. This gives an indication that the excess in resistivity bears a closer relation to dislocations than to vacancies introduced during cold work.

The dislocation density is also calculated using Bailey's expression [99] (see section 1.1.1). The theoretically calculated dislocation density, which is also plotted in figure IV-9, increases linearly with true strain. The reason behind the discrepancy between the theoretical and the experimentally calculated dislocation densities is likely due to the generally made observation that theoretical expressions such as Bailey's do not take into consideration all the physical phenomena leading to defect creation and annihilation. Not being able to determine the exerted effort in the cold rolling operations, the stress used in Bailey's expression was obtained from the plasticity function of the material, as determined from tensile tests which do not faithfully reproduce the cold rolling conditions (see annex I for details on the determination of the plasticity function) . Another reason lies in the fact that the dislocation density calculated from DSC measurements may be overestimated. It is very likely that a certain degree of dislocation rearrangement may have occurred during the recovery stage corresponding to the first peak.

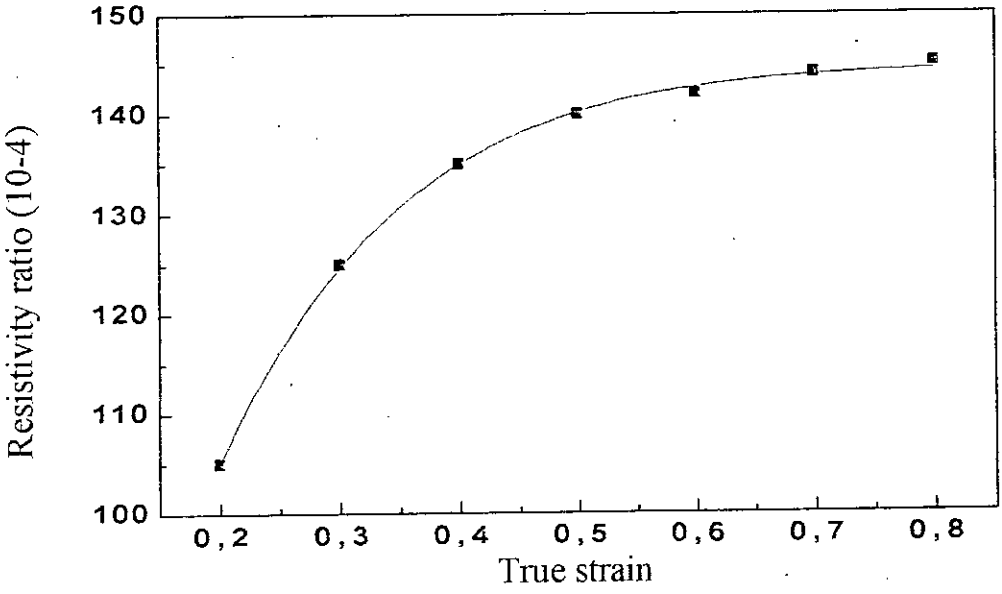

Figure IV-8. Variation of resistivity ratio with true strain

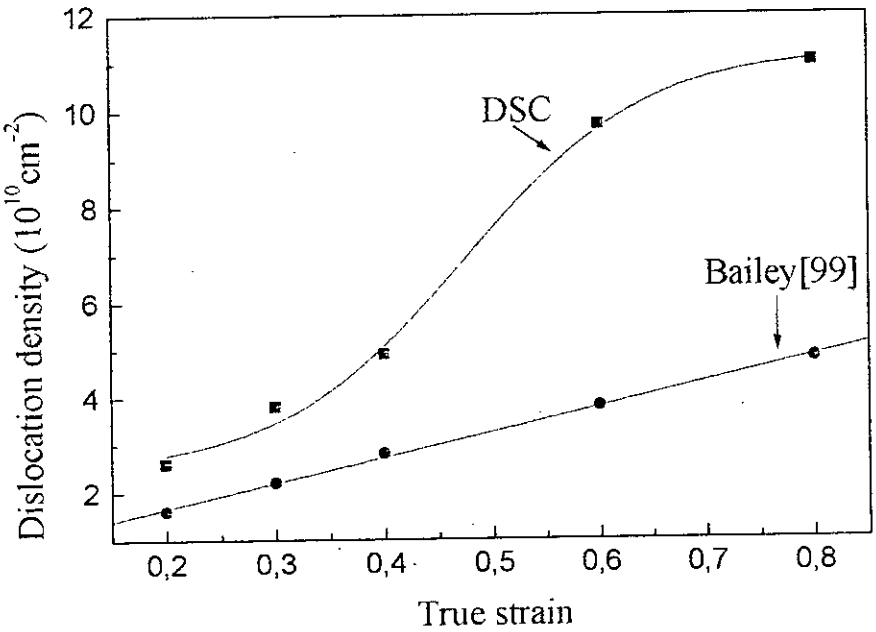

Figure IV-9. Variation of dislocation density with true strain, calculated from the second peak of the DSC curves of figureIV-4(b) and from Bailey's expression.

1.3.2 Recrystallisation kinetics

Recrystallisation kinetics during isothermal heat treatments at 455°C, are studied by microhardness testing and in-situ SEM observations. The study is carried out at one single temperature in order to minimise the experimental parameters so that a comparison between the obtained kinetics is made considerably easier. The temperature of 455°C is chosen because, as it can be easily seen from the DSC results, besides being a recrystallisation temperature for all strains greater than 0.2, it is situated at the offset of the recrystallisation peak corresponding to 0.2 strain.

The results of the microhardness tests indicate that for deformations less than 0.2, the microhardness does not undergo any significant change after a heat treatment of 2 hours at 455°C. For deformations greater than 0.5, the microhardness is fully recovered in less than 5 minutes, a time insufficient to allow the recrystallisation kinetics to be followed with this technique. The value of 0.2 is thus confirmed to be the critical deformation for the onset of recrystallisation at 455°C. Figure IV-10, represents the hardness against annealing time at 455°C for 0.2, 0.3 and 0.5 true strains.

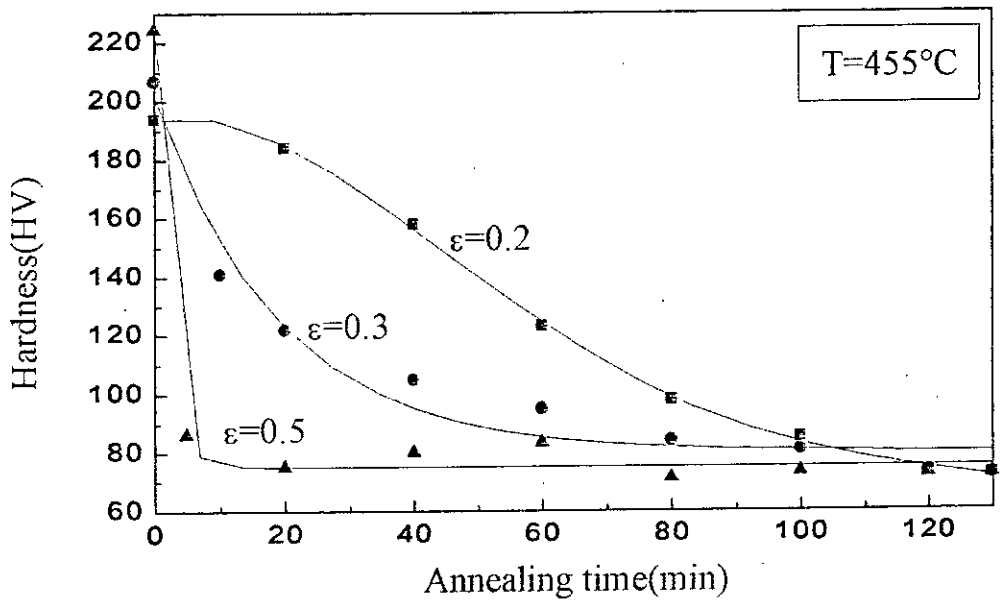

Figure IV-10. Microhardness against annealing time at 455°C for nickel cold rolled to 0.2, 0.3 and 0.5 true strains.

The fraction of recrystallised area, as determined from in-situ SEM observations, is plotted against annealing time at 455°C for deformations ranging from 0.25 to 1.12 (figure IV-11) . The curves have a sigmoidal form and exhibit an incubation time which decreases with increasing deformation. They also show that as the deformation ratio increases, the times for the starting and finishing of recrystallisation are shifted towards shorter times as more clearly seen on figure IV-12.

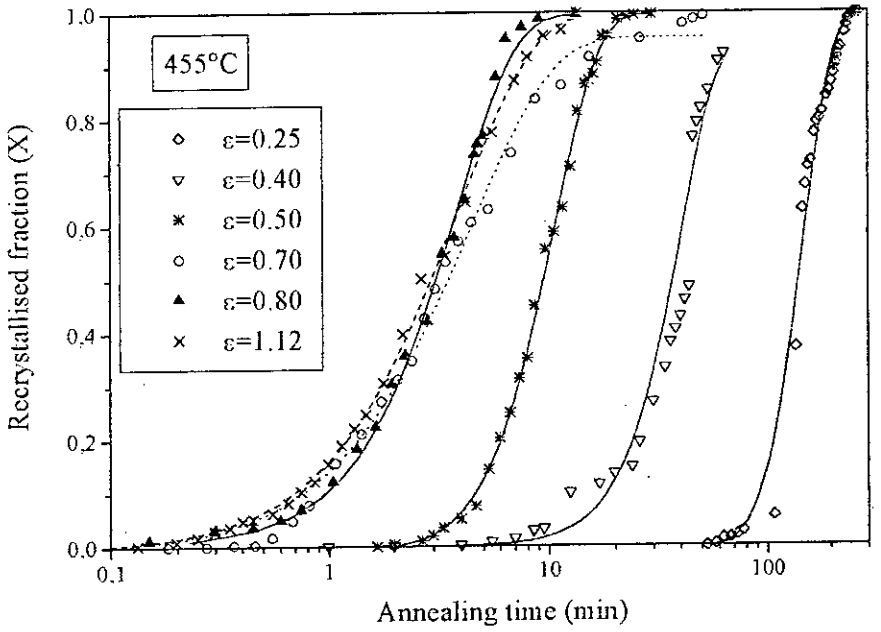

Figure IV-11. Fraction of recrystallised area versus annealing time at 455°C for nickel cold rolled to true strains ranging from 0.25 to 1.12.

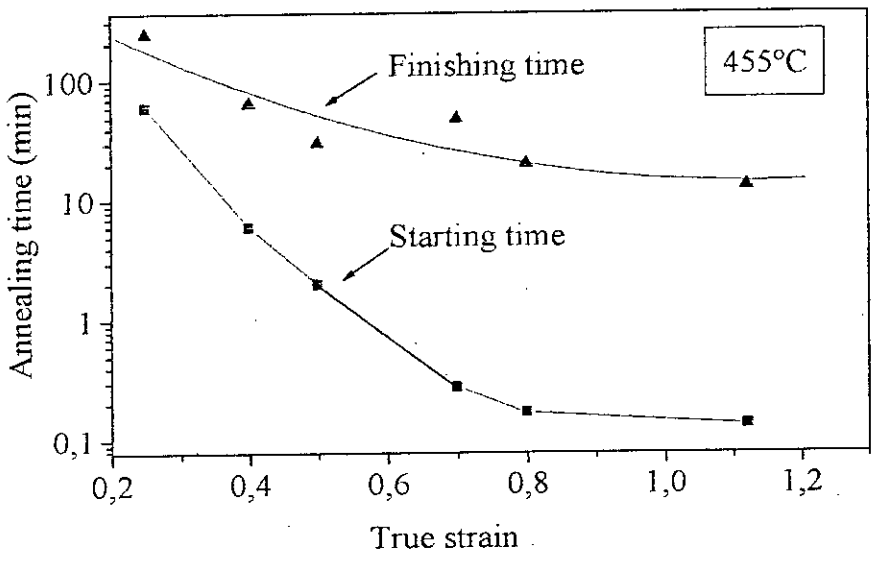

Figure IV-12. Recrystallisation starting and finishing times at 455°C for nickel cold rolled to true strains ranging from 0.25 to 1.12.

Figure IV-13 represents double log plots in accordance with the JMAK equation.

The relationship is fairly linear although some deviation is seen at low and high values of recrystallised fraction. A least squares regression yields a value of the JMAK exponent , n, between **1.36** and **2.12**. Table IV-4 summarises the main data deduced from the JMAK plots.

ε	0.25	0.4	0.5	0.7	0.8	1.12
n	2.12	2.01	1.83	1.46	1.48	1.36
k	$5.36\text{x}10^{-5}$	$4.7\text{x}10^{-4}$	$1.56\text{x}10^{-2}$	$5.7\text{x}10^{-2}$	$1.35\text{x}10^{-1}$	$1.64\text{x}10^{-1}$
t_s	60 min	6 min	2 min	16 s	10 s	8 s
t_f	4 h	64 min	30 min	48 min	20 min	13 min

Table IV-4. Data deduced from the JMAK type plots. t_s and t_f are the recrystallisation starting and finishing times respectively.

Figure IV-14 represents plots of n and k against true strain. With increasing true strain, n decreases and k increases to reach stabilisation at high strains. Coupled with the experimental observation that recrystallisation is much quicker at high strains, this clearly indicates that the constant k bears a stronger relationship with recrystallisation kinetics than does the exponent n.

The JMAK theory suggests, however, that n should lie between **3** and **4**. This deviation from the experimentally found values is accounted for by the fact that the in-situ SEM observations do not confirm the assumptions underlying the JMAK theory. These assumptions stipulate that the nucleation sites are randomly distributed and that the rates of both the nucleation and growth remain constant throughout the entire recrystallisation process.

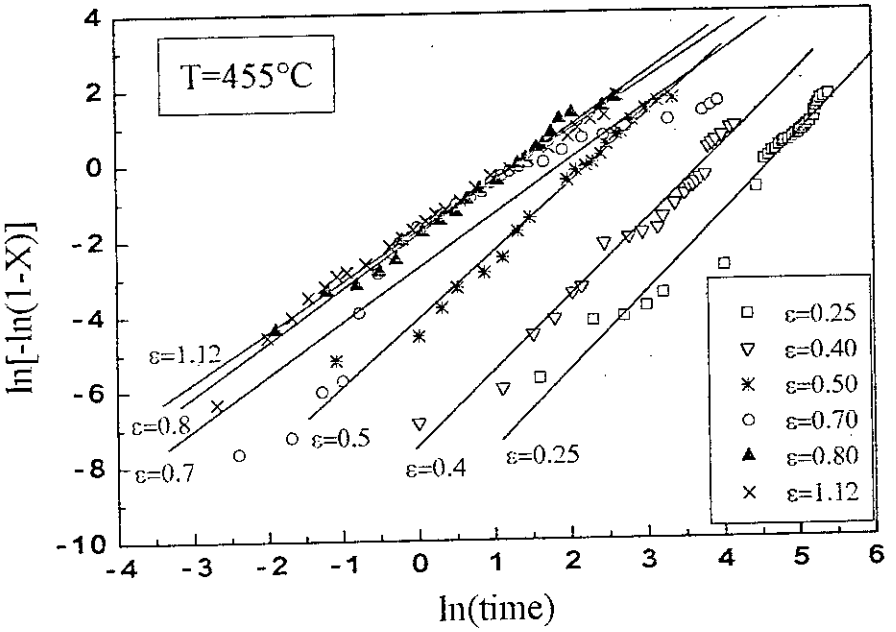

Figure IV-13. Double log plots , derived from the JMAK equation, for nickel cold rolled to various true strains and then heat treated at 455°C.

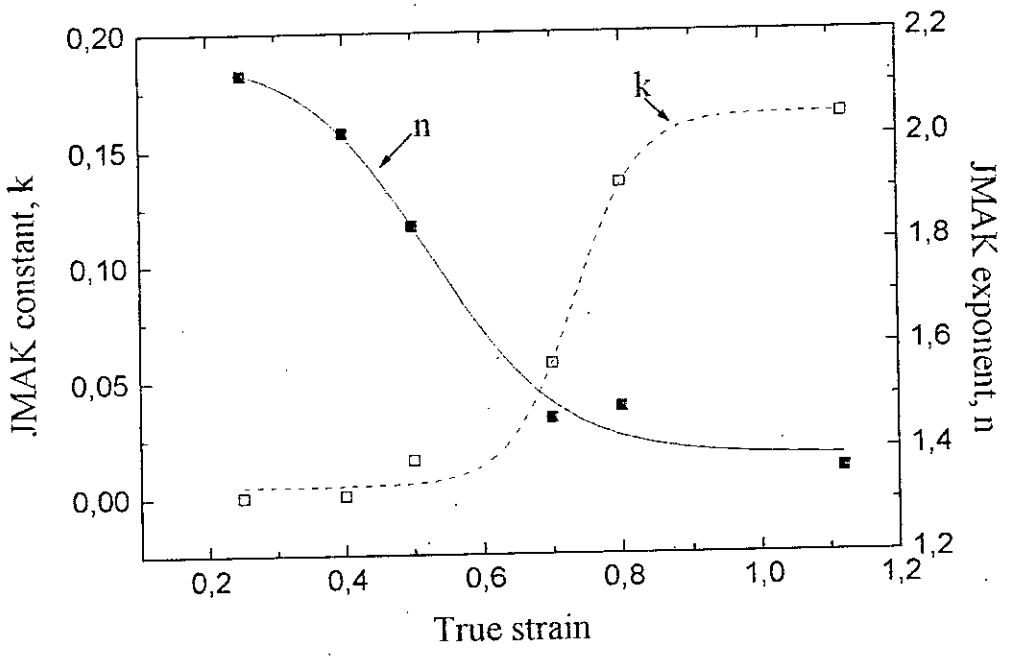

Figure IV-14. JMAK constant, k, and exponent, n, against true strain.

The in-situ investigation carried out in this work shows that nucleation sites are not randomly distributed, as shown by micrographs (a) to (d) of figure IV-15. Nucleation is rather seen to occur at preferential sites such as grain boundaries. Evidence for non-random site distribution in several other materials is reported in the literature [110]. On the scale of a single grain, nucleation of recrystallisation is found to be inhomogeneous. On a larger scale, it is found that not all grains recrystallise at the same rate, and that it is this large scale heterogeneity, attributed to texture effects, that is frequently the main cause of inhomogeneous recrystallisation.

In a recent paper, Marthinsen and Ryum [120] have shown by numerical simulation that the variation of the JMAK exponent is closely related to the spacial distribution of nucleation sites. If the nucleation sites are randomly distributed, the exponent remains equal to 2 during the entire transformation, but in the case of a very high density of GB sites, the exponent decreases to 1 during recrystallisation and then increases again to reach the value of 2 at the end of the evolution process.

2. Surface segregation of sulphur taking place during the annealing of cold worked nickel: Auger electron spectrometry

2.1 Introduction

Auger electron spectroscopy is widely used in surface analysis for its good in-depth resolution. The mean free path of Auger electrons does not exceed a few tens of Angstroms, which limits the analysis to a depth of the order of two to three atomic layers. The detection limit although not very high (≈1%), remains sufficient for our purpose.

It is generally accepted that the concentration of an element X in a matrix is proportional to the ratio of its peak height to that of the matrix ,i.e. :

$$C_X = \alpha.\left(\frac{H_X}{H_{mat}}\right),$$

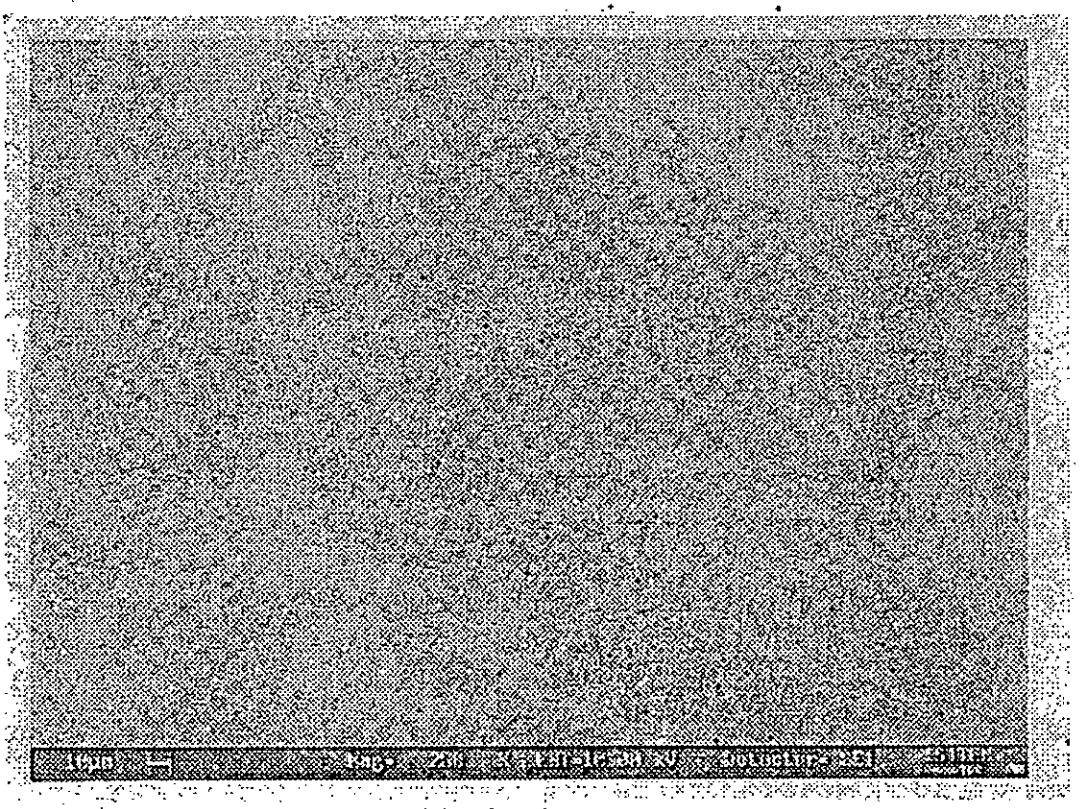

(a) 10 min

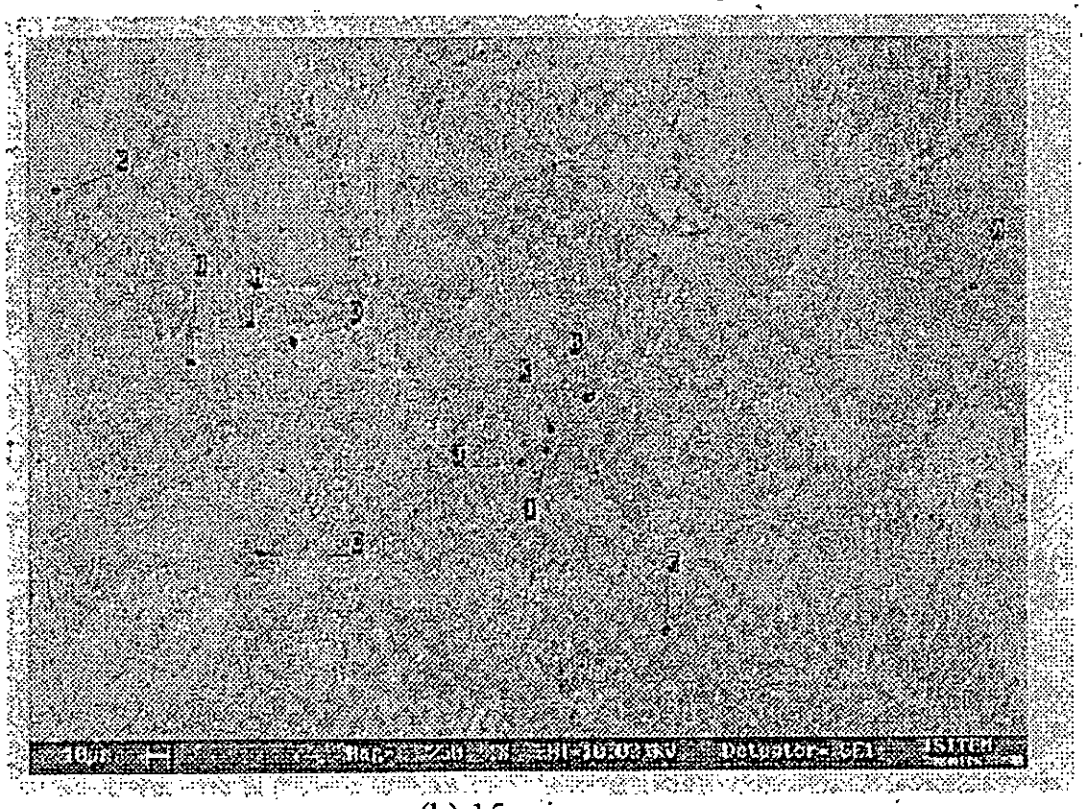

(b) 15 min

Figure IV-15. SEM micrographs showing the in-situ observation of the evolution of the microstructure at 455°C. Material deformed to 0.4 true strain.

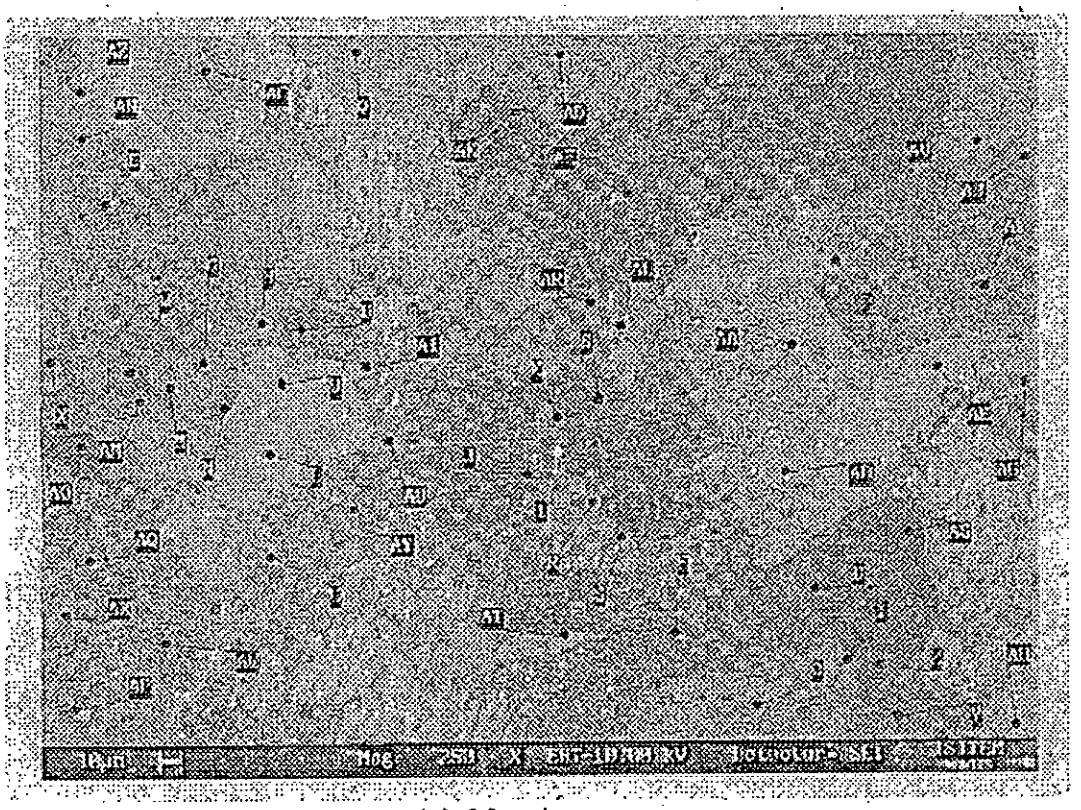

(c) 30 min

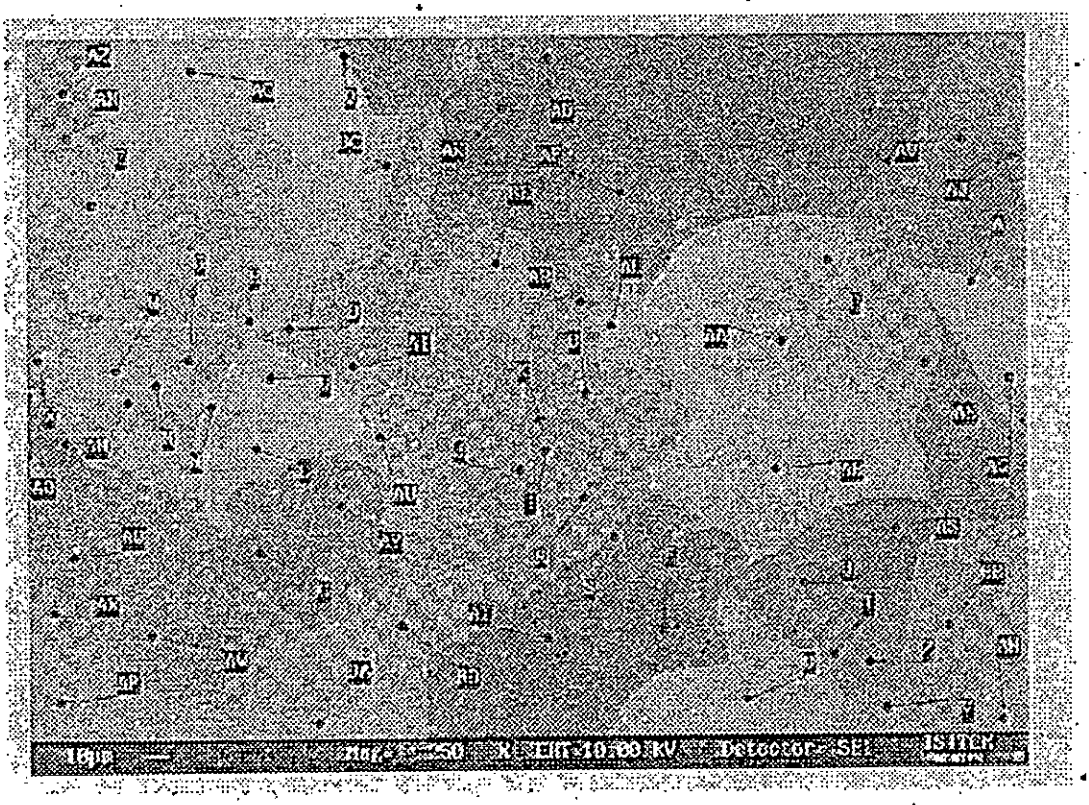

(d) 50 min

Figure IV-15 (followed). The letters indicate the recrystallizing grains.

where α is the calibration constant for element X and was found elsewhere [55] to be equal to **0.48**.

In the case of sulphur on the surface of polycrystalline nickel, the expression above becomes :

$$C_S = \alpha.10.54x10^{14}.\frac{H_S}{H_{Ni}} \quad (\text{at .cm}^{-2}),$$

where 10.54 x 10^{14} at.cm^{-2} is the density of a polycrystalline nickel surface [121]

2.2 Equipment and procedure

The equipment used is a cylindrical mirror analyser RIBER ISA, model ASC 2000. The pressure inside the analysis chamber was maintained at a level below 5.10^{-8} Pa. The primary beam energy and current were set at E_p=3 keV and I_p=0.1μA,respectively. The spatial resolution in these conditions is of the order of 1μm. The spectra are recorded in differential mode, d[E.N(E)]/d(E), between 0 and 900 eV with a modulation amplitude of 3eV (peak to peak).

Before their introduction into the Auger spectrometer, the specimens are prepared in the following manner :

The specimens are cut from sheets which were annealed (5 hours at 850°C) inside evacuated silica capsules and then cold rolled in small passes (< 0.05 mm each) in order to avoid excessive heating. The final dimensions of the specimen are obtained by mechanical polishing using abrasive paper and then a diamond suspension (down to 1μm surface finish). The specimen is then electropolished as described before and then finally washed in an acetone bath. The specimens, 5mm x 1mm x 0.5mm, are spot welded on a resistance heated tantalum ribbon. The temperature of the specimen is measured by a chromel-alumel (type K) thermocouple made of two 50μm diameter wires, also spot welded on the specimen. Temperature regulation is provided by a low thermal inertia digital regulator, enabling a stabilisation of a temperature of 500°C in less than 30 seconds.

Isothermal runs are carried out at the two temperatures of 315°C (corresponding to the end of the vacancy elimination peak on the DSC curve) in order to study the effect of the vacancy elimination stage on segregation, and 455°C in order to study the role of the recrystallisation stage.

2.3 Results and discussion

Nickel displays several Auger peaks as shown on figure IV-16. The high energy peak (848eV) is found to be more appropriate to use for the determination of the peak heights ratios for the following reasons :

- The high energy peak is found to be superimposed on a flat continuous background , which leads to a better accuracy in the determination of the ratio peak/background.
- The high energy peak is much less affected by the presence of a segregated layer.

An apparent diffusion coefficient can be calculated, using McLean's model, provided the segregation kinetics present a linear part with respect to $\sqrt{t}$. The model yields the following expression :

$$C_S = \frac{2.C_V.\sqrt{D^*.t}}{\sqrt{\pi}} ,$$

which can be rewritten as follows :

$$D^* = P^2.\frac{\pi}{4.C_V^2} ,$$

where C_s is given in at.cm^{-2} and C_V in at.cm^{-3}. **P** is the slope of the C_s versus $\sqrt{t}$ curve.

2.3.1 Segregation at 315°C (in the absence of recrystallisation)

The Auger runs carried out at this temperature on materials deformed to less than 0.15 were interrupted after 48 hours owing to the fact that no segregation was seen to take place. Figure IV-17 shows curves representing the ratio of the

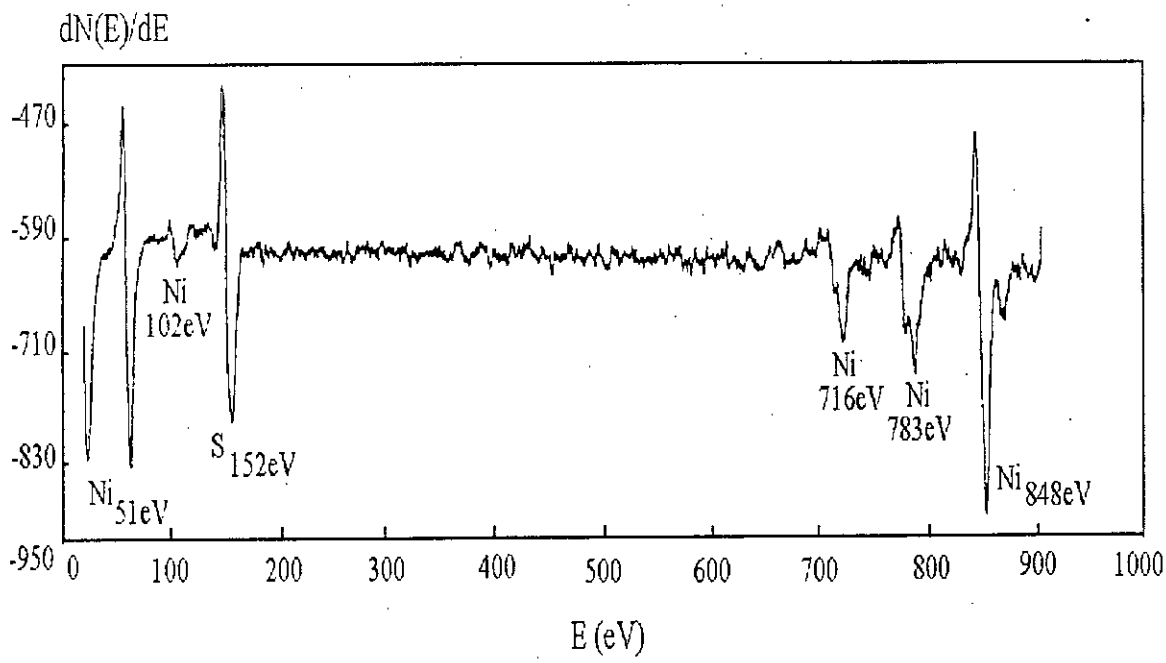

Figure IV-16. A typical Auger spectrum for nickel.

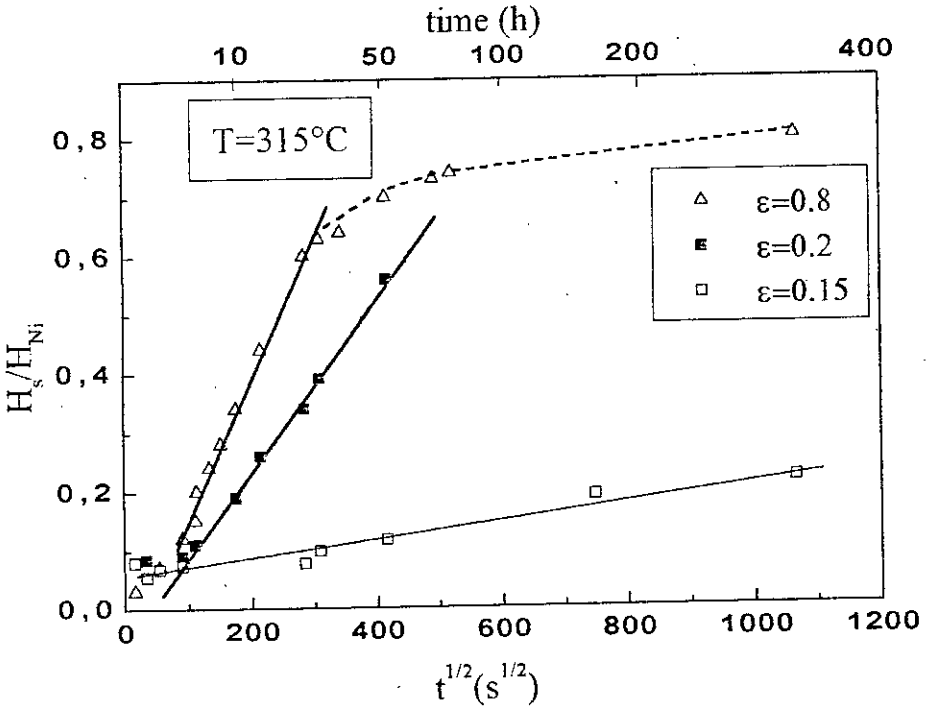

Figure IV-17. Auger peak height ratios against $\sqrt{t}$ at 315°C for nickel deformed to 0.15, 0.2 and 0.8 true strains .

sulphur peak height, H_{S152}, to that of nickel, H_{Ni848}, obtained from Auger spectra, against the square root of annealing time at 315°C, $\sqrt{t}$, for materials deformed to 0.15, 0.2 and 0.8 true strains. The curves show that the greater the strain, the quicker the steady state beyond which no segregation occurs is attained. Apparent diffusion coefficients deduced from the linear parts of the curves are given in table IV-5. The values are 5 to 8 orders of magnitude greater than the one obtained from the work of Wang and Grabke [122] on segregation in equilibrium conditions. This considerable increase in segregation kinetics can be related to the increase in diffusion short circuits resulting from cold work, as already shown by figures IV-6 and IV-9.

Deformation	0.15	0.2	0.25	0.4	0.8
Slope ($s^{-1/2}$)	$0.12x10^{-3}$	$1.57x10^{-3}$	$1.68x10^{-3}$	$2.42x10^{-3}$	$2.84x10^{-3}$
D^* ($cm^2.s^{-1}$)	$3.4x10^{-13}$	$5.9x10^{-11}$	$6.7x10^{-11}$	$1.4x10^{-10}$	$1.9x10^{-10}$
$D_{W\&G}$ ($cm^2.s^{-1}$) for equilibrium segregation	$1.6x10^{-18}$ [122]				

Table IV-5 . Apparent diffusion coefficients at 315°C.

Figure IV-18 represents the variation of the diffusion coefficient with strain. It appears that the segregation kinetics, which start by increasing with increasing strain, tend towards a stable value. This is in good agreement with the electrical resistivity against strain curve (figure IV-8), bringing more evidence of the undeniable relationship existing between segregation kinetics and defect concentration in the material. Another evidence for this relationship is given by the findings that segregation kinetics are only appreciable for deformations equal to or greater than 0.2 and that the first calorimetric peak, corresponding to vacancy annihilation, only appears for deformations greater than 0.2, which indicates that segregation accelerates only when the vacancy concentration becomes appreciable.

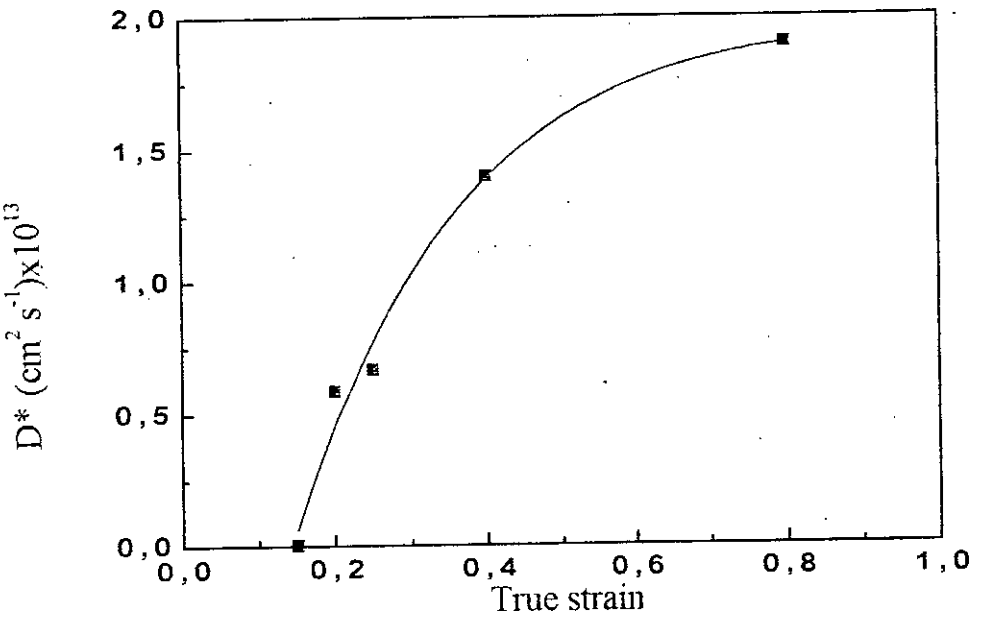

Figure IV-18. Apparent diffusion coefficient at 315°C versus true strain.

2.3.2 Segregation at 455°C (during and after recrystallisation)

Figure IV-19 shows Auger peak height ratios against annealing time at 455°C, for true strains of 0.2, 0.5 and 1.2. They exhibit, like the ones obtained at 315°C, a linear part with respect to $\sqrt{t}$ enabling an apparent diffusion coefficient to be calculated, table IV-6. The values are six to seven orders of magnitude greater than the one obtained from the work of Grabke on equilibrium segregation [122]. The diffusion coefficient, when plotted against true strain, increases up to 0.2 true strain and then falls off to finally reach a stable value, as shown in figure IV-20.

ε	Slope ($s^{-½}$)	D^* ($cm^2.s^{-1}$)	$D_{W\&G}$ ($cm^2.s^{-1}$) [122]	$D^*/D_{W\&G}$
0.1	0.032	1.44×10^{-8}	3.10×10^{-15}	5×10^6
0.15	0.048	5.5×10^{-8}	3.10×10^{-15}	18×10^6
0.2	0.061	8.89×10^{-8}	3.10×10^{-15}	28×10^6
0.25	0.039	3.6×10^{-8}	3.10×10^{-15}	12×10^6
0.3	0.034	2.71×10^{-8}	3.10×10^{-15}	8×10^6
0.5	0.027	1.8×10^{-8}	3.10×10^{-15}	6×10^6
0.8	0.035	2.94×10^{-8}	3.10×10^{-15}	9×10^6
1.2	0.032	2.41×10^{-8}	3.10×10^{-15}	8×10^6

Table IV-6 . Apparent diffusion coefficients at 455°C.

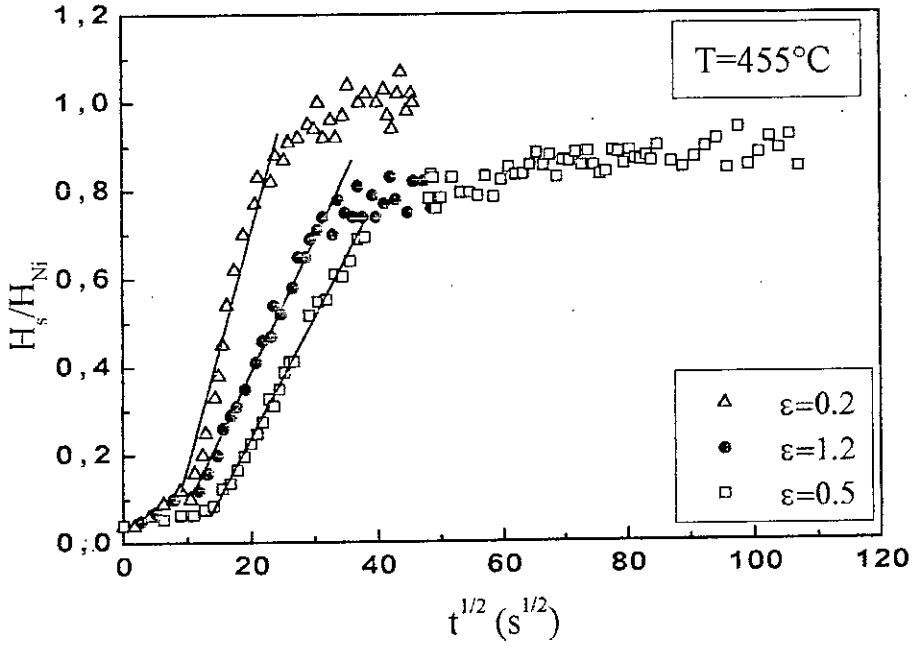

Figure IV-19. Auger peak height ratios against √t at 455°C for nickel deformed to 0.2, 0.5 and 1.2 true strains .

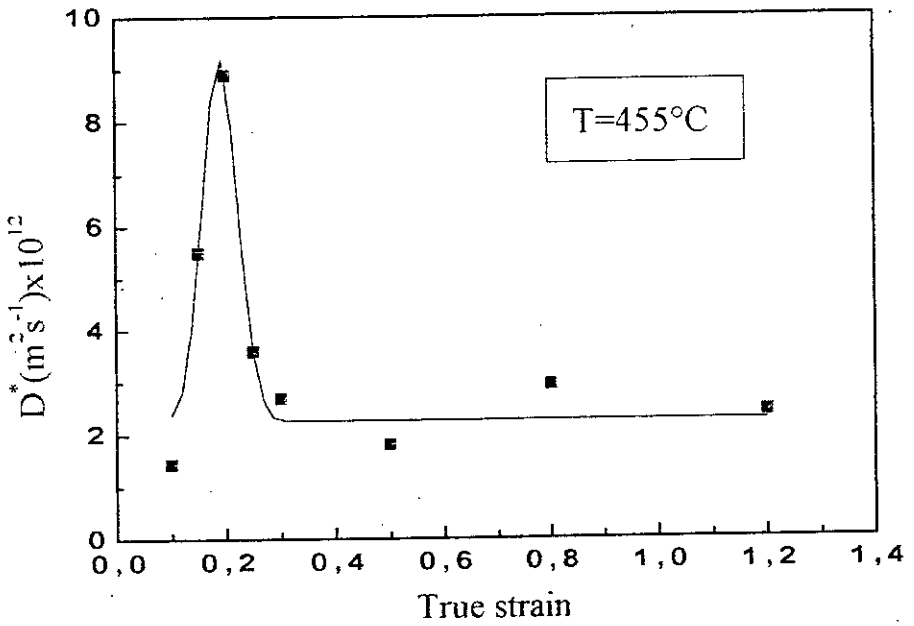

Figure IV-20. Apparent diffusion coefficient at 455°C, versus true strain.

A comparison between recrystallisation kinetics and segregation kinetics enables us to account for the observed behaviour.

Figure IV-21 shows surface segregation and recrystallization kinetics represented together on the same plots for materials deformed to 0.25, 0.5, 0.8 and 1.12 true strains. Both kinetics follow sigmoidal type tendencies, indicating a similarity in behaviour between recrystallization and superficial sulphur segregation.

For the material deformed to 0.25 true strain, surface saturation with sulphur is achieved after 40 minutes of treatment, well before the beginning of recrystallization which only starts after 60 minutes of treatment. This clearly indicates that segregation for this material takes place in the deformed material and during the recovery process. It also indicates that the acceleration of segregation is not due to recrystallization but rather due to the acceleration of diffusivity in the deformed material. Segregation takes place in this stage by diffusion of sulphur in the bulk and through the dislocation pipes and grain boundaries.

Recrystallization of the material deformed to 0.5, starts within 2 minutes of heat treatment and finishes after about 30 minutes. Saturation on the other hand is achieved after 40 minutes. Segregation therefore takes place mostly in a recrystallizing material. This behaviour can be explained in terms of the impurity drag theory first put forward by Cahn [118] and further developed by Lucke and Stüve [119]. This theory considers two cases :

- Under certain conditions of temperature, driving force and impurity concentration, the moving grain boundary drags with it the impurity atmosphere.
- If these conditions are not gathered, the GB would break away from the impurity atmosphere and continues its movement with an even greater speed.

This deformation seems to satisfy the conditions necessary for the sulphur atoms to be dragged with the moving grain boundaries in the course of recrystallization, and the acceleration of segregation kinetics in this case can

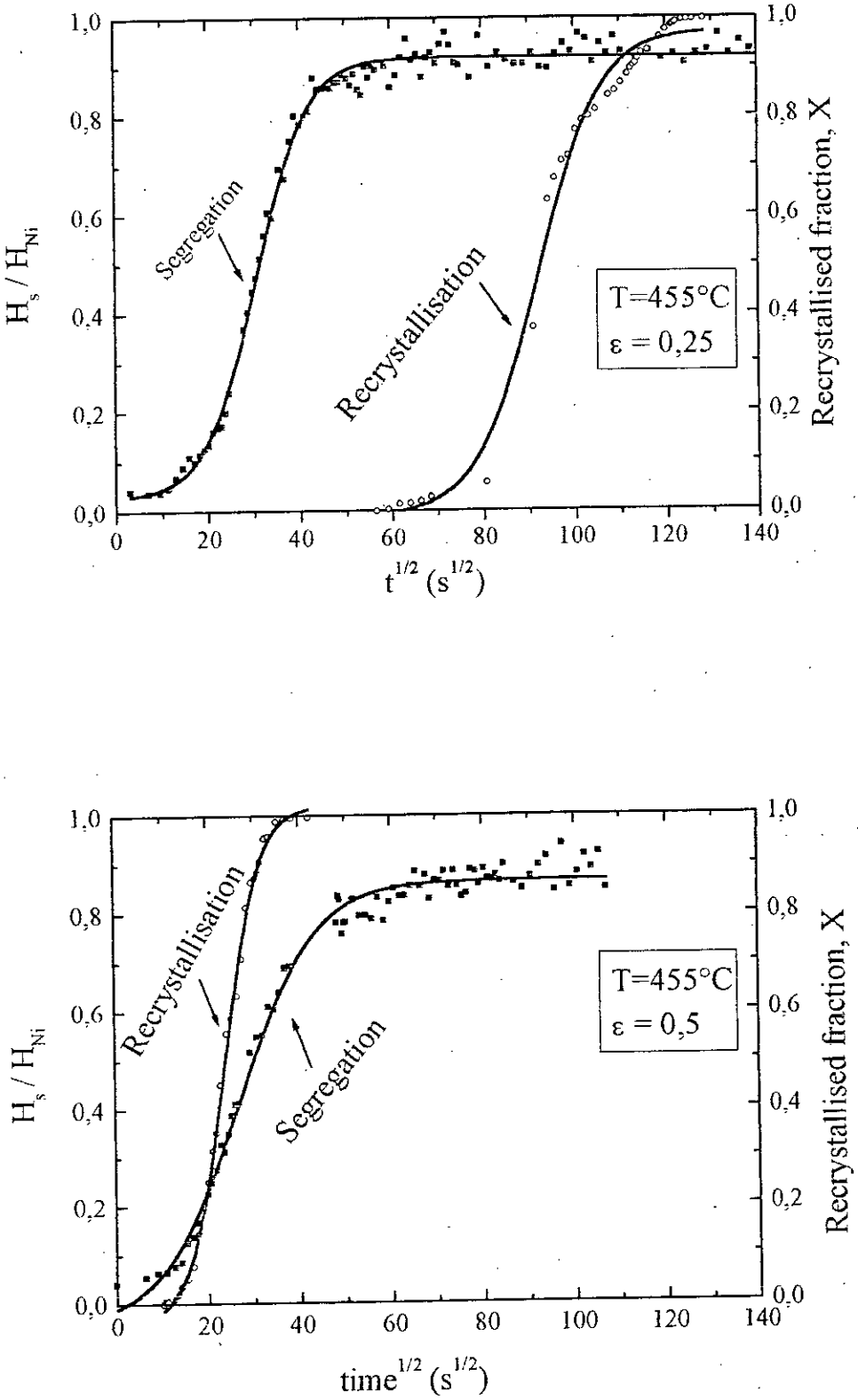

Figure IV-21. Segregation and recrystallisation kinetics for 0.25 and 0.5 true strains.

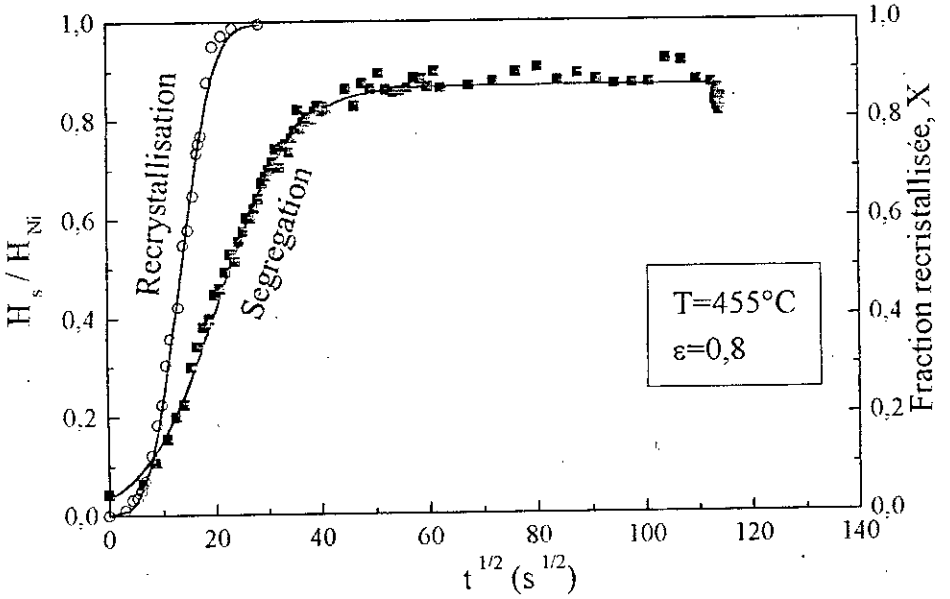

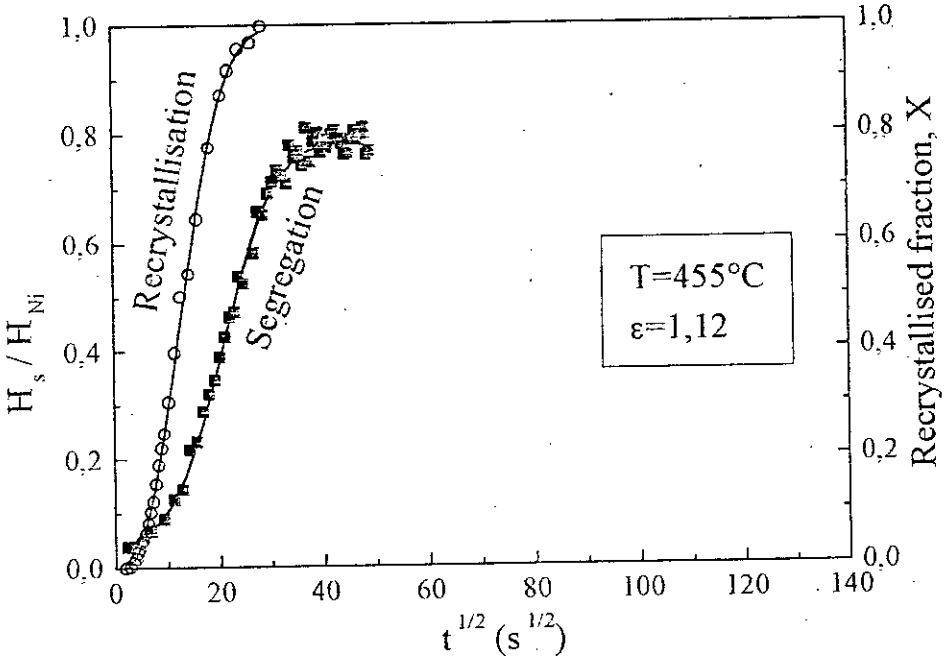

Figure IV-21.(followed). Segregation and recrystallisation kinetics for 0.8 and 1.12 true strains.

therefore be rightly attributed to recrystallization. Some segregation does however take place in a recrystallized material. The mechanism that can be suggested here involves diffusion from sulphur rich regions near the surface and/or impurity drag during the post-recrystallization grain growth stage.

The materials deformed to 0.8 and 1.12 show similar behaviours in that recrystallization starts within seconds and ends after about 13 minutes for both of them. Surfaces saturation with sulphur also takes the same time for both of them, i.e. 26 minutes, indicating that in this case saturation lags behind recrystallization. The rapidity of recrystallization in comparison with surface saturation can be explained again by the impurity drag mechanism. The driving force for recrystallization, a function of the stored energy and hence the amount of deformation, is so high that in the progress of recrystallization, the moving grain boundaries manage to break away from the sulphur atmospheres leaving them behind.

A comparison between the diffusion coefficients (Table IV-6) of the lightly deformed materials ($\varepsilon \leq 0.25$), where segregation takes place almost exclusively in a deformed matrix, and of the heavily deformed materials, where segregation occurs in a recrystallizing or recrystallized matrix, enables us to conclude that segregation kinetics are higher during recovery than during recrystallization. Although no in-situ investigation was performed on the material deformed to 0.2 true strain, its recrystallization kinetics can be predicted from the work done on other deformations. Since recrystallization starting time increases with decreasing deformation (table IV-4), it is fairly reasonable to think that recrystallization would start for this deformation after an incubation time greater than 60 minutes (t_s for 0.25 true strain), and segregation would therefore occur during recovery and not during recrystallization, thus accounting for the high diffusion coefficient observed for this strain.

3. Effect of sulphur segregation on the intergranular properties of nickel

3.1 Intergranular brittleness

3.1.1. Introduction

Direct Auger analysis of grain boundaries is a rather cumbersome technique, as already mentioned. Besides requiring the presence of hydrogen in order to fracture the specimen inside the Auger chamber, the method suffers from another problem : some grain boundaries may inevitably resist failure if segregation is insufficient and are therefore not analysed. Furthermore, since every GB is quite unique, a great number of GB's has to be analysed in order to obtain a meaningful mean value. For all these reasons, tensile testing is undertaken as an indirect method of investigating intergranular segregation and its effect on both the strength and ductility of the material .

Before going into the details of the experiments, some pertinent definitions concerning *ductility* and *brittleness* are given in the following .

The terms *ductile* and *brittle* are commonly taken as self descriptive, but care should be taken in using them. They are used to indicate the general plasticity at fracture, relying on such quantities as the elongation at fracture (ductility) and the presence of necking to indicate whether the material is ductile or brittle. A difficulty here is to decide how much ductility is required to place the material in a ductile class ; there is no common value to be used. More pertinent to our interests is that the terms ductile and brittle are used to distinguish ductile and brittle fracture, both the macroscopic and microscopic aspects. The void coalescence mechanism (on a microscopic scale) of crack formation involves plastic deformation by slip. Thus this mechanism is referred to as ductile. However, it is possible to have cracks form and fracture occur by this mechanism, yet the material shows no obvious or little macroscopic plastic deformation. On this basis, the fracture would be categorised as brittle. In our case the terms *ductile* and *brittle* are used to describe the macroscopic aspects of fracture and are not based on the microscopic mechanisms. The following

characteristics, adapted from VanderVoort [123], are used to distinguish between the two types of fracture.

Ductile fracture :

- A relatively large amount of plastic deformation precedes the fracture.
- Shear lips are observed at the fracture termination areas.
- The fracture surface is fibrous or has a matte or silky texture.
- The cross section at the fracture is reduced by necking.

Brittle fracture

- Little or no visible plastic deformation precedes the fracture.
- The fracture is flat and perpendicular to the surface of the specimen.
- The fracture surface appears granular or crystalline and is highly reflective to light. Facets are also observed.

Another preoccupation stems from the consideration that the main object of the work is not only to determine whether impurity segregation *embrittles* the material but also whether this *embrittlement* is intergranular as a consequence of sulphur segregation to grain boundaries. It is worth emphasising that not all intergranular failures are *brittle*.

Taking all the above considerations into account, the elongation at fracture is taken as a measure of ductility . Observations of the fracture surfaces under the SEM are undertaken to determine whether the fracture was effectively intergranular.

3.1.2. Experimental procedure

The tensile specimens of form and dimensions shown in figure IV-22 were machined from strips taken from sheets cold rolled to the desired thickness. These dimensions were imposed by the limitation in the quantity of material available. This limitation also necessitated great care to be taken when preparing the specimens. All sides of the gauge length were mechanically polished down

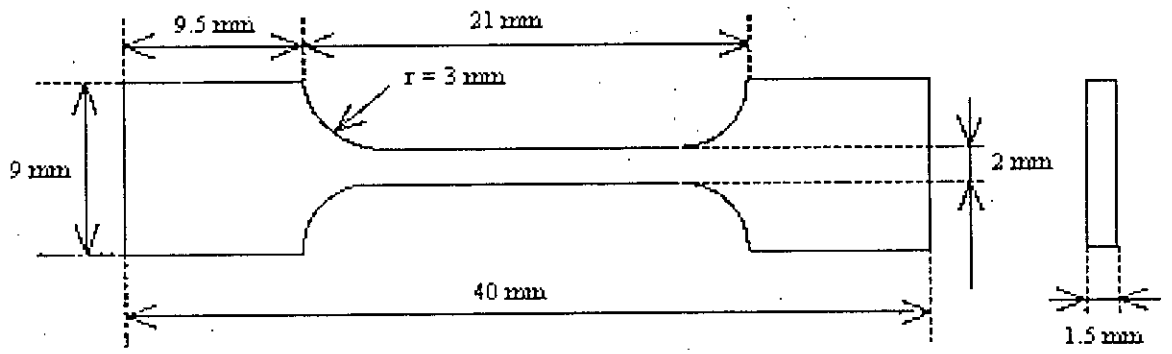

Figure IV-22. Tensile test specimen

to 3mm surface finish in order to avoid cracks initiators. The specimens were then heat treated at 455°C inside sealed silica capsules under a residual atmosphere of argon. The cross head speed of the tensile machine, a Heckert FU-1000 e, was set at 2 $mm.min^{-1}$. The specimens were kept submerged in liquid nitrogen during the entire test duration.

The results are given in the form of curves representing the variation of the stress and the strain to failure with recrystallisation time, each point of the graph being due to only one test piece because of the limitation in the quantity of the material. Because of the same limitation, only the strain of 0.2 was studied.

3.1.3. Results and discussion

The results of tensile tests performed on the material deformed to 0.2 true strain and then heat treated at 315°C indicate that no appreciable embrittlement is achieved even after 350 hours of annealing. This may be attributed to the existence of two competing mechanisms : recovery which tends to increase the deformation capacity of the metal and intergranular segregation which tends to reduce it. The diffusion kinetics at this temperature are so slow that they do not lead to any homogeneous distribution of sulphur in grain boundaries.

Figures IV-23 represents the variation of both the stress and the strain to failure with annealing time at 455°C for the material deformed to 0.2 true strain. This strain was chosen because of the high apparent diffusion coefficient associated with it. The absence of the great scatter, usually inherent to this kind of test, indicates the importance of the specimen preparation stage and the efficiency of the polishing procedure. The stress to failure decreases with annealing time and the material loses more than 75% of its deformation capacity after just 70 minutes of annealing.

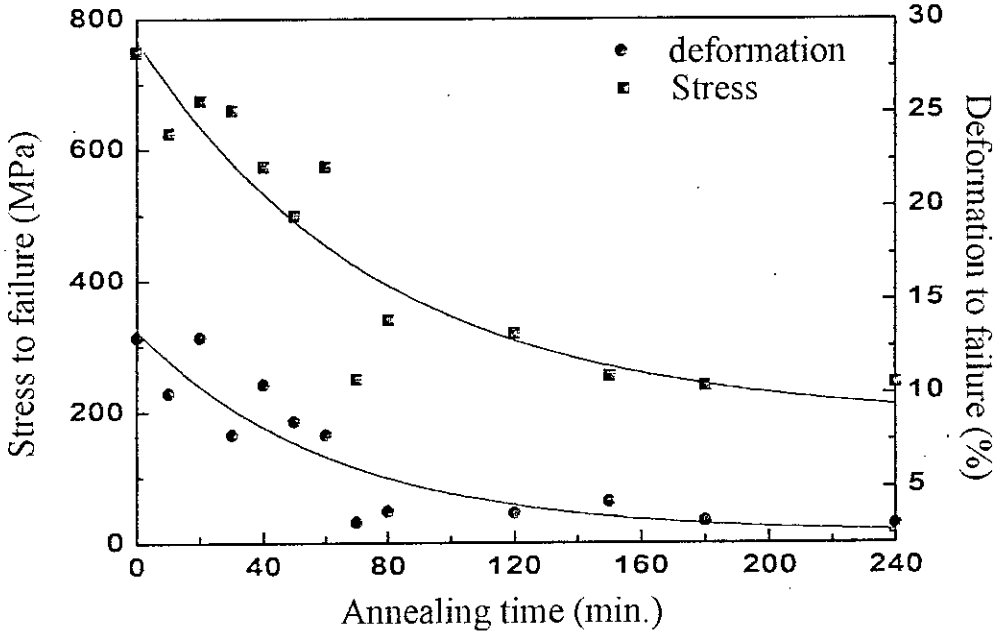

Figure IV-23. Variation of stress and strain to failure with annealing time for the material deformed to 0.2 true strain and then heat treated at 455°C.

The micrographs of figure IV-24 show mostly intergranular brittle fracture for the material cold rolled to 0.2 true strain and then heat treated for 70 min at 455°C in contrast to a mixed type fracture for the same material heat treated at the same temperature for only 20 minutes. This therefore indicates that the undertaken heat treatment led to a pronounced embrittlement of the material. Bearing in mind that, for this strain, surface saturation with sulphur is obtained after 35 minutes, the embrittlement can therefore be attributed to the segregation of sulphur to the grain boundaries of nickel. The time lag between maximum brittleness (70 minutes) and surface saturation (35 minutes) sustains this explanation since it reinforces the idea according to which surface saturation precedes grain boundary segregation because of the already mentioned difference in free energy between the two segregation processes.

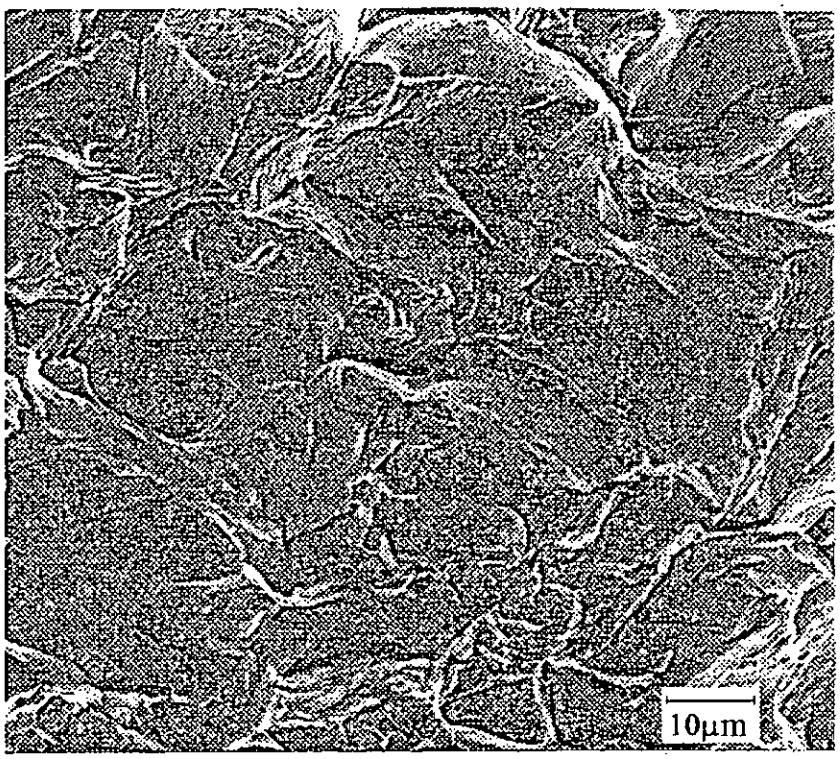

(a)

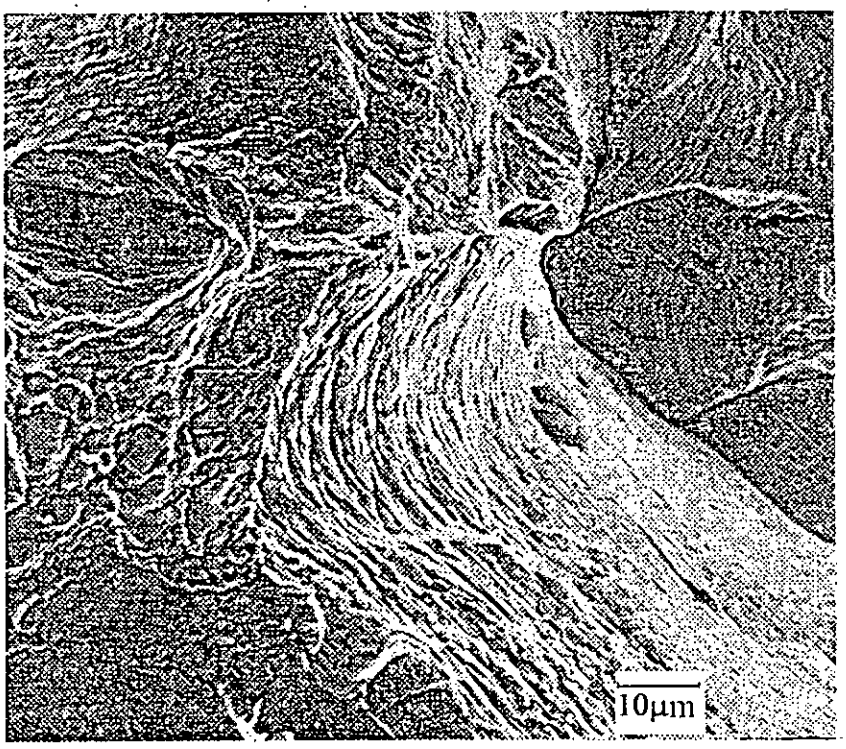

(b)

Figure IV-24. SEM fractographs of the material cold rolled to 0.2 true strain and then heat treated at 455°C for 70min (a) and 20min (b).

Larere [55], who carried out an AES investigation on sulphur segregation to the grain boundaries of a similar grade nickel, put forward the following empirical relationship linking the sulphur concentration in the GB's (atom %), $C_s^{g.b}$, to the stress to failure at 77K, σ_R:

$$C_s^{g.b} = \frac{\sigma_0 - \sigma_R}{1450}.$$

σ_0 is the stress to failure in the absence of segregation. Although this relationship was obtained in equilibrium conditions for a nickel containing 20ppm of sulphur, it is reasonable to apply it to our case, since intergranular brittleness depends on the concentration of sulphur in the GB's and not on the way that led the impurity to be there. Fig IV-25 represents the evolution of σ_R, measured experimentally, and $C_s^{g.b}$, calculated using Larere's relationship, with $\sqrt{t}$ at 455°C for the material deformed to 0.2 true strain. The GB saturation curve shows that GB segregation, which starts at a time corresponding to surface saturation, coincides with a beginning in the fall of the stress to failure, and that minimum stress to failure corresponds to a sulphur concentration of 0.35. This value is fairly near to the concentration at saturation which was found by Larère [55] to be equal to 0.45. Grain boundary segregation kinetics follow the same sigmoidal form as surface saturation kinetics, from which an apparent diffusion coefficient can be calculated using McLean's model. The calculated value of $2.87 \times 10^{-8} cm^{-2}$, although of the same order of magnitude, is smaller than the value calculated for surface segregation ($8.89 \times 10^{-8} cm^{-2}$). This is understandably so because as recovery proceeds the short circuit concentration in the material decreases. The ratio of the time to grain boundary saturation to the time to surface saturation is smaller than the ratio of the respective diffusion coefficients, because the decrease in diffusion coefficient for GB segregation is

counterbalanced by the diffusion path to the GB's being smaller than the diffusion path to the free surface.

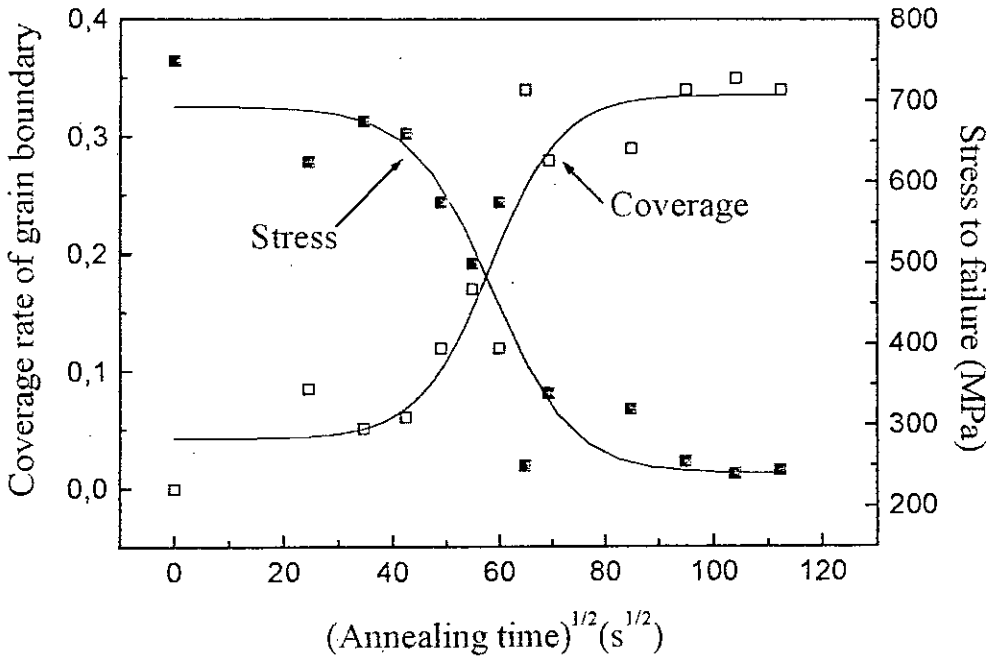

Figure IV-25. Stress to failure and GB concentration with sulphur against annealing time at 455°C for the material deformed to 0.2 true strain.

3.2 Intergranular corrosion

Intergranular corrosion is another property giving indirect evidence of grain boundary segregation.

The work carried out consisted first of all of determining the polarisation curve of the material and then determining the working conditions for the intergranular attack (intergranular grooving) leading to the determination of the extent of intergranular corrosion as indicated by the intergranular groove parameters; angle and depth (see CH.I, section 3). The evolution of the corrosion current density was also investigated.

3.2.1 Experimental procedure

3.2.1.1 Determination of the polarisation curve

The polarisation curve was determined using potentiodynamic techniques. Figure IV-26 shows a schematic representation of the apparatus used. The experimental conditions are listed below:

- Equipment : Princeton applied research computer driven EG&G potentistat / galvanostat, model 263A, version 211.
- Software : Princeton applied research, model 352/252 corrosion analysis software, version 2.23.
- Technique : potentiodynamic
- Medium : a 2N aqueous sulphuric acid solution, at 25°C, chosen in order to avoid a rapid attack of the surface and to ensure mass transport controlled kinetics [124,125].
- Counter electrode : platinum
- Reference electrode : Saturated Calomel (SCE)
- Scanning rate : 1 $mV.s^{-1}$.
- Deaeration : bubbling of nitrogen through the solution.

The results are recorded as **I** versus **E** curves, where **I** is the current density and **E** is the potential.

3.2.1.2 Electrochemical grooving of the grain boundaries

Grooving of the grain boundaries was obtained by a controlled potential coulometry technique. In order to obtain a preferential attack of the grain boundaries, the specimen is subjected to tests carried out according to experimental conditions established by Baunier et al [64], whereby a constant quantity of electricity is passed through the specimen, at a potential in the transpassive peak of the polarisation curve, in order to obtain the dissolution of a constant thickness of the material. The dissolution at the grain boundaries is hence quantified by the intergranular groove parameters; angle and depth. The

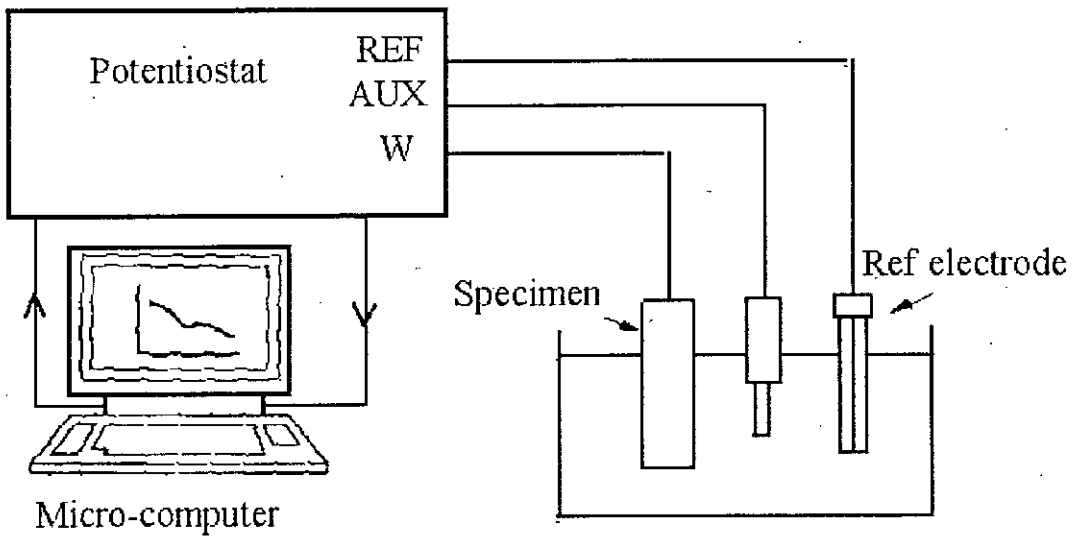

Figure IV-26. Experimental set up for the electrochemical tests.

apparatus used is a computer controlled equipment which enabled the tests to be run automatically once the conditions are set. The experiments were run in the following conditions :

- Equipment : same as for polarisation curve
- Software : Princeton applied research, research electrochemistry software model 270/250, version 4.23.
- Technique : Potentiostatic, controlled potential coulometry (CPC). The experiment is stopped once a quantity of electricity of 15 $C.cm^{-2}$ is delivered, thus ensuring that a constant thickness of material is dissolved on all specimens.
- Medium : a 2N aqueous sulphuric acid solution at 25°C.
- Counter electrode : platinum
- Reference electrode : Saturated Calomel (SCE)
- Working potential : 1450 mV, a potential corresponding to $\frac{3}{4} I_{2\,max}$, where I_{2max} is the maximum current density of the transpassive peak on the polarisation curve, attributed to intergranular corrosion [64].
- Deaeration : bubbling of nitrogen through the solution.

The experiment is stopped automatically once a quantity of electricity of 15 Coulombs/cm^2 is sent through the specimen.

The groove parameters (angle and depth) are measured in a Stereoscan 440 scanning electron microscope of Leika Cambridge, using a computer software named Leo. The specimen stage was tilted to an angle of 70° in order to be in an adequate measuring position. A minimum of fifteen measurements were carried out on each specimen in order to obtain a representative mean value. The results are presented in the form of graphs representing the evolution of the groove angle and depth with annealing time after deformation.

SEM micrographs showing a selection of grooved grain boundaries are gathered in annex two.

3.2.1.3 Evolution of the corrosion current density with annealing time

The specimens, cold rolled and then annealed as described before, were subjected to corrosion tests using an EG&G Park corrosion testing equipment, model 350A. The experimental conditions were as follows :

- Technique : potentiodynamic.
- Medium : 2N H_2SO_4 solution at 26°C.
- Counter electrode : platinum
- Scanning rate : 10 $mV.s^{-1}$.
- Reference electrode : Saturated Calomel.
- Deaeration : bubbling of nitrogen through the solution.

The results were recorded in the form of E versus **Log(I)** curves, where E is the potential and I is the corrosion current density.

3.2.2. Results and discussion

3.2.2.1 Polarisation curve of Ni 270

The polarisation curve for the material is presented in figure IV-27. An active peak and a transpassive peak, separated by a region where the metal is passive, are observed. The gradient of the ascending part of the active peak characterises the dissolution rate of the metal. The value of the passivation potential, E_p, translates the ease with which the passive layer is formed, whereas the value of the current, I_p, characterises its protectiveness.

The presence of a segregated layer on the surface modifies to a great extent the characteristics of the curve as shown on figure IV-28. The dissolution rate is

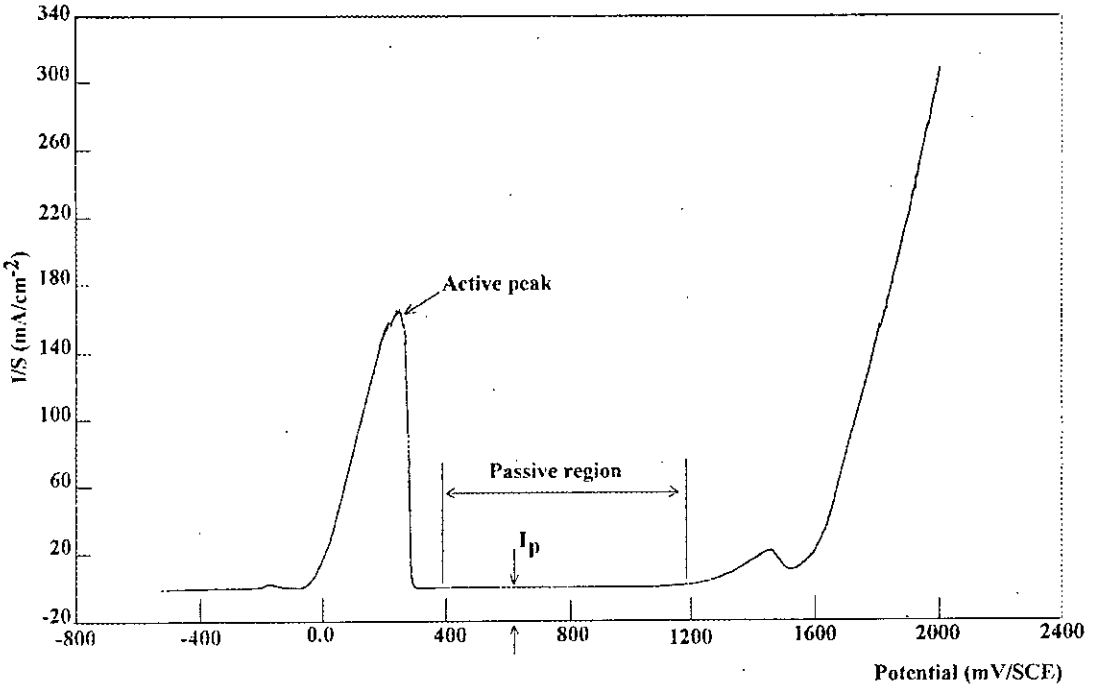

Figure IV-27. Polarisation curve of nickel.

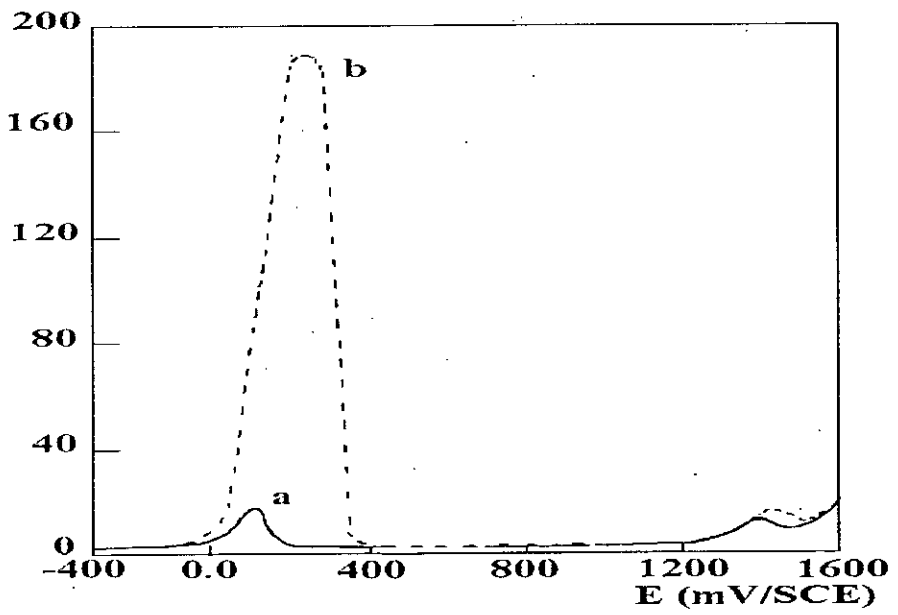

Figure IV-28. Effect of segregation on polarisation curve
(a) annealed 5h at 850°C (non deformed)
(b) deformed to 0.2 true strain and then annealed for 70 min. at 455°C.

increased translating a catalytic effect of sulphur on the attack of nickel. The formation of the NiO passive layer is found to be retarded if not eliminated all together, by the sulphur atoms preventing the OH^- ions from taking part in the formation of the layer [64]. This results in the sulphur layer remaining on the surface whereas the nickel goes into solution as a result of its bonds being weakened.

Figure IV-29 represents the transpassive part of the polarisation curve. It shows that the maximum current at the transpassive peak is equal to 11.8 mA. The potential corresponding to ¾ that value (8.85 mA), i.e. 1450 mV, was chosen as a working potential in the potentiostatic electrochemical grooving of the grain boundaries described above.

3.2.2.2 Intergranular corrosion

Figure IV-30 represents the variation of the groove angle and height with annealing temperature for specimens cold rolled and non cold rolled. The angle at 455°C for the non cold worked material is nearly twice that of the cold worked material. This illustrates quite well the difference between non equilibrium and equilibrium segregation, for which the diffusion coefficients are too low at this temperature to activate the migration of the impurity (sulphur) atoms. As the temperature increases, the behaviour of the cold worked material tends towards that of the non deformed material, i.e. towards equilibrium conditions, as shown by the groove angle and height which tend towards similar values for both materials. It is worth noting that the height varies inversely to the angle. A deep low angle groove highlights a localised intergranular attack in opposition to a shallow groove. At 850°C, the homogenisation temperature, segregation is negligible for both materials.

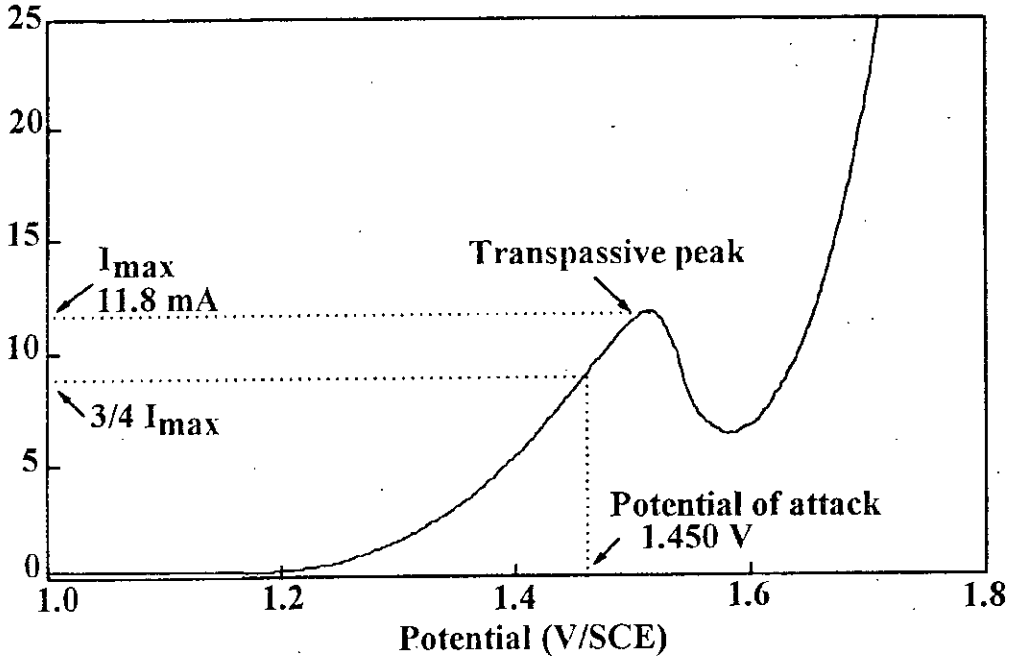

Figure IV-29. Transpassive part of the polarisation curve for nickel.

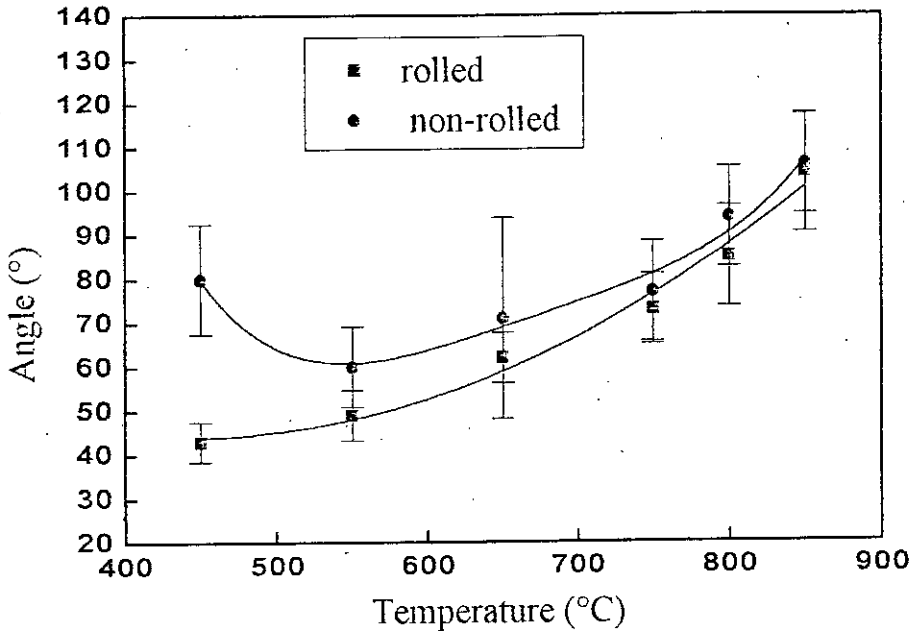

(a)

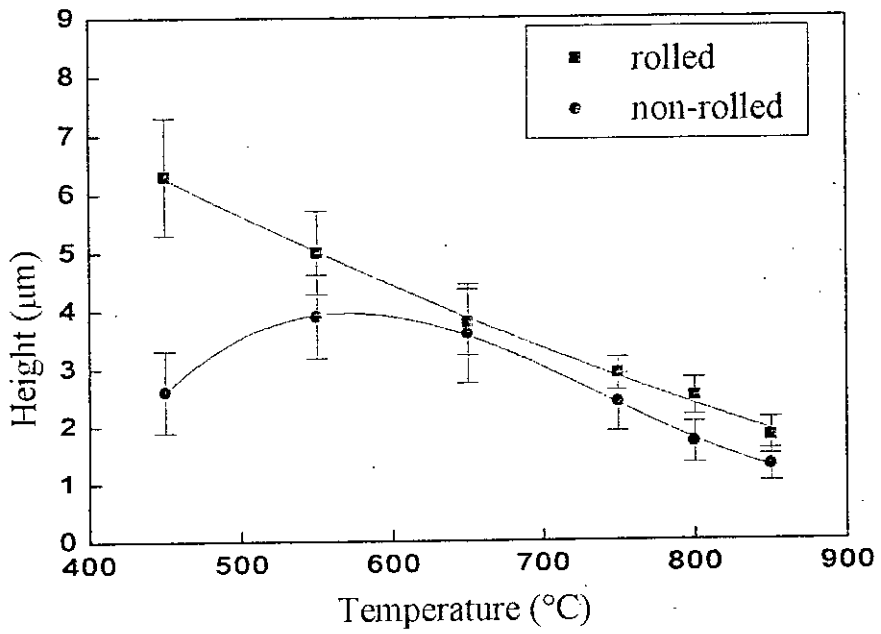

(b)

Figure IV-30. Variation of intergranular groove angle (a) and height (b) with annealing temperature for the materials non-rolled and cold rolled to 0.2 true strain. Isochronous anneals of 70 minutes.

Figure IV-31 shows the variation of the groove angle and height with annealing time at 455°C for the material cold rolled to 0.2 true strain. The angle decreases whereas the height increases with time, indicating that the longer the annealing time, and hence the nearer the material is to its recrystallised state, the more localised (decreasing α, increasing H) the intergranular attack is. Both curves tend towards stabilisation after an annealing time of 70 minutes. This is in good agreement with the tensile tests. It can therefore be concluded that recovery induced grain boundary segregation results in an enhancement of intergranular corrosion. In other words, the observed intergranular attack is an indirect evidence of grain boundary segregation of sulphur occurring during the recovery of the deformed material.

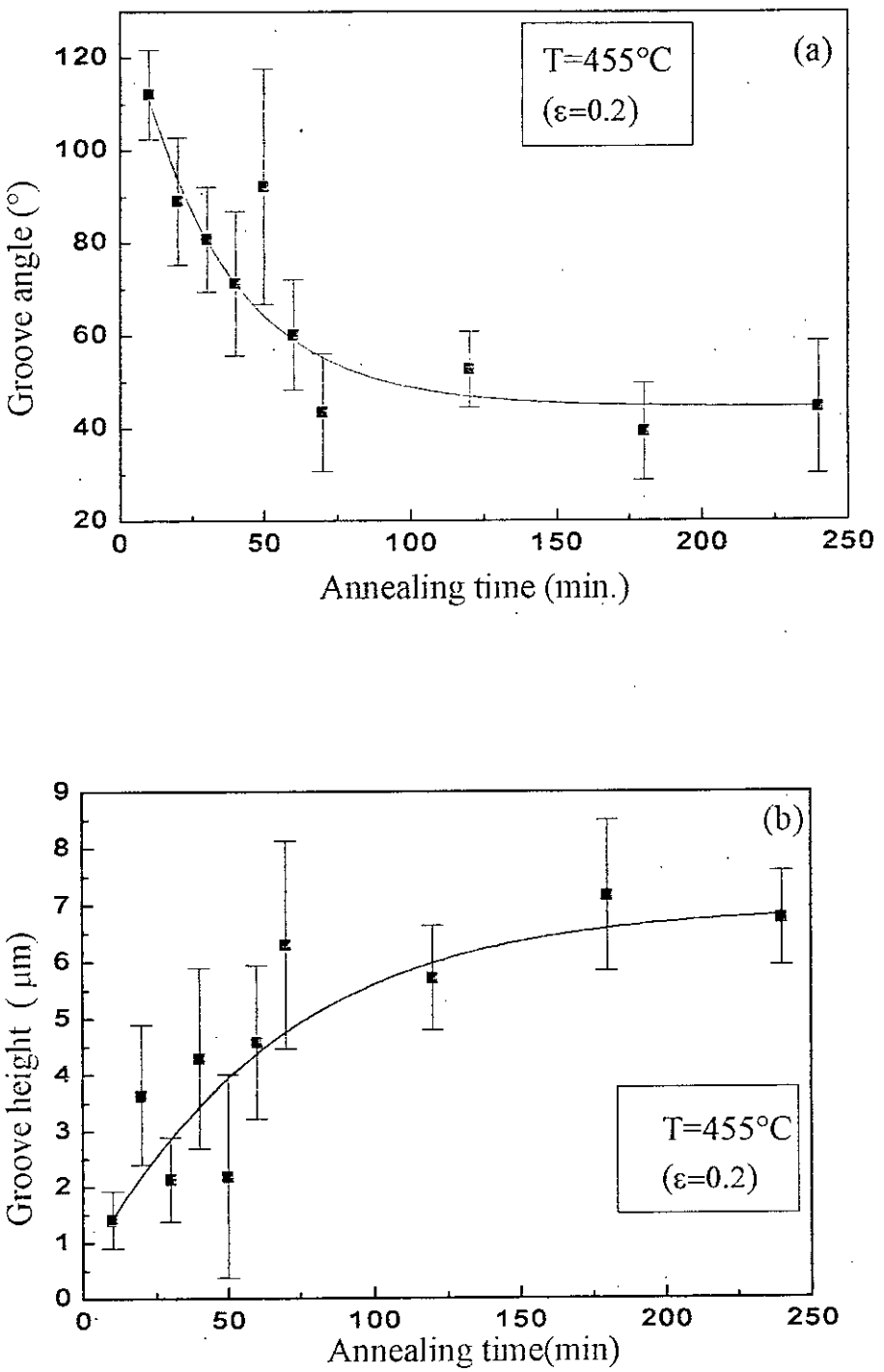

Figure IV-31. Variation of intergranular groove angle (a) and height (b) with annealing time at 455°C for the material cold rolled to 0.2 true strain.

Furthermore, the corrosion current density is shown to increase with annealing time ,figure IV-32 , indicating a deleterious contribution of recrystallisation, and hence segregation, to the corrosion process. The curve has a sigmodal form and tends towards stabilisation at the already mentioned annealing time of 70 minutes, corresponding to the end of the recovery process.

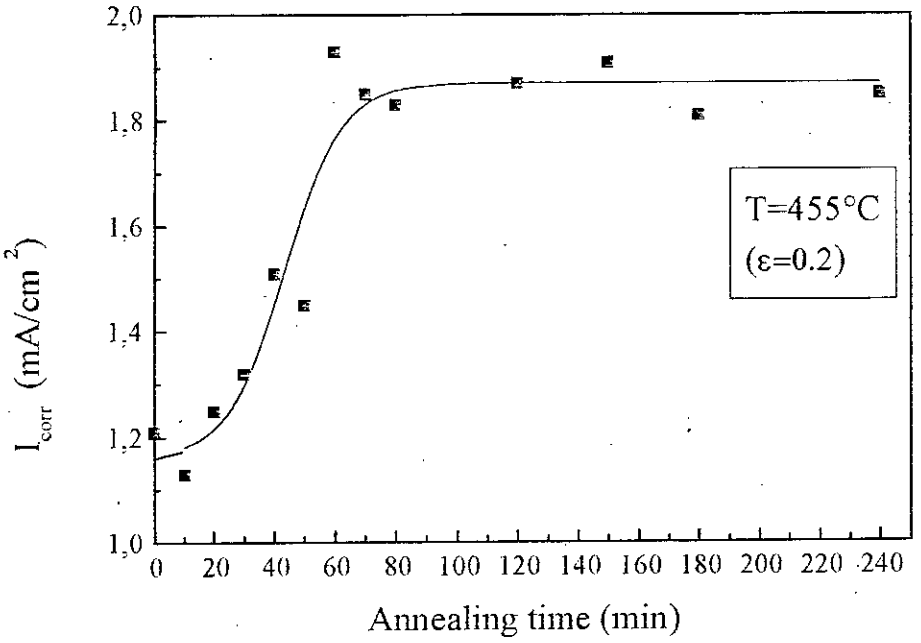

Figure IV-32. Corrosion current density versus annealing time at 455°C for the material cold rolled to 0.2 true strain.

4. A comparison between surface and grain boundary segregation

A stabilisation in the curves presented and discussed above is perceived as indicating a saturation of the interface with sulphur. The Auger results indicate that surface saturation with sulphur is generally attained before any stabilisation in any of the intergranular properties (stress and deformation to failure, groove parameters) is observed. This time lag can be explained in terms of the reduction in free energy associated with surface and with grain boundary segregation. The reduction in free energy associated with surface segregation (-140 $kJ.mol^{-1}$[93]) is more important than that associated with grain boundary segregation (-98 $kJ.mol^{-1}$[93]). Grain boundary saturation and its effects on the properties are therefore only observed once the surface had been saturated. In other words, before the grain boundaries can be saturated, surface saturation has first to be attained.

CHAPTER V

SULPHUR SEGREGATION TAKING PLACE DURING THE RECOVERY OF QUENCHED NICKEL

In this chapter, the results of an investigation carried out on the role of quenching vacancies are presented and discussed.

The chapter is divided into three main parts. The first part presents the thermodynamic and kinetic aspects of vacancy creation and elimination. The second part describes the experimental techniques and procedures used to produce, eliminate and study the consequences of vacancy elimination on sulphur segregation kinetics to the free surface and to the grain boundaries. The results are presented and discussed in the third part.

1. Introduction

1.1 Vacancy formation and elimination

There are three main experimental methods of obtaining, at low temperature, vacancies in concentrations well above the equilibrium concentration. These are :

- Quenching from a sufficiently high temperature
- Irradiation with high energy particles
- Cold working .

The first method is by far the most widely used due to its simplicity, and is therefore the one that has been chosen in the present work .

1.1.1 Thermodynamics of vacancy formation

A vacancy is created when an atom is ejected from its normal site and driven to the free surface without a considerable change in the surface energy. The free energy of formation of a vacancy is given by the following relationship:

$$G_v^f = H_v^f - T.S_v^f ,$$

where S_v^f is the entropy due to the change in the elastic constants (*i.e.*, the vibration frequency) near the vacancy, and H_v^f is the enthalpy at constant temperature and pressure and is given by the following expression:

$$H_v^f = E_v^f + P.V_v^f$$

The first term represents the change in internal energy due to the formation of the vacancy and the second term represents the work done against the external forces due to the change in volume. E_v^f is of the order of 1eV and $P.V_v^f$ is , under normal pressure, of the order of 10^{-5} eV and can therefore be neglected [126].

The free energy of a perfect crystal in which ***n*** vacancies are introduced is given by :

$$G = n.G_v^f - T.S_c \qquad (S_c \text{ is the entropy of configuration})$$

$$G = n.H_v^f - T.(n.S_v^f - S_c)$$

The equilibrium vacancy concentration corresponds to the minimum free energy of the system :

$$\frac{\delta G}{\delta c} = 0 \Rightarrow \frac{C_v}{1 - C_v} = e^{\frac{-G_v^f}{k.T}} .$$

For C<<1, the expression above becomes :

$$C_v = e^{\frac{S_v^f}{k}} . e^{\frac{-H_v^f}{k.T}} .$$

At normal pressure, the enthalpy of formation can reasonably be approximated to the energy of formation and the expression ,therefore, becomes :

$$C_v = e^{\frac{S_v^f}{k}} . e^{\frac{-E_v^f}{k.T}} .$$

This last expression can be used to calculate the equilibrium vacancy concentration in a pure metal, at any temperature, provided the enthalpy and entropy of formation are both known.

In the case of dilute solutions, the equilibrium vacancy concentration is given by [127]:

$$C_v = Z.C_I . e^{\left(-\frac{E_v^f + E_{v-I}}{k.T}\right)} + (1 - Z.C_I) . e^{\left(\frac{E_v^f}{k.T}\right)} ,$$

where Z is the co-ordination number, C_I is the impurity concentration and E_{v-I} is the energy of interaction between the vacancy and the impurity atom.

1.1.2 Thermodynamic and kinetic aspects of vacancy elimination

Vacancies in supersaturation obtained after a quenching operation are in a metastable state. Their elimination is achieved through either their elimination at well known sinks (free surfaces, grain boundaries, dislocations...etc.), or their coalescence to form cavities or dislocation loops. The temperature intervals of vacancy elimination are determined by carrying out a series of isochronous anneals at increasing temperatures, until a physical quantity characterising the

vacancies (electrical resistivity, for example) is completely altered. The elimination kinetics in isothermal conditions can after that be known by studying the evolution of the physical quantity with time.

The jump frequency of a migrating vacancy is given by [127] :

$$\gamma_s = Z.\gamma.e^{\left(\frac{S_m}{k}\right)}.e^{\left(\frac{-H_m}{k.T}\right)} \quad ,$$

where γ is the initial frequency with which the defect attacks the energy barrier and the exponential term indicates the probability of the defect having sufficient energy to overcome the barrier. Z is the co-ordination number ; H_m and S_m are the enthalpy and entropy of vacancy migration respectively.

In the case of a fully annealed metal, vacancy elimination is carried out on a random basis, i.e. the only acting forces are of a thermodynamic origin, excluding all kinds of interactions (vacancy-vacancy, vacancy-dislocation). The vacancies will hence be eliminated in sinks such as grain boundaries and free surfaces. The number, dn, of vacancies which are eliminated in a time interval, dt, is proportional to the number, n, of vacancies initially present at time, t :

$$dn = -K_1.n.dt \quad ,$$

K_1 is the speed of the elimination reaction and is given by :

$$K_1 = \alpha.Dv \quad ,$$

where D_v is the diffusion coefficient of the vacancies, and α is a coefficient that depends only on the density of the sinks and their distribution. The equation above giving dn can therefore be rewritten as follows :

$$\frac{dC}{dt} = -\alpha.D_v.C \quad ,$$

the integration of which gives :

$$C = C_0.e^{(-\alpha.D_v.t)} \quad ,$$

C_0 being the initial vacancy concentration.

1.1.3 Investigation techniques for the study of quenching vacancies

Numerous techniques have been deployed for the study of vacancies in quenched metals. Direct observation techniques , such as field emission microscopy, were successfully tried [128]. The variation of density was also taken as an indication of the presence of vacancies[129,130]. The shortcomings of this technique rely in the fact that its accuracy increases with the volume of the material, which is in contradiction with the necessity to have high cooling rates. The modulus of elasticity is found to be very sensitive to the amount of vacancies in the material. Changes in Young's modulus after quenching of aluminium were investigated by measuring the speed of sound in the material, before and after quenching [131]. Electrical resistivity remains ,however, the most frequently used technique because of its ease and accuracy. Isochronous annealing after quenching can be used to determine the different recovery stages, whereas isothermal annealing can be used to determine the migration energy of the defect as well as the kinetics of the reaction. The curve representing the evolution of resistivity with temperature during isochronous annealing of quenched nickel shows a maximum of three recovery stages. The exact number of these stages depends on the purity of nickel as well as on the quenching atmosphere. Scherrer et al [132] found three different stages. Wuttig and Birnbaum [133] found two stages ; one at about 50°C and the other at about 130°C. They attributed them to the migration of di-vacancies (energy > 0.3 eV) and mono-vacancies (energy > 1.0 eV) respectively. Mughrabi and Seeger [134] noticed an important influence of the metal purity and quenching atmosphere on the behaviour of the nickel studied. Only one stage appeared, at about 110°C, for the pure specimens (> 99.99%), whereas a second stage appeared , at about 270°C, for the less pure material (99.9%). Scherrer *et al* [132,135] reported that the second stage appears only if the specimen contains enough impurities. Mono-vacancies are therefore preserved, according to them, only if they are associated with impurities. Wycisk *et al* [136] attributed the

third stage of their curve to the dissolution of the dislocation loops they observed after annealing at 200°C. Electron microscopy observations of these dislocation loops are widely reported in the literature [137-140].

It can be concluded from the electrical resistivity and electron microscopy studies reported above that the impurities and the quenching atmosphere have a considerable effect on the thermodynamic characteristics of vacancies (energies of formation and migration). The first stage in the resistivity versus temperature of nickel is attributed to the elimination of di-vacancies whereas the second stage, the amplitude of which increases as the purity of the metal decreases, is attributed to the elimination of mono-vacancies interacting with impurities. The third stage is attributed to the elimination of dislocation loops and small cavities which grow in the first two stages after having been created in the quenching stage.

2. Experimental procedure carried out to study the influence of quenching vacancies on sulphur segregation in Ni 270

The experimental procedure consists of producing vacancies, eliminating them and studying sulphur segregation and the resulting changes in properties accompanying the vacancy elimination process. The details are given in the following.

2.1 Vacancy production and elimination

2.1.1 Vacancy production scheme

The specimens are homogenised for 1 hour at 1200°C inside sealed silica capsules, under a residual atmosphere of argon, and then quenched by letting the capsule to fall freely on a metallic bloc submerged in water at 0°C. The capsule would then break and allow the specimen to be homogeneously quenched. Following this point defect production scheme, part of the specimens is destined

to an investigation of the vacancy elimination process, and the other part to the study of the segregation phenomenon.

2.1.2 The investigation of vacancy elimination: resistivitry measurement

The quenched specimens (ribbons of 25x2x0.5 mm^3) undergo isothermal heat treatments at temperatures ranging from 50 to 700°C inside silica capsules. They then undergo electrical resistivity measurements at 4.2K using the same apparatus as for the cold worked material.

2.2 Superficial segregation of sulphur: Auger electron spectroscopy

Surface segregation of sulphur accompanying vacancy elimination is studied using Auger electron spectroscopy, in the same conditions as for the cold worked material. In this case, the quenched specimens are isothermally heated inside the AES chamber, at various temperatures going up to 700°C.

2.3 Effect of segregation on the intergranular properties

2.3.1 Tensile testing

Intergranular brittleness resulting from grain boundary segregation of sulphur accompanying vacancy elimination is investigated by tensile tests to failure carried out at 77K instead of the cumbersome in-situ fracture tests that would be done inside the Auger spectrometer. Tensile specimens are quenched from 1200°C and then heat treated inside sealed silica capsules at temperatures going up to 750°C. They are subsequently tested in tension at 77K, until failure occurred.

2.3.2 Electrochemical testing

The consequences of sulphur segregation on the electrochemical properties of the grain boundaries were investigated in the same manner as for the cold worked material. Quenched and then annealed specimens were subjected to

controlled potential coulometry (CPC) tests in exactly the same conditions as for the cold worked material. The intergranular groove parameters (angle, height) were measured using the SEM as detailed before.

SEM micrographs representing a selection of grooved grain boundaries are presented in annex two.

3. Results and discussions

3.1 Recovery of the quenched structure

The results of the resistivity tests are presented in the form of the ratio $\Delta\rho/\Delta\rho_0$, where $\Delta\rho_0$ is the increase in resistivity due to quenching and $\Delta\rho$ is the excess in resistivity after the post-quenching anneal, with reference to the fully annealed state.

$$\Delta\rho_0 = \rho_q - \rho_A,$$

$$\Delta\rho = \rho_a - \rho_A.$$

ρ_A is the resistivity of the fully annealed material (slowly cooled from 1200°C), ρ_q is the resistivity of the quenched material and ρ_a is the resistivity of the quenched and then annealed material. A decrease in $\Delta\rho$, and hence of the ratio, represents therefore a tendency to attain the equilibrium (fully annealed) state.

The increase in resistivity after quenching, $\Delta\rho_0$, is found to be $1.8\text{x}10^{-3}$ $\mu\Omega$.cm. Figure V-1 represents the evolution of the resistivity ratio with annealing time (after quenching) at a low, an intermediate and a high temperature. The ratio decreases with increasing time for each temperature. This behaviour is consistent with the idea that as time increases, an increasing number of vacancies is annihilated leading to a decrease in resistivity. The curves also show that after 20 minutes heat treatment, all three curves tend towards a stationary value which decreases with increasing temperature, at a rate which increases with increasing temperature. This can easily be explained by the fact

that vacancy annihilation is a thermally activated process implying that the higher the temperature, the greater the number of annihilated vacancies and the quicker the annihilation process (i.e. the greater the diffusivity of the vacancies). The duration of 20 minutes is therefore taken as a heat treatment time for all the isochronous anneals.

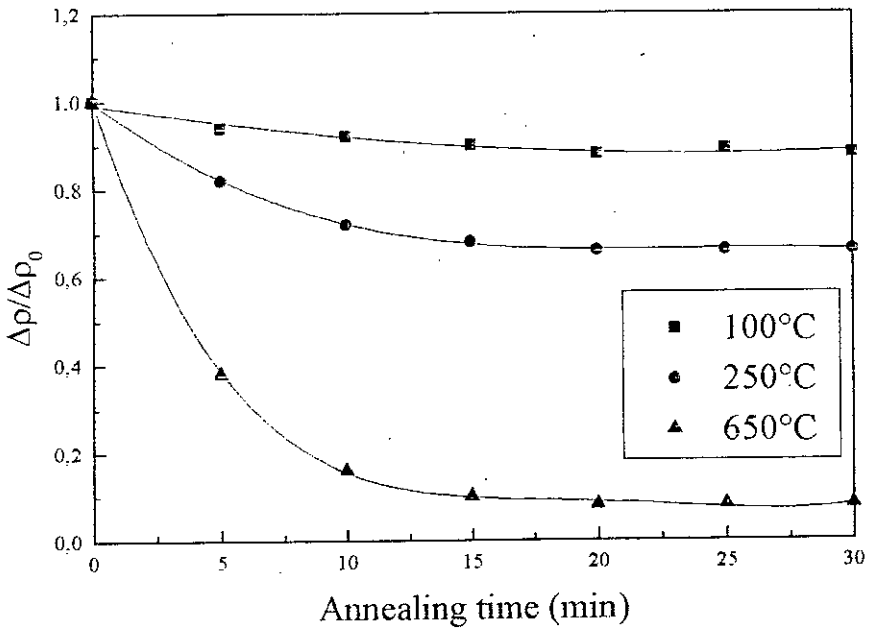

Figure V-1. Resistivity ratio against annealing time at 100, 250 and 650°C after quenching from 1200°C.

Figure V-2 represents the variation of the resistivity ratio with annealing temperature after quenching. The specimens had undergone isochronous anneals of 20 minutes at each temperature.

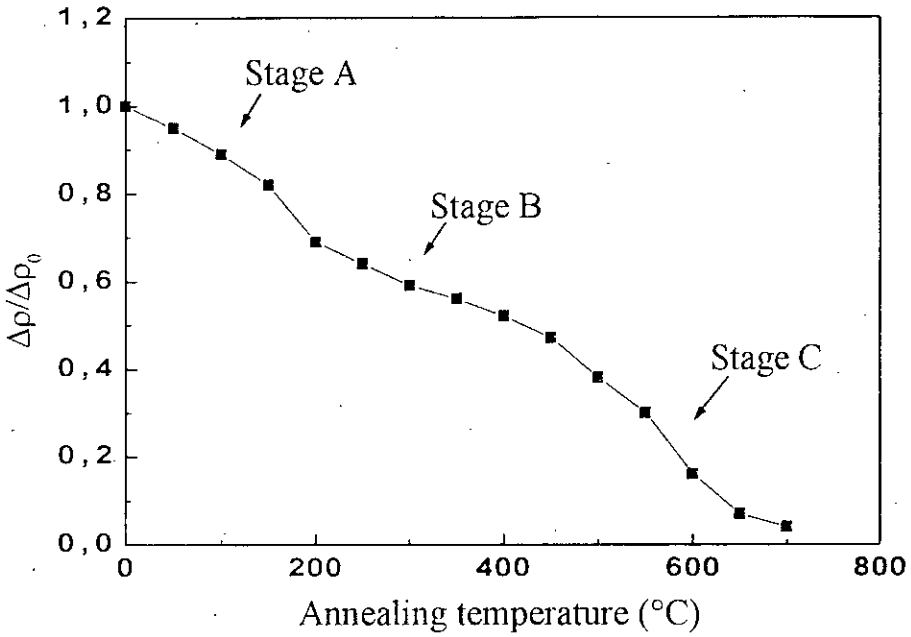

Figure V-2. Resistivity ratio versus isochronous (20 min.) annealing temperature after quenching.

The curve can be divided into three stages. The first stage (stage A) lies between 50 and 200°C and corresponds to a recovery of about 15% of the resistivity. The second stage (stage B) is centred at about 300°C and results in a recovery of resistivity of about 30%. The remaining resistivity is recovered in the last stage (stage C) which lies between 450 and 700°C.

These results are in agreement with the work reported in the literature and surveyed in section one above. The first stage is associated with the elimination of the very mobile di-vacancies which result from the coalescence, during quenching, of the monovacancies [132,135,141]. The second stage is thought to be strongly linked to the presence of impurities, and is attributed to the migration of monovacancies and vacancy-impurity (in our case vacancy-sulphur atoms) complexes existing at the end of the quenching operation

[132,135]. The form of the curve at this stage, exhibiting a decrease in recovery rate, is therefore thought to be due to the action of two mechanisms :

- a decrease in resistivity due to the elimination of vacancies and vacancy-impurity complexes on sinks (dislocations, grain boundaries, free surface) and small clusters,
- an increase in resistivity as a result of the growth of the clusters formed during quenching.

The last stage is attributed [136,140] to the dissolution of the clusters and cavities already present in the quenched material as a result of the strong interaction between vacancies reported in nickel [122].

It is worth mentioning that no experimental techniques, such as transmission electron microscopy, liable to confirm these explanations were available to us.

3.2 Surface segregation of sulphur during the annealing of quenched nickel

The obtained Auger spectra indicate that no appreciable segregation was detected below 400°C and that only sulphur segregates in appreciable amounts to the surface of nickel. The curves of figure V-3 represent Auger peak height ratios versus $\sqrt{t}$ for isothermal Auger runs carried out at 400, 500, 600 and 700°C. Assuming that the segregation kinetics can be expressed in terms of a McLean type expression, $C_s = 2.C_v.\sqrt{D^* t} / \sqrt{\pi}$, values of an apparent diffusion coefficient D* are calculated from the linear parts of the curves and gathered in table V-1, together with values, $D_{W\&G}$, reported in the literature [122] concerning the equilibrium segregation of sulphur in a nickel of similar composition. The ratio $D^*/D_{W\&G}$, which is of the order of 10^4, indicates that segregation is strongly accelerated by the presence of quenching vacancies in the material.

Figure V-4, which represents AES runs carried out at 700°C on a slowly cooled material and a quenched material, provides further evidence concerning the influence of vacancies. The surface coverage rate in the slowly cooled material is, after 10 minutes, less than 10% that in the quenched material.

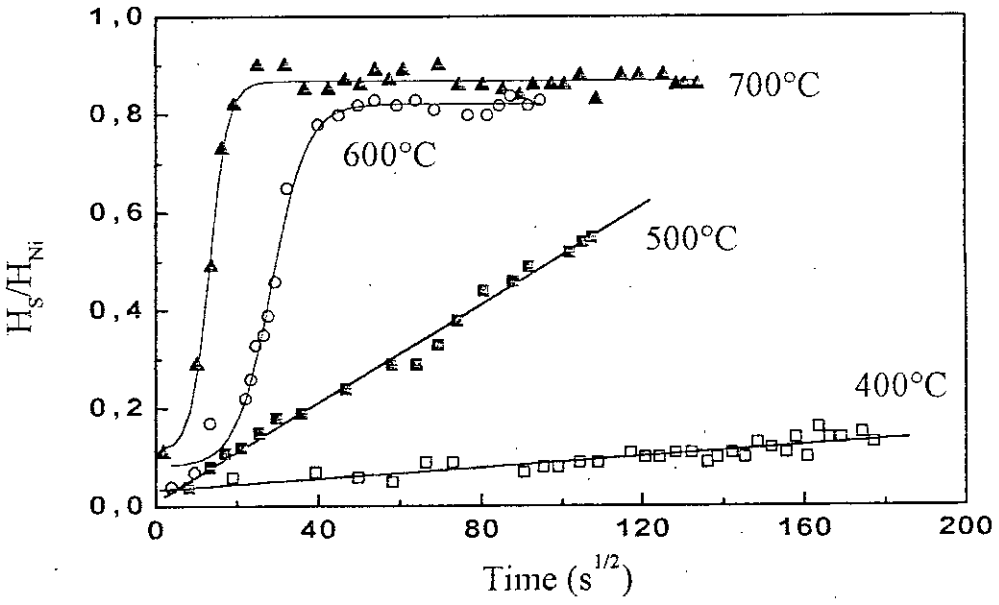

Figure V-3. Auger peak heights ratio versus annealing time for isothermal runs at 400, 500, 600 and 700°C carried out on quenched nickel .

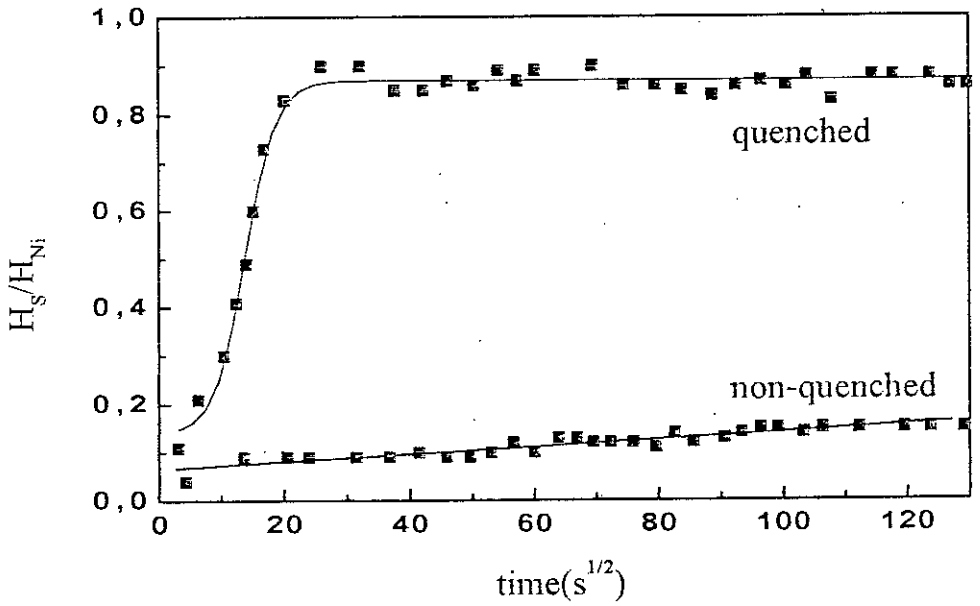

Figure V-4. Auger peak heights ratio versus annealing time for isothermal runs at 700°C carried out on a fully annealed and on a quenched specimens.

Temperature (°C)	D^* ($cm^2.s^{-1}$)	$D_{W\&G}$($cm^2.s^{-1}$) [122]	$D^*/D_{W\&G}$
400	2.1×10^{-11}	2.87×10^{-16}	7.3×10^{4}
500	5.43×10^{-10}	2.4×10^{-14}	2.3×10^{4}
600	2.1×10^{-8}	7.23×10^{-13}	2.9×10^{4}
700	7.2×10^{-8}	1.08×10^{-11}	6.7×10^{3}

Table V-1 . Apparent diffusion coefficients measured in the quenched material.

3.3 Segregation mechanism in the presence of vacancies

Sulphur segregation to the surface of quenched and then annealed nickel can be attributed to the formation and then elimination of the sulphur-vacancy complexes according to the mechanism suggested by Aust [142]. The segregation process can be described, according to this mechanism, in terms of the following stages :

Stage one concerns the metal at high temperatures, prior to quenching. Impurities such as sulphur would increase the vacancy concentration of the metal by the formation of vacancy-sulphur complexes.

Stage two, which corresponds to the material just after quenching, results in an increase in di-vacancy concentration, as a result of the interaction between mono-vacancies occurring during quenching, as well as an increase in the concentration of vacancy-sulphur complexes. Small cavities are also formed as a consequence of vacancy elimination It should however be borne in mind that although 30% of defects are lost during the quenching process, the remaining defects exist in important concentrations.

Stage three corresponds to low temperature annealing after quenching (stage A on the resistivity curve). Since it is found that heat treatments at temperatures around 100°C do not lead to any measurable surface segregation of sulphur, it is reasonable to suggest that at these temperatures, an important part of the divacancies are eliminated either in the cavities already existing at the end of

divacancies are eliminated either in the cavities already existing at the end of the quenching process, or through a coalescence process leading to the formation of very much less mobile clusters .

Stage four corresponds to heat treatments at temperatures corresponding to stage B on the resistivity curve. At this stage, monovacancies and complexes are eliminated on sinks (grain boundaries, free surface) and on cavities. Certain monovacancies also react, during their migration, with sulphur atoms to form new complexes. As a consequence of the high density of cavities in the metal, the concentration of the complexes that are eliminated on fixed sinks is fairly low leading to an undetectable sulphur concentration on the surface. This finding rather than meaning that segregation would not take place at this temperature, would more likely mean that heat treatment durations were not sufficiently long . Our work on the cold worked material showed that segregation did actually take place at 315°C.

Stage five corresponds to heat treatments at the high temperatures corresponding to the last stage (stage C) on the resistivity curve. Cavities are dissolved enabling a recombination of the complexes and their migration to the interfaces (grain boundaries, free surfaces). At the vicinity of the interface, a region of low distortion energy, the complexes are decomposed leading the vacancy to be eliminated on the interface and the sulphur atom to stay behind . This brings about an acceleration of segregation to the interface and an enrichment of its vicinity. As a result of the important quantity of sulphur accumulated just under the surface, this region becomes a source of sulphur whenever it is needed and accounts for the continuation of segregation even after the elimination of vacancies.

3.4 Effect on the intergranular properties of nickel

3.4.1 Mechanical properties

The curves of figure V-5 represents the stress versus strain curve of specimens quenched and then annealed for 100 minutes at temperatures ranging from 450 to 700°C. This particular duration is chosen because it ensures the completion of both the vacancy annihilation and the superficial segregation processes. The stress and the strain to failure decrease with increasing annealing temperature after quenching, with the decrease in strain being less pronounced. The low degree of embrittlement as depicted by the week sensitivity of the strain to failure is attributed to the short heat treatment duration. To highlight the effect of heat treatment time, tests were carried out on specimens isothermally heat treated at 650°C for various periods of time after quenching. This temperature is chosen in particular because it is high enough for pronounced defect annihilation and too low to cause equilibrium segregation. The curves of figure V-6 show that both the stress and the strain to failure decrease in the same fashion to reach minimum values for annealing times between 2 and 4 hours, before increasing again to recover their original values after about 20 hours of annealing. Tests carried out by Larere [55] on nickel in equilibrium conditions (fully annealed), containing 10ppm sulphur, revealed that maximum brittleness is attained after 13 days of heat treatment at 625°C. This clearly highlights the outstanding effect of defect annihilation in speeding up the segregation process.

The fracture surfaces represented in the SEM micrographs of figure V-7 show shiny, smooth intergranular facets for the material heat treated 3 hours at 650°C compared to mixed facets for the specimen heat treated 1 hour at the same temperature.

Guttmann [143] and Messmer and Briant [69]suggest that this embrittlement is due to the formation of a segregation layer, in the form of a two dimensional metal-impurity compound, over the whole interface and that the recovery coming after that is due to the conversion of the two dimensional compound into

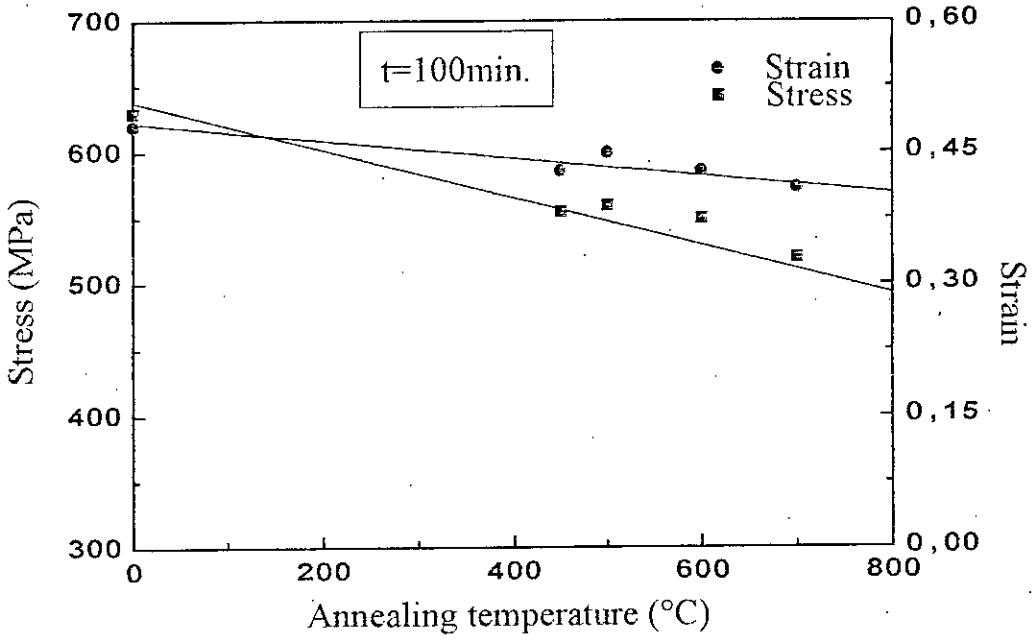

Figure V-5. Stress and strain to failure versus annealing temperature after isochronous (100 min.) anneals carried out on quenched nickel.

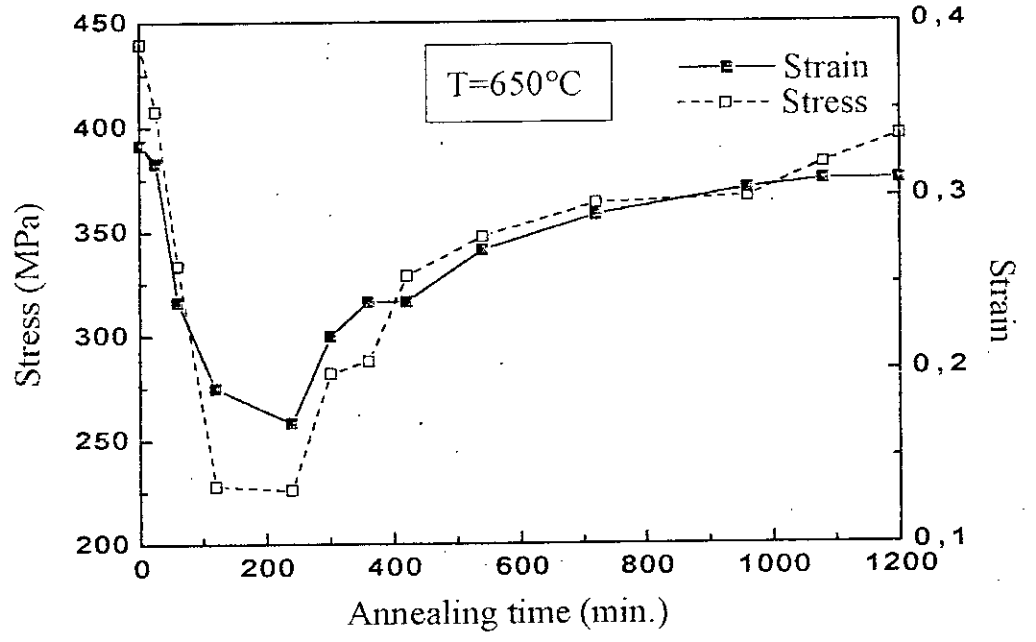

Figure V-6. Stress and strain to failure versus annealing time at 650°C of quenched nickel .

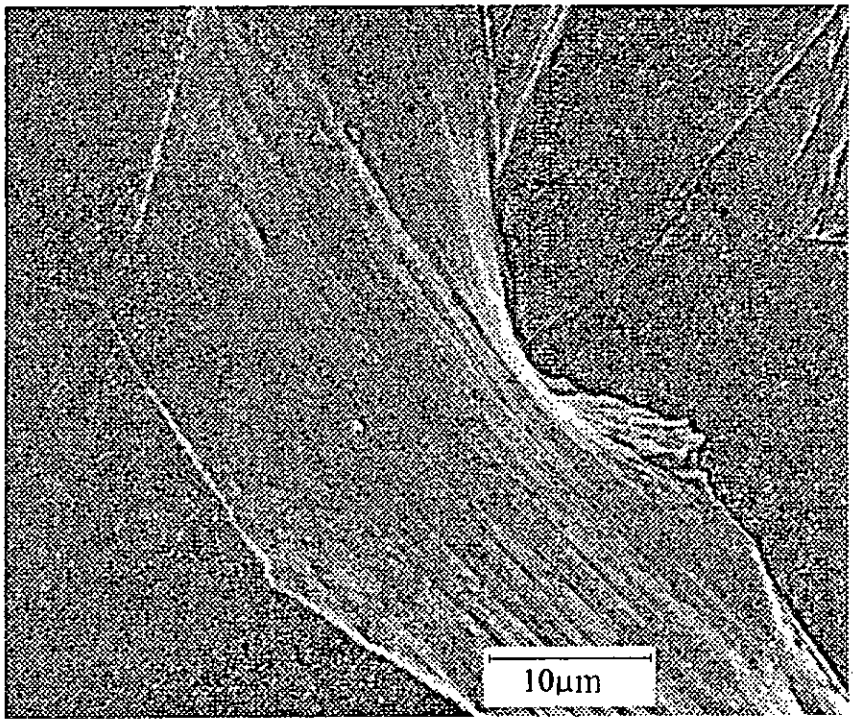

(a)

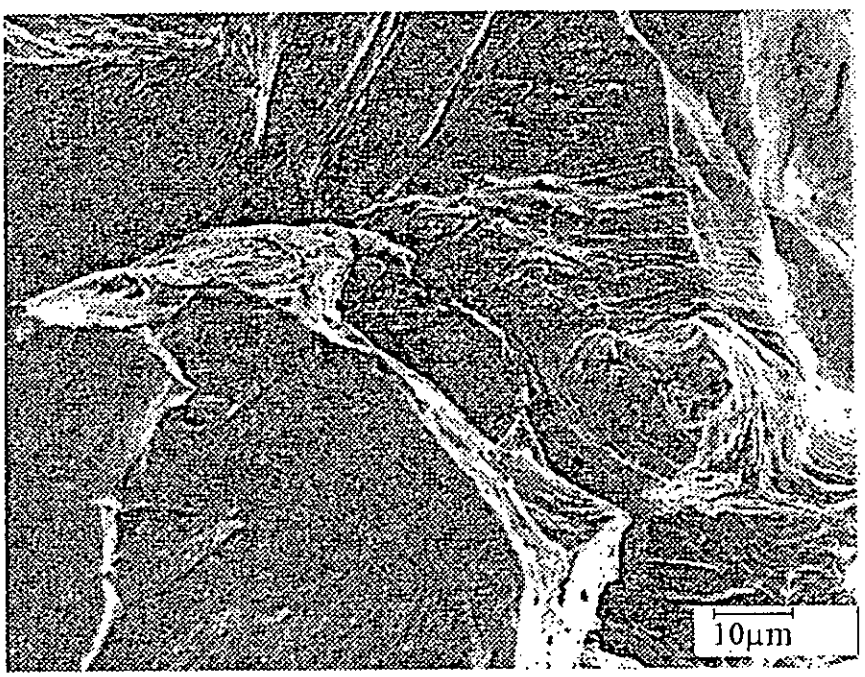

(b)

Figure V-7. SEM fractographs showing (a) smooth intergranular facets for the quenched material heat treated for 3 hours at 650°C, and (b) mixed facets for the same material heat treated for 1 hour at the same temperature.

a three dimensional compound localised at only a few points of the interface. Again, the speed of the recovery process should be noted : 20 hours are sufficient for nearly full recovery in non-equilibrium conditions whereas 90 days are necessary in equilibrium conditions [55]. This acceleration is explained by the contribution of vacancies to the acceleration of the reaction of conversion from a 2D to a 3D compound.

The application of the following empirical relationship:

$$C_S^{gb} = \frac{\sigma_0 - \sigma_R}{700},$$

found by Larère [55] concerning equilibrium segregation of sulphur in pure nickel containing 5ppm sulphur to quenched and then annealed nickel yields the curves of figure V-8. The concentration is seen to increase with annealing time at 650°C to reach the maximum value of 0.3 at a time corresponding to minimum stress to failure, i.e. 2 to 4 hours. The fall in concentration, corresponding to an increase in stress to failure, observed after that highlights the recovery process and can be related to the formation of the localised three dimensional nickel sulphide; Ni_3S_2.

It is worth mentioning that Larère [55] put forward two empirical relationships linking the GB concentration to the stress to failure; one for the material containing 20 ppm sulphur and another for the one containing 5 ppm sulphur. We found that the former was applicable to the deformed material and the latter to the quenched material. The only explanation that we can suggest for this lies in the difference in segregation kinetics which are greater in the deformed material than in the quenched material. The deformed material behaves as if it contained more sulphur than the quenched material.

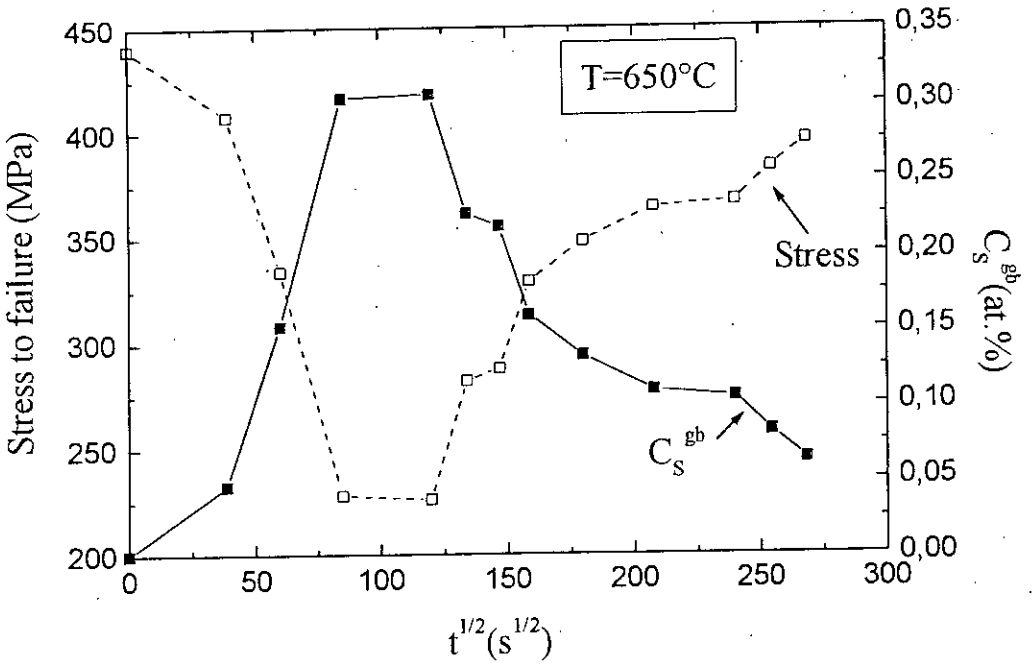

Figure V-8. Stress to failure and C_S^{gb}, calculated from Larère's expression [55] against annealing time at 650°C.

3.4.2 Electrochemical properties

The results of the CPC tests are given in the curves of figure V-9 which represent the evolution of the intergranular groove angle and height with annealing time, after quenching, at 650°C . The curves clearly show maximum intergranular attack, depicted by maximum groove height and minimum angle, for an annealing time of 3 hours. This is in very good agreement with the tensile tests which give maximum brittleness for an annealing range of 2 to 4 hours. For annealing durations greater than 4 hours, the intergranular electrochemical properties are also recovered, in the same way the mechanical properties are, indicating that the three dimensional nickel-sulphur compound is too localised to have any considerable effect on the electrochemical properties.

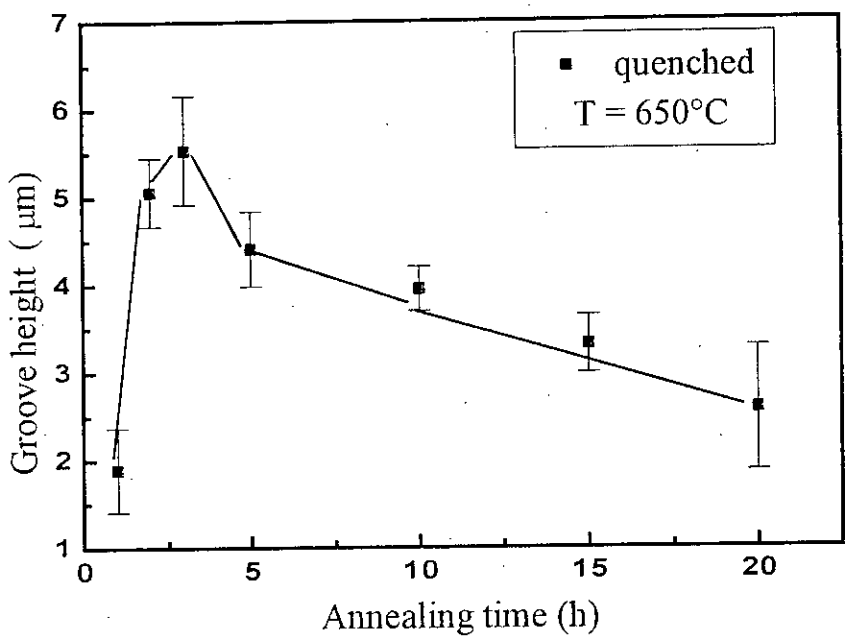

(a)

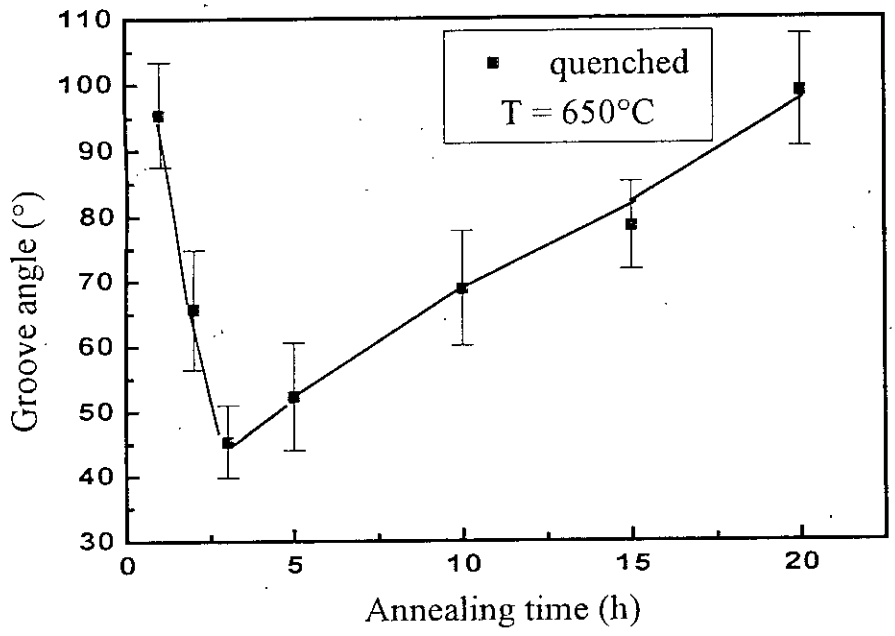

(b)

Figure V-9. Groove height (a) and angle (b) versus annealing time at 650°C of quenched nickel.

The results of the tensile and the electrochemical tests highlight the time lag between surface and grain boundary segregation, observed before for the cold worked material. Surface saturation is attained after only 40 minutes at 600°C, whereas more than 2 hours are necessary to attain grain boundary saturation.

CHAPTER VI
SEGREGATION MECHANISMS IN QUENCHED AND IN COLD WORKED NICKEL

This chapter summarises the mechanisms of sulphur segregation to the interfaces (grain boundaries, free surface) occurring during the annealing of both quenched and cold worked nickel.

1. Mechanisms of sulphur segregation in quenched and then annealed nickel

Sulphur atoms-vacancy interactions leading to sulphur segregation to the surface of quenched and then annealed nickel can be summarised in the following stages:

I) At high temperature, prior to quenching.

The vacancy concentration of the metal increases as a result of the formation of vacancy-sulphur complexes.

II) After quenching, before annealing:

- The interaction between mono-vacancies occurring during quenching results in an increase in di-vacancy concentration.
- The interaction between sulphur atoms and vacancies results in an increase in the concentration of vacancy-sulphur complexes.
- Small cavities are also formed as a consequence of vacancy elimination.

III) Low temperature annealing after quenching (up to 200°C, stage A on the resistivity curve).

At these temperatures, it is found that :

- No measurable surface segregation of sulphur is detected
- 15% of the excess in resistivity is recovered.

It is therefore reasonable to deduce that at these temperatures, an important part of the di-vacancies are eliminated either in the cavities already existing at the end of the quenching process, or through a coalescence process leading to the formation of very much less mobile clusters .

IV) Heat treatments at intermediate temperatures (200°C<T<400°C, stage B on the resistivity curve).

At these temperatures, it is found that:

- 30% of the excess in resistivity is recovered

- No appreciable segregation is detected

It reasonable then to explain the vacancy elimination process as follows: mono-vacancies and complexes are eliminated on sinks (grain boundaries, free surface) and on cavities. Certain mono-vacancies also react, during their migration, with sulphur atoms to form new complexes.

The non-detection of segregation can be explained as follows:

As a consequence of the high density of cavities in the metal, the concentration of the complexes that are eliminated on fixed sinks (grain boundaries, free surface) is fairly low leading to an undetectable sulphur concentration on the surface. This does not mean that segregation would not take place at this temperature, but rather means that the heating durations are not sufficiently long. The work on the cold worked material did actually show that segregation took place at 315°C.

V) Heat treatments at high temperatures (T≥400°C, stage C on the resistivity curve).

The observed decrease in resistivity and highly accelerated segregation can be explained in terms of the following sequence of events:

- Cavities are dissolved enabling a recombination of the complexes and their migration to the interfaces (grain boundaries, free surfaces).
- At the vicinity of the interface (a region of low distortion energy) the complexes are decomposed leading the vacancy to be eliminated on the interface and the sulphur atom to stay behind . This brings about an acceleration of segregation to the interface and an enrichment of its vicinity.
- As a result of the important quantity of sulphur accumulated just underneath the interface, this region becomes a source of sulphur whenever it is needed and accounts for the continuation of segregation even after the elimination of vacancies.

The diagram of figure VI-1 summarises the sequence of events leading to sulphur segregation during the annealing of quenched nickel.

2. Mechanisms of sulphur segregation in cold rolled and then annealed nickel

2.1. Segregation in the absence of recrystallisation

This type of segregation is made in evidence by the AES runs carried out at 315°C. The predominant role of vacancies at this stage is unambiguously evident. The true strain at which a notable increase in segregation kinetics is observed corresponds to nearly that at which a considerable increase in vacancy concentration is also observed. The role played by dislocations can be highlighted by looking at the apparent diffusion coefficients obtained from Auger analyses performed at 400°C on the quenched specimen ($2.1 \times 10^{-11} cm^2 s^{-1}$) and at 315°C on the specimen deformed to $\varepsilon = 0.2$ ($5.9 \times 10^{-11} cm^2 s^{-1}$). It is found that even though the deformed specimen was analysed at a lower temperature, the surface segregation kinetics on it are greater. This can be explained by a difference in microstructure. The quenched material has a coarse grained structure (500μm) with a dislocation density of the order of 10^8 cm^{-2}, whereas the cold worked material has a finer structure (80μm) and a high dislocation density of the order of 10^{10} cm^{-2}. This implies that in the case of the cold rolled material, besides the contribution due to vacancies detailed above, a considerable contribution to the diffusion process is made by the short circuits (grain boundaries, dislocations) existing in greater quantities.

In the light of this, the mechanism that can be suggested for segregation taking place at this stage can be summarised in the following sequence of events:

- Vacancies generated by cold work combine with sulphur atoms to form vacancy-sulphur complexes.
- In the course of the heat treatment following cold work, the migrating vacancies drag with them the sulphur atoms towards vacancy sinks (dislocations, grain boundaries, free surface).

- Sulphur atoms diffuse along dislocations towards the grain boundaries and then towards the surface or directly towards the surface.
- The sulphur in the grain boundaries diffuses towards the surface until this latter is saturated.

2.2. Segregation during and after recrystallisation:

We have shown that for the material deformed to true strains less or equal to 0.25, segregation takes place during recovery and is completed before recrystallisation starts. The mechanism that can be suggested is therefore the one based on the contribution of vacancies and dislocations detailed above.

For greater strains, the impurity drag theory [118,119] seems to hold. The mechanism that can be suggested on the basis of this theory can be summarised as follows:

- for strains less or equal to 0.5, the moving boundaries of the recrystallizing grains drag with them the sulphur atoms leading to the formation of sulphur atmospheres at the vicinity of the interface.
- For strains greater than 0.5, the grain boundaries manage to break away from the sulphur atmospheres leaving them behind, and resulting in the completion of recrystallisation before segregation. The sulphur sources thus formed continue to feed the grain boundaries which in turn feed the surface until saturation of this latter is achieved.

The diagram of figure VI-2 summarises the mechanisms of sulphur segregation occurring during the annealing of cold worked nickel.

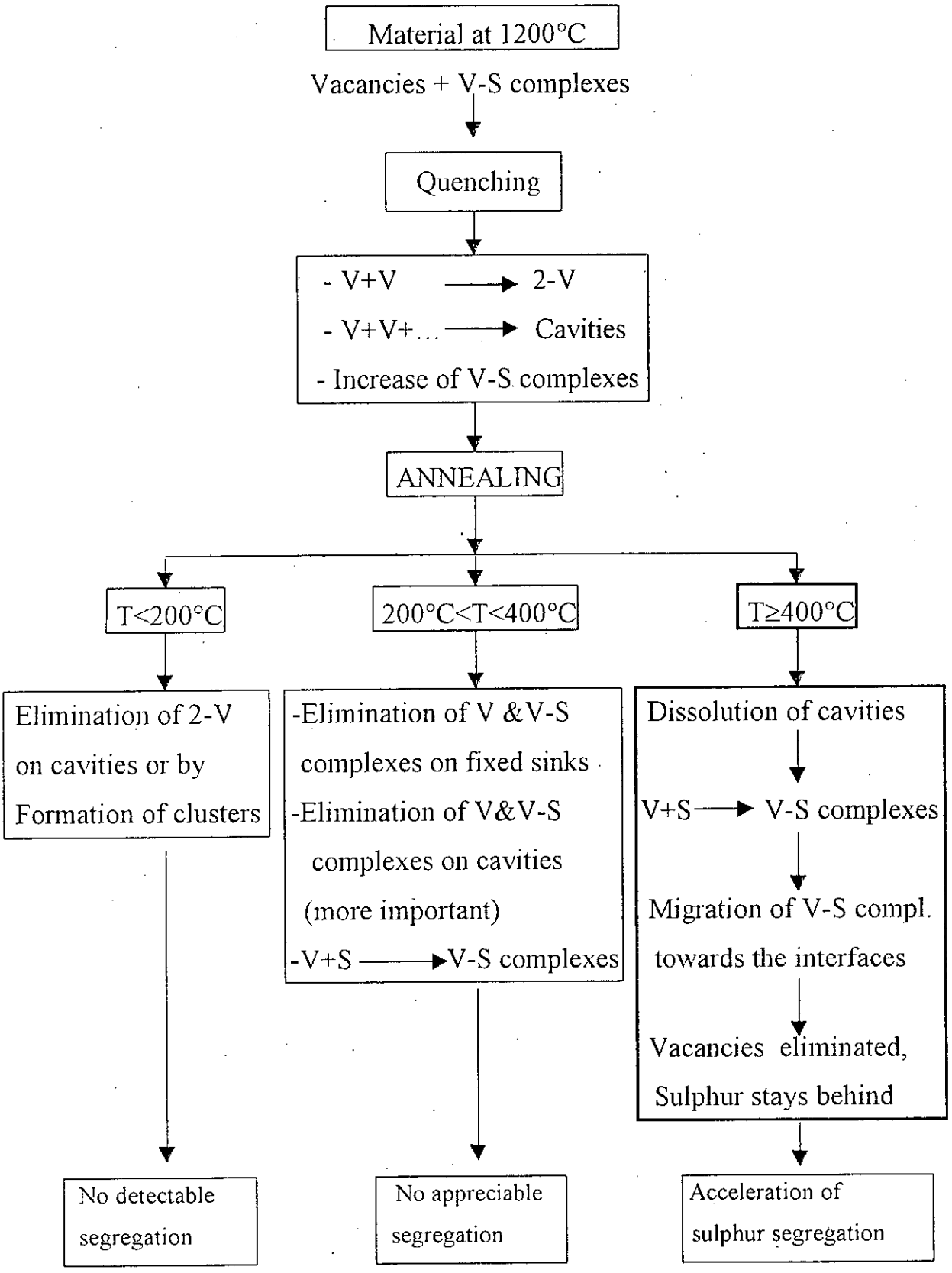

Figure VI-1. Diagram representing the segregation mechanisms operating during the annealing of quenched nickel (V: vacancy, S: sulphur, 2-V: di-vacancy).

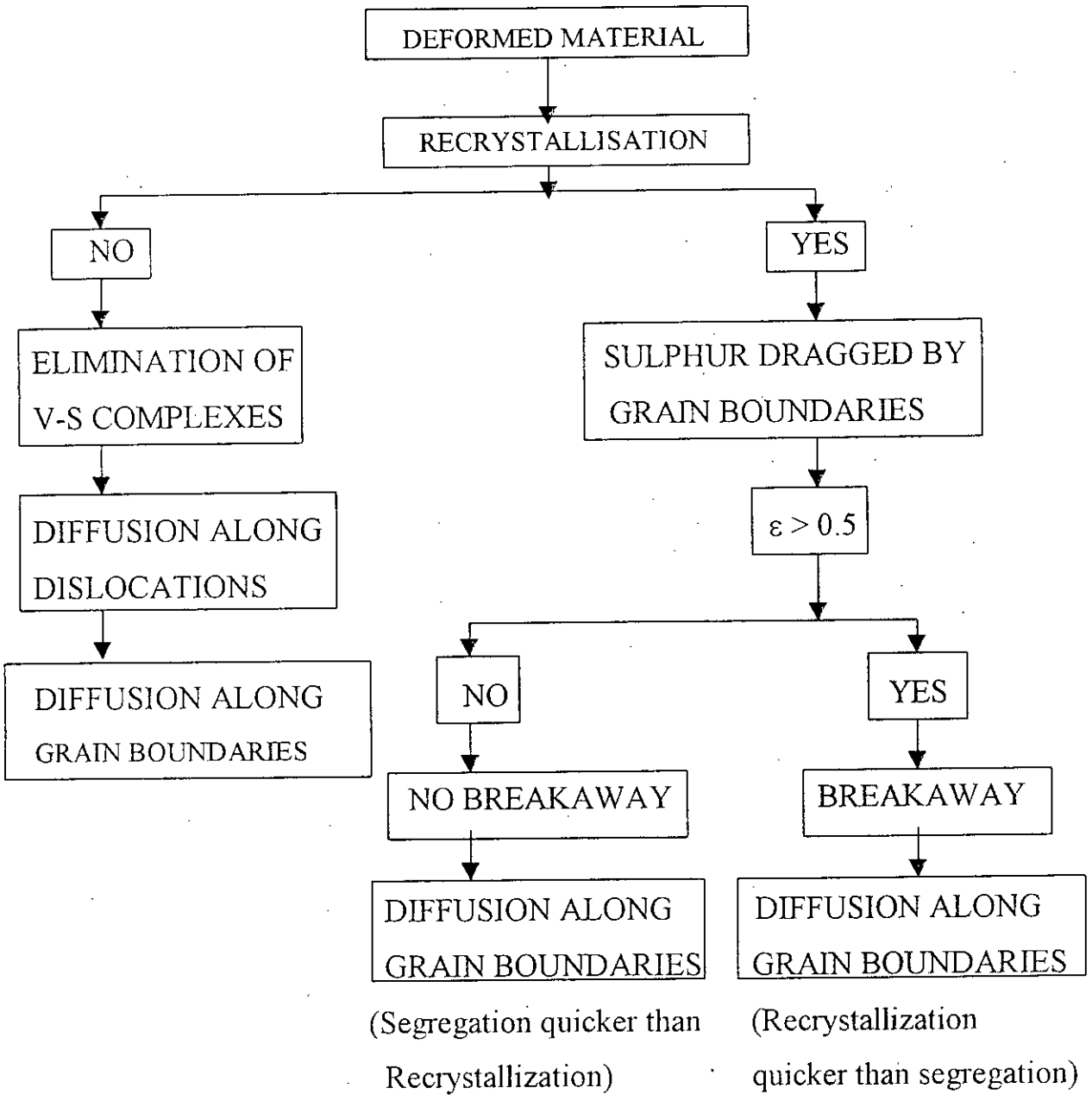

Figure VI-2. Diagram representing the segregation mechanisms operating during the annealing of cold worked nickel.

CONCLUSIONS

The results obtained in this work enable us to come to the following conclusions :

- The return of high purity nickel, originally in a metastable state (quenched, cold worked), to its equilibrium state results in the segregation of sulphur to the interfaces (grain boundaries, free surface) at a rate several orders of magnitude greater than that usually taking place in equilibrium conditions (a fully annealed material heat treated for long periods of time at relatively high temperatures).
- The vacancies created by quenching or cold work contribute to the acceleration of the segregation kinetics by dragging sulphur atoms with them during their movement in the course of a heat treatment.
- The increase in dislocation density resulting from cold work leads to an increase in diffusion short circuits. Grain boundaries of the recrystallising structure collect the sulphur diffusing along dislocation lines and drive it to the free surface as long as this latter is not saturated.
- The time lag between surface segregation and intergranular segregation is due to the transfer of sulphur from the GB's to the surface via grain boundary diffusion resulting from the difference in free energy between the two interfaces. Grain boundary segregation is therefore established only once the flux of atoms from the GB's to the surface is stopped, i.e. only once the surface concentration has reached its maximum.
- Sulphur segregation associated with the recovery and recrystallisation of a cold worked metal occurs at a rate 10^5 to 10^8 greater than that taking place in equilibrium conditions, with the maximum rate corresponding to annealing at the right temperature a material strained to a critical value. For strains below this critical value, the acceleration of segregation is attributed to the role played by the crystal defects in speeding up diffusion. For strains slightly above that value, the acceleration is due to the sulphur atoms being dragged by the moving grain boundaries. For much greater strains, the grain

boundaries breakaway from the sulphur atmospheres leaving them behind. This brings about a decrease in segregation kinetics to attain a value which is independent of strain.

- Surface saturation with sulphur is attained after annealing times ranging from a few minutes to tens of minutes, except at the low temperatures (~ 300°C) where longer periods (days) are necessary. The times at these low temperatures are of the same order (if not less) as those leading to equilibrium segregation although the temperatures are much lower.
- Moving grain boundaries, dislocations and vacancies lead to an accumulation of impurities, and hence the formation of impurity atmospheres, near the interfaces. These atmospheres are the real source of segregation acceleration. This particular point seems to be characteristic of dynamic segregation. The concentration profile, in the case of equilibrium segregation, reaches a minimum near the interface whereas it reaches a maximum in the case of non equilibrium (dynamic) segregation.
- Grain boundary segregation results in a loss of strength and ductility as shown by a decrease in the stress and the strain to failure with annealing time. The corrosion behaviour, besides being largely affected as shown by an increase in corrosion current density with annealing time, becomes more and more concentrated at the grain boundaries with increasing annealing time.
- Quenching vacancies result in the segregation of sulphur to nickel interfaces at a rate of up to 10^4 greater than that observed during equilibrium segregation.
- Segregation occurring during the annealing of quenched nickel continues well after the resistivity is entirely recovered. This is due to the accumulation of important quantities of sulphur near the interfaces.
- The purity of the metal seems to play a controversial role. A deterioration in intergranular properties is indeed obtained in a material of a very high purity.

This behaviour can reasonably be explained as follows :

The purification of a metal while obviously bringing about a decrease in sulphur concentration, leads also to a decrease in vacancy sinks such as impurity micro-precipitates. The remaining sulphur, although in reduced quantities, thus acquires a greater long range diffusivity. Moreover, the recrystallisation temperature of a metal increases with increasing impurity concentration and might even be pushed beyond a temperature where interfacial segregation is small and therefore undetectable. In the particular case of nickel, it is observed that , due to various interactions in the segregated layer, grain boundary segregation falls off rapidly at relatively high temperatures so that it becomes negligible above 800°C. A nickel of 99.5% purity recrystallises at about 850°C, and therefore shows no dynamic segregation with recrystallisation. This clearly emphasises the limitations of purification as a means of reducing intergranular brittleness.

It should however be noted that not all segregations are deleterious. Although sulphur segregates to grain boundaries of both nickel and silver, only the former is found to suffer from this segregation. The segregation of boron to the grain boundaries of nickel is found to have a strengthening effect, and very small quantities of this element are usually added to nickel base superalloys to increase their resistance to creep [69].

ANNEX I

Determination of the plasticity function of nickel 270.

Introduction

The plasticity function is aimed at finding a relationship between the uniaxial stress and true strain in order to be able to use Saada's [100] and Bailey's [99] expressions to calculate the vacancy concentration and dislocation density.

Procedure

A tensile test was carried out on a fully annealed (7h at 1000°C) cylindrical specimen. The testing conditions are as follows:

Temperature of the test: ambient.

Initial dimensions of the specimen: d_0=6 mm, l_0=105mm

Strain rate: 2 mm.min^{-1} (3.3x10^{-4} s^{-1})

The tensile force and cross-head displacement are continuously recorded.

In the range of uniform deformation ($0<\varepsilon<0.46$) the uniaxial stress and the true strain are given by:

$$\sigma = \frac{4.F}{\pi.d^2} \quad , \qquad \varepsilon = \ln(\frac{l}{l_0}) = 2.\ln(\frac{d_0}{d}) \quad ,$$

where F is the tensile force, d and l are the diameter and length of the specimen, d_0 and l_0 are the initial diameter and length of the specimen.

The stress and strain can therefore be related as follows:

$$\sigma = \frac{4.F.e^{\varepsilon}}{\pi.d_0^2} \quad .$$

In the necking range, the stress in the plane of maximum necking (minimum diameter) is obtained from the following expression [144]:

$$\sigma = K.\frac{4.F}{\pi.d^2},$$

K, a correction factor, is given by:

$$K = \frac{1}{\left(1+\frac{4.R}{d}\right).\ln\left(1+\frac{d}{4.R}\right)},$$

where $\boldsymbol{R}$ is the curvature radius of the necking profile, $\boldsymbol{d}$ is the minimum diameter at the neck.

Figure A-1 represents the plasticity function for deformations of up to ε=1. Failure of the specimen occurred at a strain of 2.5

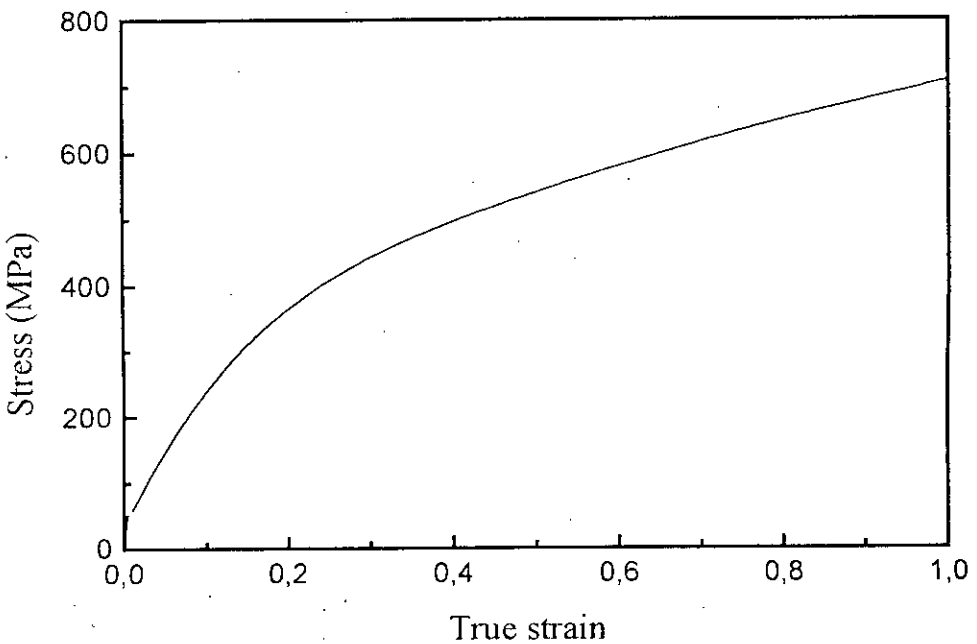

Figure A-1. Plasticity curve of Ni 270.

ANNEX II

Scanning electron microscope micrographs showing the intergranular grooves as obtained from the controlled potential coulometry tests

A) COLD ROLLED MATERIAL

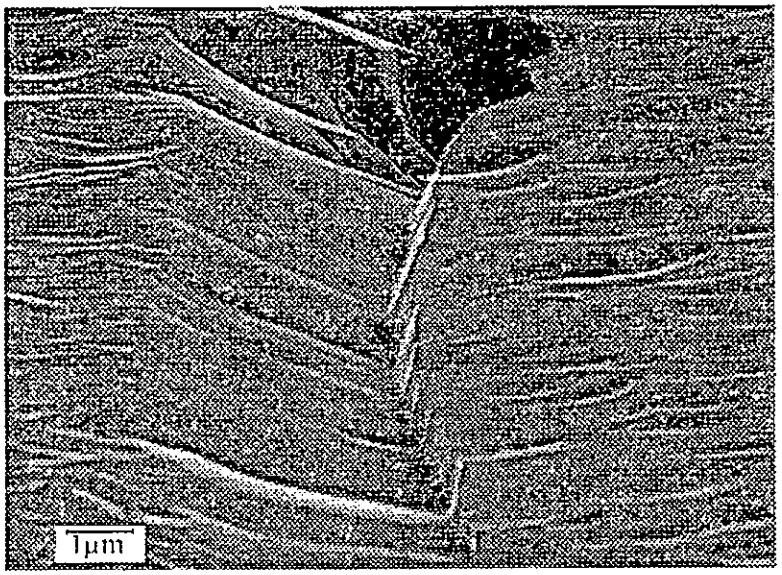

(a) 10 min

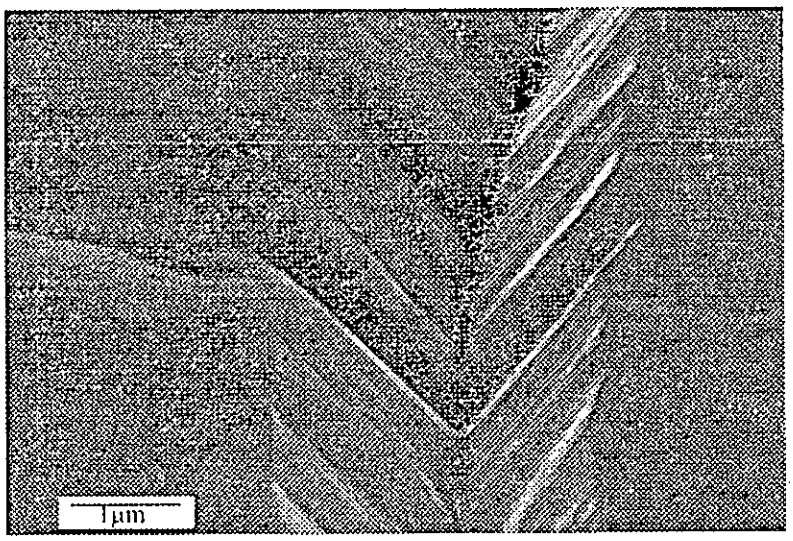

(b) 20 min

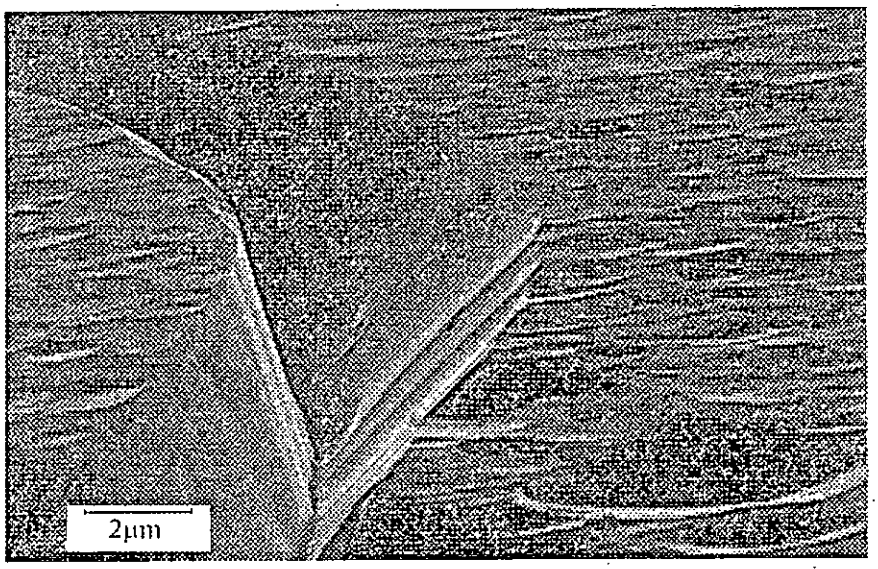

(c) 30 min

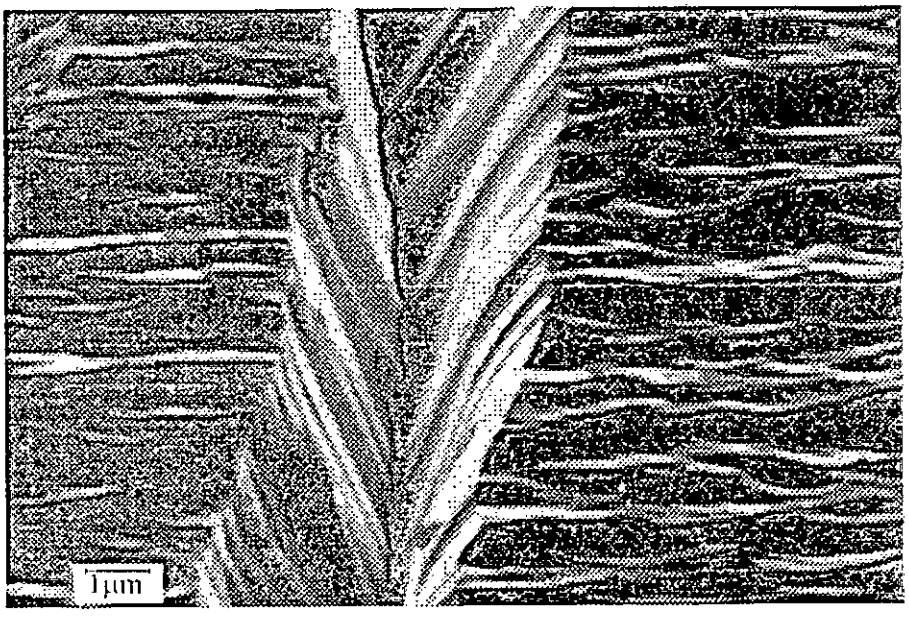

(d) 40 min

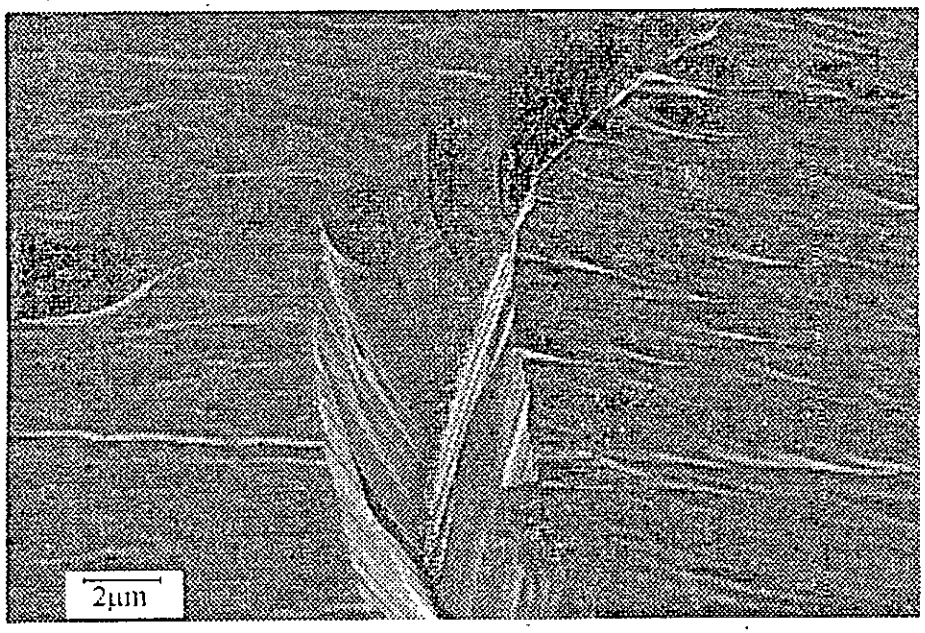

(e) 50 min

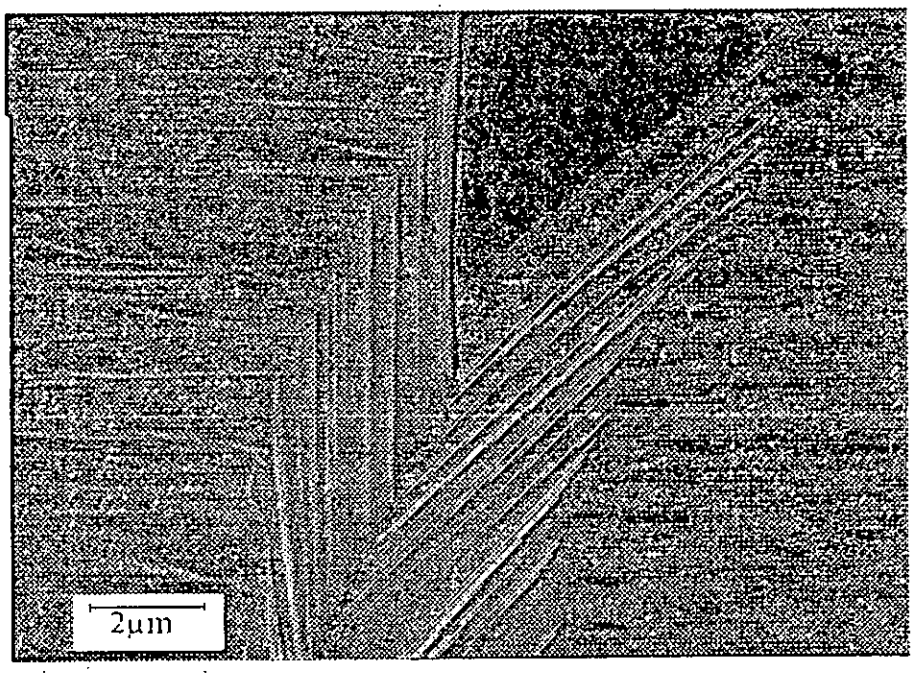

(f) 60 min

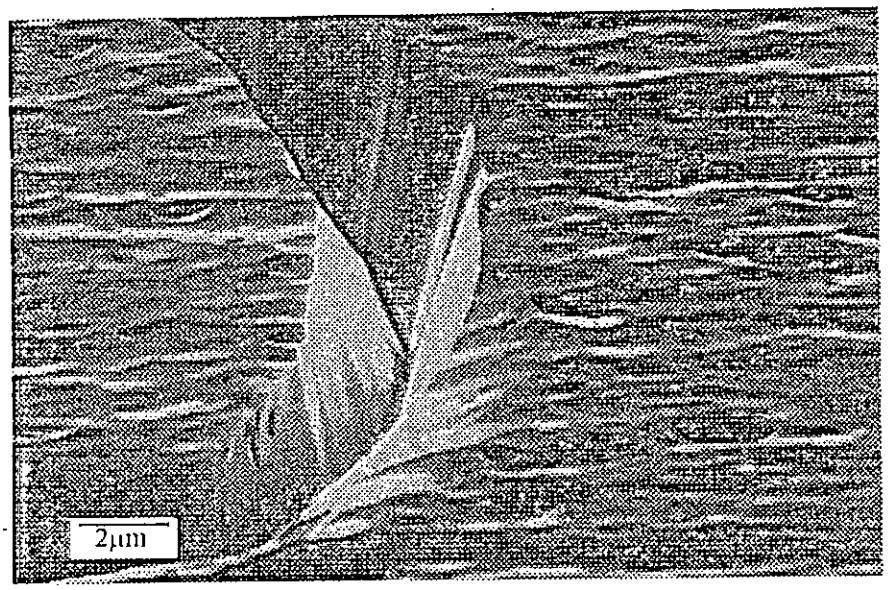

(g) 70 min

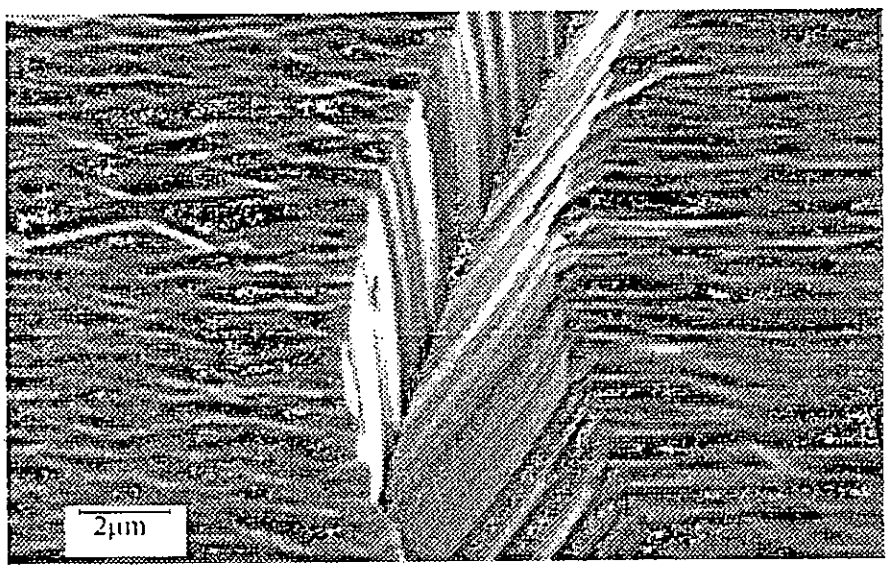

(h) 180 min

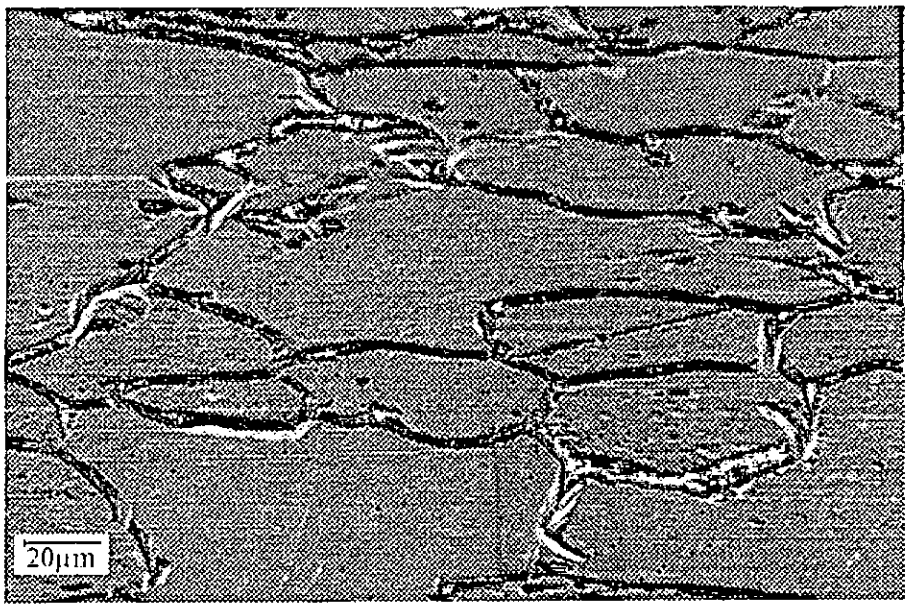

(i) 70 min

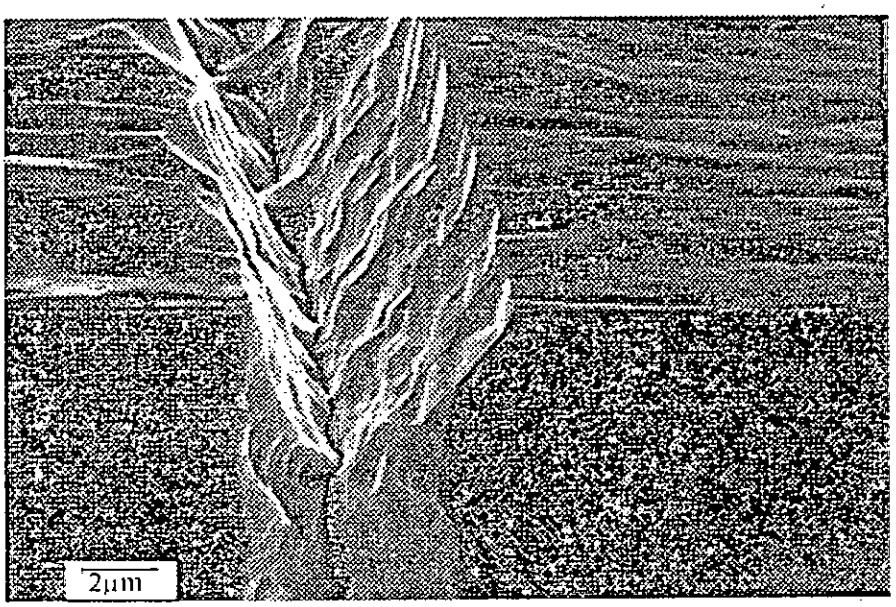

(j) 70 min

Figure A-II-1. SEM micrographs showing the intergranular grooves for the material cold rolled to 0.2 and then heat treated at 455°C for different periods of time. (i) low magnification.(j) the edge of the specimen.

B) QUENCHED MATERIAL

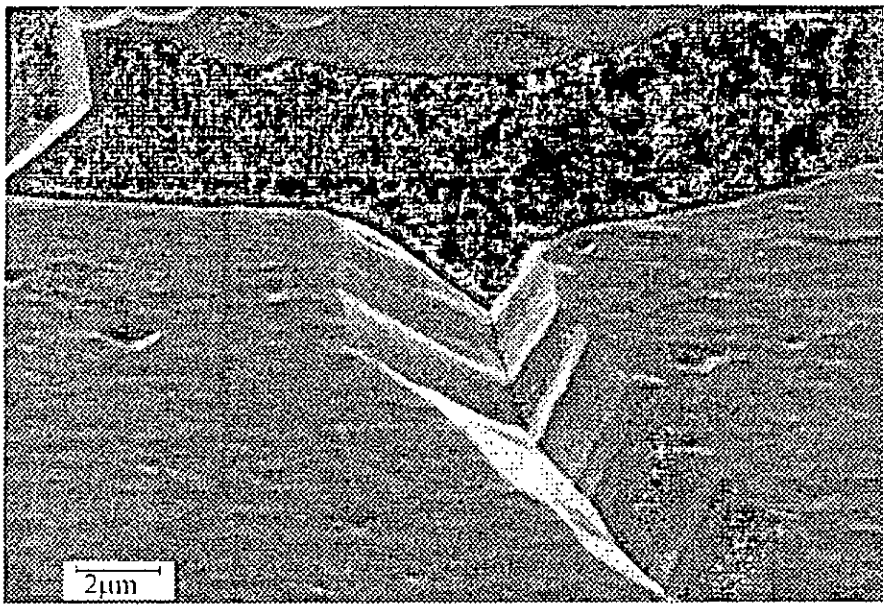

(a) 1 h.

(b) 2 h.

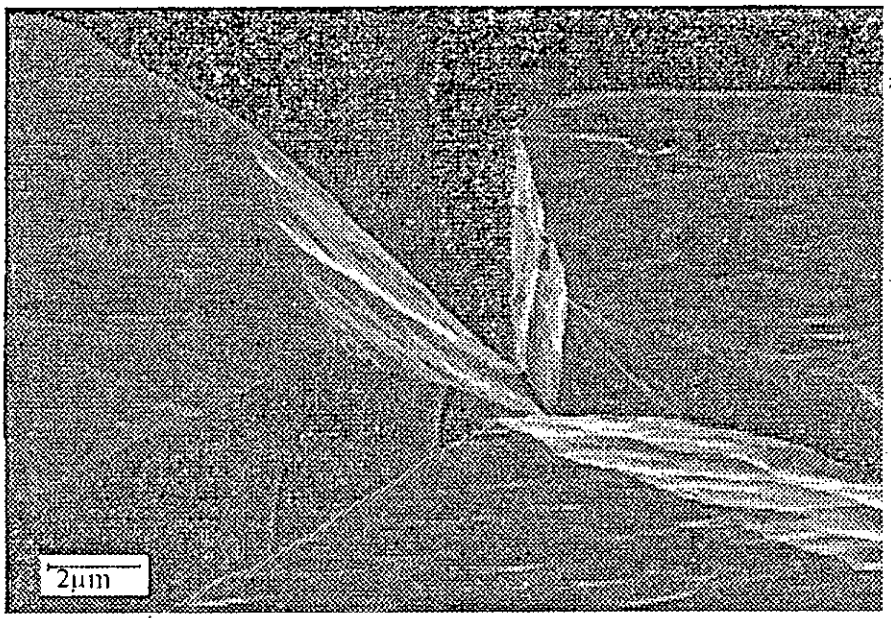

(c) 3 h.

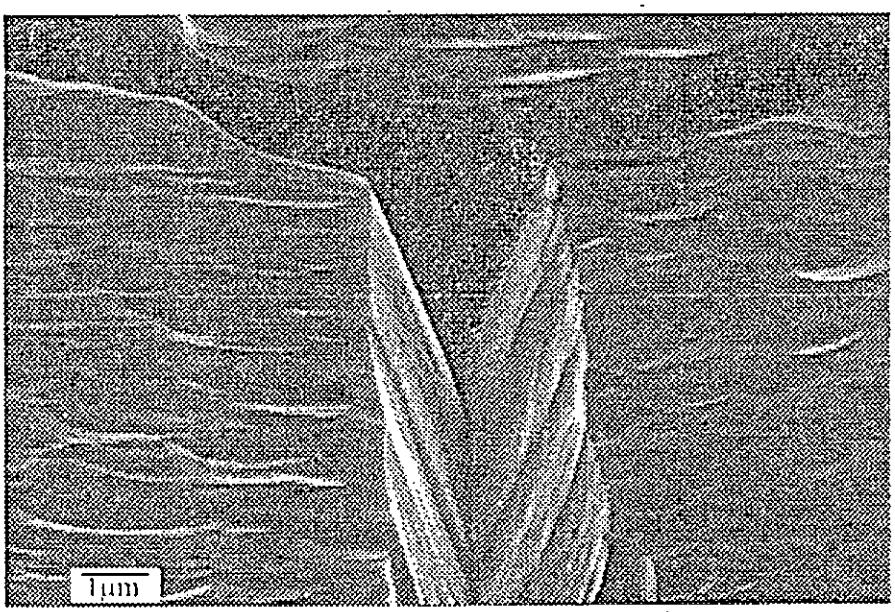

(d) 5h.

(e) 15 h.

(f) 20 h.

Figure A-II.2. SEM micrographs showing the intergranular grooves for the material quenched and then heat treated at 650°C for different periods of time. (e): the attack ceases to be concentrated at the GB's.

REFERENCES

1. K.T. Aust, R.E. Hanneman, P. Niessen and J.H. Westbrook, *Acta Metall.*, **16**, 291(1968) .
2. D. Udler and D.N. Seidman, *Acta metall.*, **42**, 1959(1994)
3. E. Rabkin, *Mater. Lett.*, **25**, 199(1995)
4. M.P. Seah and E.E. Hondros, *Proc. R. Soc. A*, **335**, 191(1973).
5. M.P. Seah and C. Lea, *Phil. Mag.*, **31**, 627(1975).
6. L. S. Chang, E. Rabkin, B.B. Straumal, S.Hofmann, B.Baretzky and W. Gust, *Defect and Diff. Forum*, **156**, 135(1998).
7. L. S. Chang, B. Straumal, E. Rabkin, W. Gust and F. Sommer, *J. Phase Equilibria*, **18**, 128(1997)
8. E.D. Hondros, M.P. Seah and C. Lea, *Metals Mater.*, January 1976, **26**.
9. H.R. Tipler and D. McLean, *Metals Sci. J.*, **4**, 103(1970).
10. D. Gupta, C.K. Hu and K.L. Lee, *Defect and Diff. Forum*, **143-147**, 1397(1997)
11. E. Glickman and M. Molotskii, *Mater. Lett.*, **26**, 65(1996).
12. T. Surholt, C. Minkwitz and Chr. Herzig, *Acta Mater.*,**46**, 1849(1998)
13. P.E.J. Flewitt and R.K. Wild, *Mater. Sci. Forum*, **294-296**, 297(1999).
14. J.C. Kim, N.H. Heo, J.G. Na J.S. Woo and G.M. Kim, *Scripta Mat.*, **38**, 1071(1998)
15. C. Lea and M.P. Seah, *Scripta Metall.*, **9**, 583(1975)..
16. A.V. Krajnikov, M. Militzer and J. Wieting, *Mater. Sci. Tech.*, **13**, 877(1997)
17. M. Militzer and A.V. krajnikov, *Mater. Sci. Forum*, **294-296**, 435(1999)
18. M. Jenko, F. Vodopivec, H.J. Grabke, H. Viefhaus, B. Pacek, M. Lucas and M. Godec, *Steel Research*, **65**, 500(1994)
19. M. Jenko, M. Godec, H. Viefhaus and H.J. Grabke, *Mater. Sci. Forum*, **294-296**, 747(1999)

20. C.S. Lin, M. Meshii and C.C. Cheng, *Galvatech '95 Conf. Proc.*, ISS, Warrendale, PA, 485(1995)
21. C.S. Lin and M. Meshii, *Galvatech '95 Conf. Proc.*, ISS, Warrendale, PA, 335(1995)
22. V. Rangarajan, R. Toncheff and L.L. Franks, *Metall. and Mater. Trans.*, **29A**, 2707(1998)
23. J.A. Smith and W.E. Martinsen, *Bull. Am. Ceram. Soc.*, **52**, 855(1973).
24. R. Hales, A.C. Hill and R.K. Wild, *Corrosion Sci.*, **13**, 325(1973).
25. G.M. Scamans and A.S. Rehal, *J. Mater. Sci.*, **14**, 2459(1979).
26. M. Menyhard, M. Yan and V. Vitek, *Acta Metall. Mater.*, **42**, 2783(1994)
27. S.H. Na, M.S. Yang and S.W. Nam, *Scripta Metall.*, **32**, 627(1995)
28. X.Y. Liu and J.B. Adams, *Acta Mater.*, **46**, 3467(1998)
29. P. Doig, J.W. Edigham and M.H. Jacobs, *Phil. Mag.*, **31(2)**, 285(1975).
30. C.R. Shastry and G. Judd, *Met. Trans.*, **2**, 779(1972).
31. T. Malis and M.C. Chaturvedi, *J. Mater. Sci.*; **17**, 1479(1982).
32. J.R. Galvele and S.M. de Micheli, *Corrosion Sci.*, **10**, 795(1970).
33. S. Maitra and G.C. English, *Metall. Trans.*, **12A**, 535(1981).
34. S.C. Byrne, in « Aluminium alloys, physical and mechanical properties », Vol.II, ed. E.A. Stark and T.H. Sanders,, Warley (UK), 1095(1986).
35. E.C. Bain, R.H. Aborn and J.B. Rutherford, *Trans. Amer. Steel Treating Soc.*, **21**, 481(1933).
36. E.L. Hall and C.L. Briant, *Metall. Trans.A*, **15A**, 793(1933).
37. Seizaboro Abe, Masao Kajima and Juzo Hosoi, *Proc. Seventh Int. Congress on Metallic Corrosion*, Rio de Janeiro, 1978, p. 887.
38. R. Carnahan and C.W. Jewett, Proc. Electric Power Research Institute Conf. on BWR Corrosion, Chemistry and Radiation Control, Palo Alto, California, 1984.
39. P.L. Anderson, Paper 85, Corrosion 87, San Francisco, California.
40. T.M. Devine, C.L. Briant and B.J. Drummond, *Scripta Metall.*, **14**,

1175(1980).

41.E.P. Simonen and S.M. Bruemmer, *J . Nuc. Mater.*, **239**, 193(1996)

42. E.P. Simonen and S.M. Bruemmer, in Microstructure Evolution During Irradiation, MRS Symposium, **439**, 569(1996)

43. E.P. Simonen and S.M. Bruemmer, *Mater. Sci. Forum*, **294-296**, 755(1999)

44. C.L. Briant and S.K. Banerji, in « Embrittlement of engineering alloys », Academic Press, New York, 1983, p. 21.

45. C.L. Briant and P.L. Andersen, *Metall. Trans.A*, **19A**, 495(1988).

46. H. Hanninen and E. Minni, Technical Research Center of Finland, Report 32/1981, Espoo, Finland, Oct.1981.

47. C.L. Briant, *Metall. Trans.A*, **16A**, 2061(1985).

48. C.L. Briant, *Metall. Trans.A*, **18A**, 691(1987).

49. C.L. Briant, *Scripta Metall.*, **21**, 71(1987).

50. C.L. Briant, *Surf. And Interface Anal.*, **13**, 209(1988).

51. C.L. Briant and R.A. Mulford, *Metall. Trans.A*, **13A**, 745(1982).

52. A. Larere, M. Guttmann, P. Dumoulin and C. Roques-Carmes, *Acta Metall.*, **30**, 686(1982).

53. C. Lea and M.P. Seah, *Phil. Mag.*, **35**, 213(1977).

54. F. Garzarolli, D. Alter and P. Dewes, *Proc. Second Int. Symposium on Environmental Degradation of Materials in Nuclear Power Systems-Water Reactors*, American Nuclear Society, Monterey, CA, 1986,p. 131.

55. A. Larère, Thèse de Doctorat d'Etat, Univ. Paris XI, 1983, p. 268.

56. D. McLean, Grain Boundaries in Metals, Clarendon Press, 1957, p. 116.

57. R.H. Fowler, *Proc. Cambridge Phil. Soc.*, **31**, 260(1935).

58. P. Rabu, G. Saindrenan, A. Caprani, T. Jaszay and J.P. Frayret, *J. of Applied Electrochem.*, **22**, 57(1992).

59. L. Baunier, *J. de Physique*, C6, suppl.43, 271(1982).

60. C.Gabrielli, *Métaux Corrosion Industrie*, **573**, 71(1973).

61. B.W. Lifka and D.D. Sprowls, *ASTM Spec. Tech. Publ.*, USA, **516**,

120(1972).

62. A. Desestret and M. Froment, *Mem. Sci. Rev. Metal.*, LXII n°2, 135(1965).
63. M. Froment, *Int. Coll. On grain boundaries in metals*, J. Physique, C4, suppl.10, 371(1975).
64. L. Beaunier, M Froment and C. Vignaud, *Electrochimica Acta*, **25**, 1239(1980).
65. M.P. Seah, *Surf. Sci.*, **53**, 1686(1975).
66. C.L. Briant, *Met. Trans.*, **21A**, 2339(1990).
67. E.D. Hondros and M.P. Seah, *Scripta Metall.*, **6**, 1007(1972).
68. W. Losh, *Acta Metall.*, **27**, 1885(1979).
69. R.P. Messmer and C.L. Briant, *Acta Metall.*, **30**, 457(1982).
70. J. Cabane, in « Les joints de grains dans les métaux », les éditions de physique, France, 1984, p. 161.
71. J.W. Gibbs, Collected Works, New York, 1929.
72. I. Langmuir, *J. Am. Chem. Soc.*, **40**, 1371(1918).
73. R.H. Fowler and E.A. Guggenheim, in « Statistical thermodynamics », Cambridge University Press, 1965.
74. M. Lagües, *Philips Res . Reports Suppl.*, **5**, 1976.
75. M. Guttman, Doctorate thesis, Paris XI, 1974.
76. M. Guttman, Surf. Sci, **53**, 213(1975).
77. J. Oudar, *Mater. Sci. Eng.*, **42**, 101(1980)
78. Y. Zhang, F. Zhu and J. Xiao, *Scripta Metall.*, **25**, 1617(1991)
79. A.S. Gay, A. Fraczkiewicz and M. Biscondi, *J . de Phys.*, 6 C2, 153(1996)
80. I. Baker, O. Klein C. Nelson and E.P. George, *Scripta Metall.*, **30**, 863(1994)
81. A.S. Gay, A. Fraczkiewicz and M. Biscondi, *Materials Sci. Forum*, **294-296**, 453(1999)
82. V.V. Sagaradze, V.A. Shabashov, T.M. Lapina and V.L. Arbuzov, *Phys. Met. Metallography*, **78**, 414(1994)

83. B.N. Goshchitskii, M.A. Kirk, V.V. Sagaradze and S.S. lapin, *Nanostructured Materials*, **9**, 189(1997)
84. V.V. Sagaradze, A.G. Mukoseev, V.A. Shabashov and S.S. lapin, *Mater. Sci. Forum*, **294-296**, 759(1999)
85. X.L. He, M. Djahazi, J.J. Jonas and J. Jackman, *Acta Metall. Mater.*, **39**, 2295(1991)
86. R.G. Faulkner, S. Song and P.E.J. Flewitt, *Metall. Mater. Trans.*, **27A**, 3381(1996)
87. J. Kameda and T.E. Bloomer, *Acta Mater.*, **47**, 893(1999)
88. P.D. Merica, *Trans. Am. Soc. Steel Treatm.* , 1054 (1929)
89. M. Massard, *Traitement de Surface*, **20**, 42 (1973)
90. P.D. Merica and R.G. Waltemberg, U.S. Nat. Bur. of St., Tech. Paper n°281, 2 (1925).
91. K.M. Olsen, C.F. Larkin and P.H. Shmitt, *J. of Trans. Am. Soc. Met.*, **53**, 349 (1961)
92. D.A. Oliver, *Royal Mint Report*, **3**, April 20 (1965)
93. F.G. Wilson and F.B. Pickering, *J. Iron Steel Inst.*, **210**, 37(1972).
94. N. Barbouth and J. Oudar, *C.R. Acad. Sci.*, Paris, Série C, 269(1969).
95. R.J. Brighman, H. Neumeyer and J.S. Kirkaldy, *Canadian Metallurgical Quarterly*, **9**, 525 (1970).
96. M. Hansen, Constitution of Binary Alloys, McGraw Hill Book Company, 1958.
97. T. Furu, R. Orsund and E. Nes, *Acta Metall. Mater.*, **43**, 2209(1995)
98. E. Nes, , *Acta Metall. Mater.*, **43**, 2189(1995)
99. J.E. Bailey, *Phil. Mag.*, **8**, 223 (1963).
100. G. Saada, *Acta Metall.*, **8**, 166 (1961).
101. P. Merklin, Thèse de Doctorat d'Etat., Université Paris VI, (1972).
102. M. Ferry and F.J. Humphreys, *Acta Metall. Mater.*, **44**, 1293(1996)
103. F.J. Humphreys, *Acta Mater.*, **45**, 4231(1997)

104. C.J. Simpson, W.C. Winegard and K.T. Aust, in « Grain boundary structure and properties », Edited by G.A. Chadwick and D.A. Smith, Academic Press, London, 1976, p. 201.
105. L.M. Clarebrough, M.E. Hargreaves, M.H. Loretto and G.W. West, *Acta Metall.*, **8**, 797 (1960).
106. A. Sosin and J.A. Brinkman, *Acta Metall.*, **7**, 478 (1959).
107. W.A. Johnson and R.F. Mehl, *Trans. Am. Inst. Min. Ingrs.*, **135**, 416(1939).
108. M. Avrami, *J. Chem. Phys.*, **7**, 1103(1939).
109. A.E. Kolmogorov, Akad Nauk SSSR, *Izv. Ser. Mat.*, **1**, 355(1937).
110. F.J. Humphreys and M. Hatherly, in « Recrystallisation and related annealing phenomena, Pergamon Press, 1995.
111. A.D. Rollett, D.J. Srolovitz, R.D. Doherty and M.P. Anderson, *Acta Metall.*, **37**, 627(1989).
112. B. Hutchinson, S. Jonsson and L. Ryde, *Scripta Metall.*, **23**, 671(1989).
113. R.A. Vandermeer and P. Gordon, *Trans. Met. Soc. AIME*, **224**, 221(1962).
114. K. Marthinson, O. Lohne and E. Nes, *Acta Metall.*, **37**, 135(1989).
115. T. Furu, K. Marthinson and E. Nes, *Mater. Sci.Technol.*, **6**, 1093(1990).
116. H.W. Hesselbarth and I.R. Göbel, *Acta Metall. Mater.*, **39**, 2135(1991).
117. K. Lücke and K. Detert, *Acta Metall.*, **5**, 628 (1957).
118. J.W. Cahn, *Acta Metall.*, **10**, 789 (1962).
119. K. Lüke and H.P. Stüve, in « Recovery and recrystallisation of metals », edited by L. Himmel, Interscience, New York, 1963, p.171.
120. K. Marthinsen and N. Ryum, *Acta Metall. Mater.*, **46**, 1127(1997)
121. M. Perdereau and J. Oudar, *Surf. Sc.*, **20**, 80(1970).
122. S.J. Wang and H.J. Grabke, *Z. Metallkde.*, **61**, 597(1970).
123. G.F. Vandervoort, « Visual examination and light microscopy », in Metals Handbook, 9th. ed., Vol.12 : Fractography, ASM International, Metals Park, Ohio, 1987.
124. M. Daguenet, M. Froment and M. Keddam, *J. Microscopie*, **5**, 569(1966).

125. I. Epelboin and M. Keddam, *C. r. hebd. Séanc. Acad. Sci.*, Paris, **127C**, 258(1964).
126. J. Hillairet, Défauts ponctuels dans les solides, Ecole d'été de Confolant, Les éditions de physique, Orsay, Paris, 1977.
127. W.M. Lomer, Vacancies and other point defects in metals and alloys, Inst. of Metals, 79(1959).
128. E.W. Muller, *J. of Jap. Phys. Soc* ., **18**, Suppl.(II,1), 1963.
129. W.J. Sutern and M.S. Wechsler, *J. Appl. Phys.*, **38**, 1509(1957).
130. J.I.Takamura,Lattice defects in quenched metals, Academic press, 1965,p.521
131. R.C. Foleiler and F.R. Brotzen, *Acta Metall.*, **7**, 716(1959).
132. S. Scherrer, G. Losers and B. Deviot, International Conf. On Vacancies and Interstitials in Metals, Jülich, 167(1968).
133. M. Wuttig and H.K. Birnbaum, *J. of Phys. and Chem. of Solids*, **27**, 225(1966).
134. H. Mughrabi and A. Seeger, *Sol. Stat. Phys.*, **19**, 251(1967).
135. S. Scherrer and B. Deviot, *J. Phys.*, **33**, 895(1972).
136. W. Wycisk and M. Feller-Kniepmeier, *J. of Nuclear Materials*, **69&70**, 616(1978).
137. R.E. Smallman, K.H. Westmacott and J.H. Coiley, *J. Inst. Met.*, **88**, 127(1959).
138. S. Mader, A. Seeger and E. Simsch, *Z. Metalkunde*, **52**, 785(1961).
139. M. H. Loretto and L.M. Clarebrough, *Phil. Mag.*, **15**, 134(1967).
140. G. Lozes, Thèse de Doctorat d'Etat, Université de Nancy, France, 1969.
141. S. Scherrer, Thèse de Doctorat d'Etat, Université de Nancy, France, 1970.
142. K.T. Aust, R.E. Hannema, P. Niessen and J.H. Westbrook, *Acta Metall.*, **16**, 291(1968).
143. M. Guttman, *Met. Trans.*, **8A**, 1383(1977).
144. B. Jaoul,Plasticité et application aux métaux, ed.DUNOD, Paris 1965, p165

RESUME

La ségrégation d'une impureté aux interfaces d'un métal peut dans certains cas conduire à la détérioration des propriétés mécaniques et électrochimiques du matériau par un affaiblissement de la cohésion intergranulaire. La ségrégation est dite d'équilibre lorsque la cinétique de recouvrement des interfaces dépend uniquement du coefficient d'hétérodiffusion de l'impureté dans le métal. Dans le cas où l'accélération des cinétiques résulte soit de l'élimination des défauts ponctuels générés par irradiation ou par trempe, soit de la recristallisation du métal, on parle alors de ségrégation hors d'équilibre ou dynamique. Dans ce travail, nous traitons le cas particulier de la ségrégation du soufre ayant lieu durant le recuit du nickel trempé et du nickel écroui.

La restauration et la recristallisation du nickel écroui sont étudiées par calorimétrie différentielle à balayage. On constate l'apparition de deux pics sur la courbe de calorimétrie. Le premier est centré aux environs de 250°C, quelque soit le taux initial de déformation, et n'apparaît que pour les taux supérieurs à 0.2. Ce pic est attribué à l'élimination des lacunes. Le second apparaît à une température qui diminue lorsque le taux de déformation augmente. Ce pic est attribué à la recristallisation du matériau écroui.

Les cinétiques de recristallisation sont étudiées au moyen de recuits in situ dans un microscope électronique à balayage et de mesures de microdureté. Les résultats sont exploités sur la base de la théorie de Johnson-Mehl-Avrami-Kolmogorov (JMAK). Les valeurs expérimentales des exposants de JMAK (n=0.7-2.1) sont plus faibles que celles prédites par la théorie et dépendent fortement du taux de déformation. La compétition entre restauration et recristallisation, et surtout la distribution non aléatoire des cites de germination, sont à l'origine des valeurs basses de l'exposant de JMAK.

Les cinétiques de ségrégation superficielle se produisant au cours de chacun des stades de restauration et de recristallisation sont enregistrées par spectrométrie des électrons Auger.

Les cinétiques obtenues sont de cinq à huit ordres de grandeur supérieures aux cinétiques de ségrégation d'équilibre. La ségrégation intergranulaire est indirectement étudiée par des essais de traction et des essais électrochimiques. Une chute de la résistance et de la déformation à la rupture, ainsi qu'une concentration de l'attaque électrochimique intergranulaire (représentée par une augmentation de la profondeur et une diminution de l'angle du sillon intergranulaire) permettent d'associer la fragilité du nickel et la diminution de sa résistance à la corrosion intergranulaire à la ségrégation du soufre aux joints de grains. En raison du transfert des atomes de soufre des joints de grains vers la surface, dû à la différence entre les énergies de ségrégation superficielle et intergranulaire, la ségrégation intergranulaire ne devient stable qu'à partir du moment où le flux intergranulaire s'annule.

L'interprétation des cinétiques de ségrégation ainsi que la confrontation avec les résultats de calorimétrie et les cinétiques de recristallisation nous conduisent à proposer les mécanismes de ségrégation suivants :

- Si la recristallisation n'a pas lieu, c'est à dire, si la température de recuit est trop basse ou si le taux de déformation est trop faible, l'accélération de la ségrégation est liée à la formation de complexes lacune-soufre qui s'éliminent sur les puits de lacunes (surface, joints de grains, dislocations) ; le soufre pouvant ensuite diffuser rapidement vers les joints de grains ou la surface le long de ces courts-circuits.
- Si la recristallisation a lieu les joints de grains en mouvement entraînent dans leur sillage une atmosphère de soufre, il peut alors se présenter deux cas : si la force motrice de déplacement du joint est inférieure à une certaine valeur, autrement dit si le taux de déformation n'est pas suffisamment élevé, le joint de grain traîne le nuage de soufre jusqu'à la fin de la recristallisation. Par contre si le taux de déformation dépasse une certaine valeur, alors le nuage de soufre est décroché du joint de grains. Les surconcentrations de soufre ainsi formées constituent une source de soufre qui va contribuer à alimenter les joints de grains, puis la surface par diffusion intergranulaire.

La restauration du matériau trempé est étudiée par mesures de resistivité. On constate l'existence de trois stades sur l'échelle de température. Le premier stade est situé entre 50 et 200°C et correspond à la restauration de 15% de la résistivité totale due à la trempe. Le deuxième stade est centré vers 300°C et correspond à la restauration de 30% de la résistivité. Le dernier stade s'étale entre 450 et 700°C et correspond au recuit de 55% de la résistivité.

Les cinétiques de ségrégation superficielle se produisant au cours de chacun des stades de restauration de la résistivité sont enregistrées par spectrométrie des électrons Auger.

Les cinétiques obtenues sont de quatre ordres de grandeur supérieures aux cinétiques de ségrégation d'équilibre. La ségrégation intergranulaire est indirectement étudiée de la même manière que pour le matériau écroui.

L'interprétation des cinétiques de ségrégation ainsi que la confrontation avec les résultats de résistivité nous conduisent à associer l'accélération de la ségrégation à la formation puis l'élimination de complexes lacune-soufre. L'élimination de ces complexes entraîne l'accumulation de quantités importantes de soufre au voisinage des interfaces, permettant ainsi la poursuite de la ségrégation bien au delà du temps nécessaire à la restauration de la résistivité.

- If recrystallization does not occur, i.e., if either the annealing temperature or the deformation ratio is low, the acceleration of segregation is attributed to the formation of vacancy-sulphur complexes which annihilate on vacancy sinks (free surface, grain boundaries, dislocations) allowing sulphur to diffuse along the short circuits towards the grain boundaries or the surface.
- If recrystallization occurs the moving boundaries of the recrystallizing grains drag with them the sulphur atmospheres. In this case, two situations are expected : if the driving force for grain boundary migration is less than a certain value, in other words if the deformation ratio is not sufficiently high, the moving grain boundary drags with it the sulphur atmosphere until the end of recrystallization. If on the other hand the deformation ratio is greater than a certain value, the grain boundary breaks away from the sulphur atmosphere. The superconcentrations thus formed constitute a sulphur source which contributes to the supply of the grain boundaries and then the surface with sulphur.

Recovery of the quenched material is investigated by electrical resistivity measurements. The resistivity versus temperature curve can be divided into three stages. The first one lies between 50 and 200°C and is associated with a recovery of 15% of the resistivity due to quenching. The second stage is centred around 300°C and is associated with a recovery of 30% of the resistivity. The last stage extends from 450 to 700°C and corresponds to a recovery of the remaining resistivity.

The segregation kinetics associated with each stage of the recovery of resistivity are investigated by AES. The recorded kinetics are four orders of magnitude greater than the equilibrium segregation kinetics. Grain boundary segregation is indirectly studied in the same manner as for the cold worked material. Segregation kinetics in association with the resitivity results enable us to suggest a mechanism for the acceleration of segregation, based on the formation and then elimination of vacancy-sulphur complexes. The elimination of these complexes leads to an accumulation of appreciable quantities of sulphur at the vicinity of the interfaces. This enables segregation to continue for time durations well beyond those necessary for the recovery of resistivity.

ABSTRACT

Impurity segregation to interfaces in metals can in certain cases lead to a deterioration of the mechanical and electrochemical properties of the material by weakening the intergranular cohesion. Segregation where the surface coverage kinetics are under the sole control of the heterodiffusion coefficient of the impurity in the metal is known as equilibrium segregation. Segregation where the kinetics undergo considerable increase as a result of point defect annihilation or recrystallisation of the metal is known as non-equilibrium or dynamic segregation. The work presented in this thesis treats the special case of segregation occurring during the annealing of quenched and of cold worked nickel.

Recovery and recrystallization of cold worked nickel is studied by differential scanning calorimetry (DSC). Two peaks appear on the DSC curve. The first one is centred around 250°C, regardless of the deformation ratio, and only appears for deformations greater than 0.2. This peak is mostly attributed to vacancy elimination. The second peak appears at a temperature which decreases with increasing deformation. This peak is attributed to the recrystallization of the material.

Recrystallization kinetics are studied by carrying out in situ anneals inside a scanning electron microscope and microhardness measurements. The results are exploited in terms of the Johnson-Mehl-Avrami-Kolmogorov (JMAK) theory. The experimentally deduced values of the JMAK exponents (n=0.7-2.1) are smaller than the theoretically predicted values and depend to a great extent on the deformation ratio. Competition between recovery and recrystallization and non random distribution of nucleation sites is at the origin of these small values.

The kinetics of surface segregation occurring at each one of the recovery and recrystallization stages are investigated by Auger electron spectrometry (AES). The recorded kinetics are several orders of magnitude greater than equilibrium segregation kinetics. Grain boundary segregation is indirectly investigated by tensile and by electrochemical tests. A fall in both the stress and strain to failure as well as an enhancement of intergranular electrochemical attack (as depicted by an increase of the depth and a decrease of the angle, of the intergranular groove) indicate a segregation induced deterioration of the intergranular properties of the material. As a consequence of the transfer of sulphur atoms from the grain boundaries to the surface (due to the difference in free energy between superficial end intergranular segregation), grain boundary segregation becomes stable only once the intergranular flux towards the surface is stopped.

The segregation kinetics associated with the DSC results and the recrystallization kinetics enabled us to come up with the following segregation mechanisms :

(continued overleaf)